Minimum Number of Accelerograms for Time-History Analysis of Typical Highway Bridges

Kang Huang

A Thesis

in

The Department

of

Building, Civil and Environmental Engineering

Presented in Partial Fulfillment of the Requirements

for the Degree of Master of Applied Science (Civil Engineering) at

Concordia University

Montreal, Quebec, Canada

July 2014

Concordia University

School of Graduate Studies

This is to certify that the thesis prepared

By: Kang Huang

Entitled: Minimum Number of Accelerograms for Time-history Analysis of Typical Highway Bridges

and submitted in partial fulfillment of the requirements for the degree of

Master of Applied Science (Civil Engineering)

complies with the regulations of the University and meets the accepted standards with respect to originality and quality.

Signed by the final examining committee:

Dr. K.Galal Chair

Dr. Y. Zeng Examiner

Dr. L. Tirca Examiner

Dr. L. Lin Supervisor

Approved by _____

Chair of Department or Graduate Program Director

_____

Dean of Faculty

Date _____

Abstract

Minimum Number of Accelerograms for
Time-History Analysis of Typical Highway Bridges

Kang Huang

Time-history analysis is the most reliable method for the assessment of the behaviour of bridges subjected to seismic loads. It has been widely used in recent years on the evaluation of the seismic vulnerability of bridges. The selection of seismic motions is one of the most important issues for the time-history analysis. This thesis discusses four different methods for obtaining spectrum-compatible acceleration time histories (i.e., accelerograms) of seismic motions. Based on these methods, four sets of accelerograms compatible with the design spectrum for Montreal were selected for this study. These included (i) scaled real accelerograms, (ii) modified real accelerograms, (iii) simulated accelerograms, and (iv) artificial accelerograms. The selected sets were used as excitation motions in the nonlinear analysis of two existing bridges in Montreal. The bridges included a three-span continuous concrete slab bridge and a three-span continuous slab-girder type bridge. These two bridges are considered to be representative of typical highway bridges in Quebec. A number of response parameters, such as, the deck displacement, bearing displacement, column curvature ductility, and base shear were used for the evaluation of the effects of the selected sets on the response of the bridges. Based on the results from the analysis, simulated accelerograms are recommended for use in the time-history analysis of the bridges. Furthermore, a study was conducted on the investigation of the minimum number of accelerograms required for both linear and nonlinear time-history analyses. Two

different scaling methods, i.e., partial area under the spectrum and the spectral acceleration at the fundamental period of the bridge, were used to obtain the bridge responses. It was found that 5 accelerograms are sufficient for the linear time-history analysis and 10 accelerograms are required for the nonlinear time-history analysis based on the results from the two bridges considered in this study.

Acknowledgments

I wish to express my sincere gratitude to my supervisor Dr. Lan Lin for her continuous support and patience during the course of this study.

Thanks are also due to professors for sharing their knowledge by offering courses that helped me in my undergraduate and graduate studies at Concordia University.

I also would like to thank my parents for their financial support, love and encouragement during my years of study in the university.

Thank you all who made my journey to higher education successful.

Table of Contents

Abstract……...iii
Acknowledgements……..v
Table of Contents…….……...vi
List of Tables…….……..ix
List of Figures……..……x

Chapter 1: Introduction 1

1.1 Motivations 1
1.2 Review of Previous Studies 4
1.3 Objectives and Scope of the Study 5
1.4 Outline of the Thesis 7

Chapter 2: Description and Modeling of Bridges 9

2.1 Introduction 9
2.2 Description of Bridges 13
2.2.1 Bridge #1 13
2.2.2 Bridge #2 15
2.3 Modeling of Bridges 16
2.3.1 Superstructure 16
2.3.2 Bearing 20
2.3.3 Columns and Cap Beams 22
2.3.3.1 Modeling the plastic hinge zones 23
2.3.3.2 Modeling columns and cap beams 27
2.3.3.3 Material properties 28
2.3.4 Abutment 28
2.4 Dynamic Characteristics of the Bridge Models 31
2.5 Seismic Analysis 35
2.5.1 Deck displacement 36

2.5.2 Expansion bearing displacement 38
2.5.3 Response of the column 39

Chapter 3: Selection of Earthquake Records 46

3.1 Seismic Hazard for Montreal 46
3.2 Scenario Earthquakes for Montreal 48
3.3 Selection of records 51
3.3.1 Set 1 - Scaled real accelerograms 52
3.3.1.1 High A/V accelerograms 53
3.3.1.2 Intermediate A/V accelerograms 55
3.3.1.3 Scaling of ground motions 56
3.3.2 Set 2 - Modified real accelerograms 57
3.3.3 Set 3 - Simulated accelerograms 59
3.3.4 Set 4 - Artificial accelerograms 61

Chapter 4: Selection of Spectrum-compatible Accelerograms for Nonlinear Time-history Analysis 63

4.1 Introduction 63
4.2 Analysis Results of the Bridge #1 65
4.2.1 Statistics results 65
4.2.2 Behavior of the Bridge #1 73
4.3 Analysis Results of the Bridge #2 76
4.3.1 Statistics results 76
4.3.2 Behavior of the Bridge #2 83
4.4 Summary 86

Chapter 5: Minimum Number of Accelerograms Required for Time-history Analysis 87

5.1 Introduction 87
5.2 Determination the Minimum Number of Accelerograms Based on Scaling to Partial Spectral Area Method 90
5.2.1 Results for Bridge #1 91
5.2.2 Results for Bridge #2 97

5.3 Determination the Minimum Number of Accelerograms Based on the Intensity Measure of Sa(T_1) 102
5.3.1 Results for Bridge #1 104
5.3.2 Results for Bridge #2 108
5.4 Summary 112
5.5 Additional Remarks 113
Chapter 6: Summary and Conclusions 114
6.1 General remarks 114
6.2 Summary of findings 116
6.3 Conclusions 118
6.4 Recommendations for future work 119
Appendix: Analysis Results Using Set 1-Real Accelerograms……...121
References……131

List of Tables

Table 2.1 Parameters used in the modeling the bilinear behavior of the expansion bearings……..22

Table 2.2 Dynamic characteristics of the bridge models from modal analysis…….....32

Table 3.1 High A/V records included in the accelerograms of Set 1…….54

Table 3.2 Intermediate A/V records included in the accelerograms of Set 1…….55

Table 4.1 Ranges of the difference (in percentage) between the largest and smallest mean responses values from the selected sets of excitations for Bridge #1……68

Table 4.2 Ranges of the difference (in percentage) between the largest and smallest mean responses values from the selected sets of excitations for Bridge #2……76

Table 4.3 Maximum mean and mean + standard deviation (M+SD) response values from the selected sets of excitations…….....85

Table 5.1 Difference (in percentage) between the response values from ensembles of simulated accelegrams and those from Ens30 for Bridge #1 based on Sa_{Area}……...…….……...96

Table 5.2 Differences (in percentage) between the response values from ensembles of simulated accelegrams and those from Ens30 for Bridge #2 based on Sa_{Area}……..……...…102

Table 5.3 Differences (in percentage) between the response values from ensembles of simulated accelegrams and those from Ens30 for Bridge #1 based on $Sa(T_1)$…….…..108

Table 5.4 Differences (in percentage) between the response values from ensembles of simulated accelegrams and those from Ens30 for Bridge #2 based on $Sa(T_1)$……112

List of Figures

Figure 2.1 Typical bridge classes in Quebec……..10

Figure 2.2 Geometric configuration of Bridge #1…….....11

Figure 2.3 Geometric configuration of Bridge #2…….….12

Figure 2.4 Scheme of the spine models in SAP2000, (a) Bridge #1; (b) Bridge #2…….....18

Figure 2.5 Determination of the geometric properties of the superstructure of bridge models using Section Designer in SAP2000, (a) Bridge #1; (b) Bridge #2…….….19

Figure 2.6 Bilinear behavior of elastomeric bearings in the longitudinal direction……...22

Figure 2.7. Mander Model for confined and unconfined concrete…….24

Figure 2.8 Stress-strain relationship for the steel……...25

Figure 2.9 Moment-curvature curves of column section, (a) Bridge #1; (b) Bridge #2…….....……..26

Figure 2.10 Multi-linear kinematic plasticity model plastic hinges…….....27

Figure 2.11 Detailed modeling of a column bent……..…….27

Figure 2.12 Abutment models, (a) Roller; (2) Simplified; (3) Spring ……...30

Figure 2.13 Mode shapes of the first three modes from the modal analysis, (a) Bridge #1; (b) Bridge #2……...…...33

Figure 2.14 Acceleration time-history of one sample record…….…….....35

Figure 2.15 Acceleration response spectrum of the sample record, 5% damping.....36

Figure 2.16 Deck displacement time histories of Bridge #1 for a record scaled to (a) 0.5Sa(T_1); (b) 2.0Sa(T_1)……..37

Figure 2.17 Expansion bearing force-displacement curves of Bridge #1 for a record scaled to (a) 0.5Sa(T_1); (b) 2.0Sa(T_1)..……39

Figure 2.18 Column (of Pier 2) displacement time histories of Bridge #1 for a record scaled to (a) 0.5Sa(T_1); (b) 2.0Sa(T_1)…….....41

Figure 2.19 Column (of Pier 1) displacement time histories of Bridge #1 for a record scaled to (a) 0.5Sa(T_1); (b) 2.0Sa(T_1)…….....42

Figure 2.20 Column (of Pier 2) moment-curvature curves of Bridge #1 for a record scaled to (a) 0.5Sa(T_1); (b) 2.0Sa(T_1)……..43

Figure 2.21 Column (of Pier 1) moment-curvature curves of Bridge #1 for a record scaled to (a) 0.5Sa(T_1); (b) 2.0Sa(T_1)……..……...45

Figure 3.1 Uniform hazard spectrum and design spectrum for Montreal, 5% damping…….....48

Figure 3.2 Seismic hazard deaggregation results for Montreal for probability of exceedance of 10% in 50 years: (a) Sa(0.2s); (b) Sa(1.0s)……50

Figure 3.3 Scaled response spectra of the accelerograms of Set 1, 5% damping……..57

Figure 3.4 Target spectrum used to generate the accelerograms of Set 2 (modified real accelerograms)……...58

Figure 3.5 Scaled response spectra of the accelerograms of Set 2, 5% damping……..59

Figure 3.6 Scaled response spectra of the accelerograms of Set 3, 5% damping……..60

Figure 3.7 Shape function used to generate artificial accelerograms of Set 4……..…62

Figure 3.8 Scaled response spectra of the accelerograms of Set 4, 5% damping……..62

Figure 4.1 Deck displacements of Bridge #1……...…66

Figure 4.2 Expansion bearing displacements for Bridge #1…….…66

Figure 4.3 Curvature ductilities of Bridge #1 (Pier 1)……...…67

Figure 4.4 Curvature ductilities of Bridge #1 (Pier 2)……...…67

Figure 4.5 Base shear for Bridge #1……...68

Figure 4.6 Coefficients of variation (COV) of deck displacements of Bridge #1……..70

Figure 4.7 Coefficients of variation (COV) of expansion bearing displacements of Bridge #1……....71

Figure 4.8 Coefficients of variation (COV) of column curvature ductilities of Bridge #1 (Pier 1)……71

Figure 4.9 Coefficients of variation (COV) of column curvature ductilities of Bridge #1 (Pier 2)……72

Figure 4.10 Coefficients of variation (COV) for base shears of Bridge #1……72

Figure 4.11 Deck displacements of Bridge #2……..……77

Figure 4.12 Expansion bearing displacements for Bridge #2……....77

Figure 4.13 Column curvature ductilities of Bridge #2 (Pier 1)……..78

Figure 4.14 Column curvature ductilities of Bridge #2 (Pier 2)……..78

Figure 4.15 Base shear for Bridge #2…….79

Figure 4.16 Coefficients of variation (COV) of deck displacements of Bridge #2……..80

Figure 4.17 Coefficients of variation (COV) of expansion bearing displacements of Bridge #2……81

Figure 4.18 Coefficients of variation (COV) for column curvature ductilities of Bridge #2 (Pier 1)…….....81

Figure 4.19 Coefficients of variation (COV) for column curvature ductilities of Bridge #2 (Pier 2)…….....82

Figure 4.20 Coefficients of variation (COV) for base shear of Bridge #2……82

Figure 5.1 Mean response spectra from simulated accelerograms of Ens5, Ens10, Ens 20, and Ens30 using the partial spectral area scaling method……..91

Figure 5.2 Deck displacements of Bridge #1 based on the intensity measure of Sa_{Area}……...92

Figure 5.3 Expansion bearing displacements of Bridge #1 based on the intensity measure of Sa_{Area}……..93

Figure 5.4 Column curvature ductilities of Bridge #1 based on the intensity measure of Sa_{Area} (Pier 1)…….....93

Figure 5.5 Column curvature ductilities of Bridge #1 based on the intensity measure of Sa_{Area} (Pier 2)…….....94

Figure 5.6 Base shears of Bridge #1 based on the intensity measure of Sa_{Area}……..94

Figure 5.7 Deck displacements of Bridge #2 based on the intensity measure of Sa_{Area}……...99

Figure 5.8 Expansion bearing displacements of Bridge #2 based on the intensity measure of Sa_{Area}……..……99

Figure 5.9 Column curvature ductilities of Bridge #2 based on the intensity measure of Sa_{Area} (Pier 1)…….....100

Figure 5.10 Column curvature ductilities of Bridge #2 based on the intensity measure of Sa_{Area} (Pier 2)…….....100

Figure 5.11 Base shears of Bridge #2 based on the intensity measure of Sa_{Area}……101

Figure 5.12 Acceleration response spectra for the records of the Ens10 scaled to spectral acceleration of 0.28g at the first mode period of the Bridge #1, T_1 = 0.81s; 5% damping……103

Figure 5.13 Mean response spectra for the records of the Ens5, Ens10, Ens20, and Ens30 scaled to spectral acceleration of 0.30g at the first mode period of the Bridge #1, T_1 = 0.81s; 5% damping…….…104

Figure 5.14 Deck displacements of Bridge #1 based on the intensity measure of $S_a(T_1)$……..106

Figure 5.15 Expansion bearing displacements of Bridge #1 based on the intensity measure of $S_a(T_1)$ ……...106

Figure 5.16 Column curvature ductilities of Bridge #1 based on the intensity measure of $S_a(T_1)$ (Pier 1)……...107

Figure 5.17 Column curvature ductilities of Bridge #1 based on the intensity measure of $S_a(T_1)$ (Pier 2)…….....107

Figure 5.18 Base shears for the Bridge #1 based on the intensity measure of $S_a(T_1)$…….....108

Figure 5.19 Deck displacements of Bridge #2 based on the intensity measure of $S_a(T_1)$……..110

Figure 5.20 Expansion bearing displacements of Bridge #2 based on the intensity measure of $S_a(T_1)$……...110

Figure 5.21 Column curvature ductilities of Bridge #2 based on the intensity measure of $S_a(T_1)$ (Pier 1)……...111

Figure 5.22 Column curvature ductilities of Bridge #2 based on the intensity measure of $S_a(T_1)$ (Pier 2)……...111

Figure 5.23 Base shears for the Bridge #2 based on the intensity measure of $S_a(T_1)$…….....112

Figure A.1 Deck displacements of Bridge #1 based on Sa_{Area}……..121

Figure A.2 Expansion bearing displacements of Bridge #1 based on Sa_{Area}.....121

Figure A.3 Column curvature ductilities of Bridge #1 based on Sa_{Area} (Pier 1)……..122

Figure A.4 Column curvature ductilities of Bridge #1 based on Sa_{Area} (Pier 2)……..122

Figure A.5 Base shears for the Bridge #1 based on Sa_{Area}…….....123

Figure A.6 Deck displacements of Bridge #2 based on Sa_{Area}……..123

Figure A.7 Expansion bearing displacements of Bridge #2 based on Sa_{Area}.....124

Figure A.8 Column curvature ductilities of Bridge #2 based on Sa_{Area} (Pier 1)……..124

Figure A.9 Column curvature ductilities of Bridge #2 based on Sa_{Area} (Pier 2)……..125

Figure A.10 Base shears for the Bridge #2 based on Sa_{Area}…….....125

Figure A.11 Deck displacements of Bridge #1 based on $S_a(T_1)$…….....126

Figure A.12 Expansion bearing displacements of Bridge #1 based on $S_a(T_1)$.....126

Figure A.13 Column curvature ductilities of Bridge #1 based on on $S_a(T_1)$ (Pier 1) ……..……..……..……127

Figure A.14 Column curvature ductilities of Bridge #1 based on on $S_a(T_1)$ (Pier 2) ……..……..……..……127

Figure A.15 Base shears for the Bridge #1 based on $S_a(T_1)$ ……...128

Figure A.16 Deck displacements of Bridge #2 based on $S_a(T_1)$…….....128

Figure A.17 Expansion bearing displacements of Bridge #2 based on $S_a(T_1)$.....129

Figure A.18 Column curvature ductilities of Bridge #2 based on on $S_a(T_1)$ (Pier 1) ……..……..……..……129

Figure A.19 Column curvature ductilities of Bridge #2 based on on $S_a(T_1)$ (Pier 2) ……..……..……..……130

Figure A.20 Base shears for the Bridge #2 based on $S_a(T_1)$ ……130

Chapter 1

Introduction

1.1 Motivations

Dynamic analysis, such as, liner time-history analysis and nonlinear time-history analysis, has been extensively used these years on the seismic evaluation of both buildings and bridges. For example, the latest edition of the building codes around the world requires using the dynamic analysis method in the design of buildings located in high seismic hazard region (e.g., ASCE 2010, European Committee for Standards, NRCC 2010). The seismic analysis methods required for the design of bridges in the current bridge codes are different than those for buildings. According to the current Canadian Highway Bridge Design Code (CHDBC 2010) and American Association State and Highway Transportation Officials (AASHTO 2010), both multi-mode spectral method and time-history analysis method can be used to determine the *design* seismic response of the regular lifeline bridges and emergency route bridges while the time-history analysis method is mandatory only for irregular bridges.

In addition to the use of the time-history analysis method to determine the *design* parameters for bridges subjected to earthquake loads, time-history analysis is also used to *evaluate* the seismic performance of existing bridges. It is necessary to mention that time-history analysis is used very often these days for the development of fragility curves for bridges which show the probability of exceeding a given damage state of a bridge for a series of seismic excitation levels. Fragility curves are used further to estimate the economic losses of bridges

for potential earthquakes in the future.

To perform dynamic analysis, acceleration time histories (i.e., accelerograms) of the seismic excitations are needed. The codes require that the accelerograms should be compatible with the design spectrum. The main issues related to the use of spectrum-compatible accelerograms are: (i) the types of accelerograms (i.e., recorded or artificial) for use in the analysis, and (ii) the method for the selection and scaling of the spectrum-compatible accelerograms. However, both CHDBC (2010) and AASHTO (2010) do not provide guidance on the foregoing issues. Currently, different methods for the selection and scaling of accelerograms are in use, but no investigations of the effects of different types of accelerograms on the nonlinear response of bridges have been conducted so far. This leads to the first objective of this study, i.e., selection of the seismic excitations for the time-history analysis of typical highway bridges.

For this purpose, two existing bridges located in Montreal which are in a moderate seismic hazard zone according to NRCC (2010), were selected for the study. The main reason that bridges in Montreal were selected is because few records from real earthquakes in eastern Canada are available. In this study, the spectrum-compatible acceleration time histories of the seismic ground motions were generated by four different methods. Based on these methods, four sets of accelerograms compatible with the design spectrum for Montreal were selected for the analysis. They are, Set 1 - scaled real accelerograms, Set 2 - modified real accelerograms, Set 3 - simulated accelerograms, and Set 4 - artificial accelerograms. Among them Set 1 consists of accelerograms obtained from earthquakes around the world, and Sets 2 to 4 can all be considered as synthetic. Each set has 30 accelerograms. Nonlinear time-history analyses were conducted by subjecting the two bridge models to the three levels of the seismic

excitations represented by each set of the accelerograms. These intensity levels were selected to cover the response of the bridge from elastic to inelastic. Among a number of response parameters from the analysis, the deck displacement, expansion bearing displacement, column curvature ductility, and base shear were used to investigate the effects of the selected sets of the accelerograms on the seismic response of bridges.

It has been noticed that the minimum number of accelerograms required for the time-history analysis is different in the different code. For example, a minimum of *three* accelerograms is required for the two-dimensional analyses of buildings according to ASCE (2010) while *five* accelerograms are required by CHBDC (2010) and AASHTO (2010). On the contrary, NIST (2011) recommends using a minimum of *30* accelerograms for the time-history analysis. Given this, the second objective of this study was to examine the minimum number of records required for the time-history analysis of bridges. To achieve this objective, a number of 5, 10, and 20 accelerograms were randomly selected from the set of 30 accelerograms that was the most suitable for the dynamic analysis as recommended by the first part of the study. Two intensity measures (i.e., the partial spectral area and the spectral acceleration at the first mode period of the bridge) and three excitation levels were used in the analysis. The responses from the different number of the accelerograms were compared with those from the 30 accelerograms in order to determine the minimum number of accelerograms that can be used in the analysis.

1.2 Review of Previous Studies

In the past, different approaches have been used for the selection and scaling of spectrum-compatible accelerograms for use in the time-history analyses. In Canada, several studies have been conducted using eight accelerograms for eastern and eight accelerograms for western Canada simulated by Atkinson and Beresnev (1998) (e.g., Tremblay and Atkinson 2001; Dincer 2003; Amiri-Hormozaki 2003). Also, different scaling methods have been used (e.g., scaling to the spectral ordinate at the fundamental building period, and scaling to the spectral area) as discussed in Amiri-Hormozaki (2003). Very recently, Atkinson (2009) generated a comprehensive library of simulated accelerograms for eastern and western Canada. Because of the lack of recorded motions from Canadian earthquakes, it is expected that these accelerograms will be extensively used in the future.

While different methods for the selection and scaling of accelerograms are in use, very few investigations of the effects of different types of accelerograms on the nonlinear response have been conducted so far. Naeim and Lew (1995) reported that accelerograms scaled in the frequency domain are not appropriate for use in the seismic design since they might have unrealistic velocities, displacements, and energy content. Lew et al. (2008) suggested that to cover all the response effects, tall buildings need to be analysed using much more ground motion accelerograms than the sets of three or seven accelerograms that are normally used in the current design practice. Naumoski et al. (2006) investigated the nonlinear responses of two 6-storey and one 5-storey buildings, and reported significant differences in the responses from the accelerograms simulated by Atkinson and Beresnev (1998) and those from scaled accelerograms. Lin et al. (2012) recommended using the records from the real earthquakes for the nonlinear time-history analysis of buildings. If such records are not available, then

simulated accelerograms that are representative of the characteristics of the ground motions at the building location can be used to determine the seismic response of the building for the design purpose.

As described in the previous section, the suggestion of the number of the accelerograms used for the time-history analysis is different in different codes. To clarify this issue, Reyes and Kalkan (2012) conducted a comprehensive study on the investigation of the number of records used in the ASCE/SEI-7 ground motion scaling procedure. In their study, structural responses were estimated based on the results from time-history analyses using 30 records, less than 7 records, and between 7 and 10 records, respectively. They concluded that the use of 7 records is sufficient to determine the *design* values of the response parameters. In the study conducted by Lin et al. (2012) it was mentioned that the responses using 10 accelerograms and 20 accelerograms were very close.

It is necessary to mention that all the studies discussed above were conducted on the buildings. Given the different mechanism of buildings and bridges, and the capacity design method for bridges in which all the inelastic deformations should occur in the substructure, e.g., bearings and columns while the superstructure (i.e. deck) should remain elastic during earthquake events, the conclusions of the studies on buildings might not be valid for the bridges. Please take note that the seismic design of buildings should satisfy the requirement of strong column-weak beam according to the National Building Code of Canada (NRCC 2010) which is completely different than the requirement of the capacity design of bridges as specified in CHBDC.

1.3 Objectives and Scope of the Study

The objectives of this study are, (i) selection the most appropriate accelerograms for

use in the time-history analysis of typical highway bridges subjected to seismic loads, (ii) investigation the minimum number of accelerograms that can be used for the liner and nonlinear time-history analyses. To achieve these objectives, the following tasks were carried out in this study:

- Select two existing bridges that are representative of typical highway bridges in Montreal.
- Collect information on the two bridges, such as, geometry configuration, reinforcement used in the components of the superstructure and substructure, material properties (such as concrete strength and yield strength of the steel bar), type of bearing, update on the original design, etc.
- Develop nonlinear models of the two bridges for use in the time-history analysis.
- Review seismic hazard for the Montreal region, and conduct seismic hazard deaggregation analysis for Montreal.
- Select four sets of accelerograms as seismic excitation.
- Conduct the nonlinear time-history analysis by subjecting the bridge models to the seismic excitations scaled to three intensity levels.
- Evaluate the seismic response of the bridges at the three intensity levels, and identify the most appropriate accelerograms for the time-history analysis among the four sets of accelerograms under investigation.
- Select 5, 10, and 20 accelerograms from the set of the accelerograms identified above, run time-history analyses using two intensity measures represented by the partial area

under the spectrum (designated as Sa_{Area}) and the spectral acceleration at the first mode period of the bridge (i.e., $Sa(T_1)$), respectively.

- Investigate the effects of different number of accelerograms on the seismic response of bridges, and report the minimum number of accelerograms that can be used in the time-history analysis.

1.4 Outline of the Thesis

The methods, analyses, and results from the study are described in 6 Chapters. Chapters 2 and 3 provide the background material (e.g., the design information on the bridges and selection of earthquake records) that is used in the study. The results from the analyses are presented in Chapters 4 and 5, and the conclusions from this research work are given in Chapter 6.

Chapter 2 describes the two bridges that are used in the analysis. These two bridges are located in Montreal, and are considered to be representative of the typical highway bridges in Quebec. The development of the nonlinear models of the bridges for use in the time-history analyses is described in detail in this chapter. The seismic performance of the bridges is also discussed.

Chapter 3 explains the selection of the earthquake records for use in the nonlinear time-history analysis. The seismic hazard for Montreal is reviewed first in this chapter. Scenario earthquakes for the bridge location for different probability of exceedance are discussed in detail. This chapter is focused on the description of the four methods that are used to generate the accelerograms for use in the analysis.

Chapter 4 provides the analysis results for the two bridges using the 4 sets of accelerograms discussed in Chapter 3. Based on the findings of the results, the most appropriate accelerograms that can be used for the time-history analysis are recommended. The behavior of the two bridges subjected to different levels of the seismic excitations is also compared.

Chapter 5 presents the results of the use of the different number of accelerogrms in the time-history analysis. Two intensity measures are used to scale the accelerograms, i.e., one is the partial area under the spectrum of an accelerogram, the other is the spectral acceleration at the fundamental period of the bridge. In the end of the chapter, recommendations are made on the minimum number of accelerograms that can be used for the linear and nonlinear time-history analyses, respectively.

Chapter 6 summarizes the key findings and conclusions from this study. Recommendations for future research are also provided.

Chapter 2

Description and Modeling of Bridges

2.1 Introduction

It is known that bridges can be categorized into different groups according to

- Span continuity, i.e., simply-supported or continuous,
- Number of spans, such as, single-span or multi-span,
- Material of construction, e.g., concrete, steel or composite material,
- Pier type, such as, wall-type pier or column bent,
- Abutment type, i.e., U-type abutment, seat-type abutment, etc.,
- Bearing type, e.g., steel bearing, elastomer bearing, etc.

Given the variety of bridges in Canada and for the purpose of this study, it is important to select bridges that are representative of typical highway bridges for the analysis. As reported by Tavares et al. (2012), there are about 2672 multi-span bridges in Quebec in which 25% of them are multi-span simply supported (MSSS) concrete girder-type bridges, 21% are multi-span continuous (MSC) concrete girder-type bridges, 11% are multi-span continuous (MSC) slab bridges, 7% are multi-span continuous (MSC) steel girder-type bridges, and 8% are multi-span simply supported (MSSS) steel girder-type bridges. The typical cross section of the

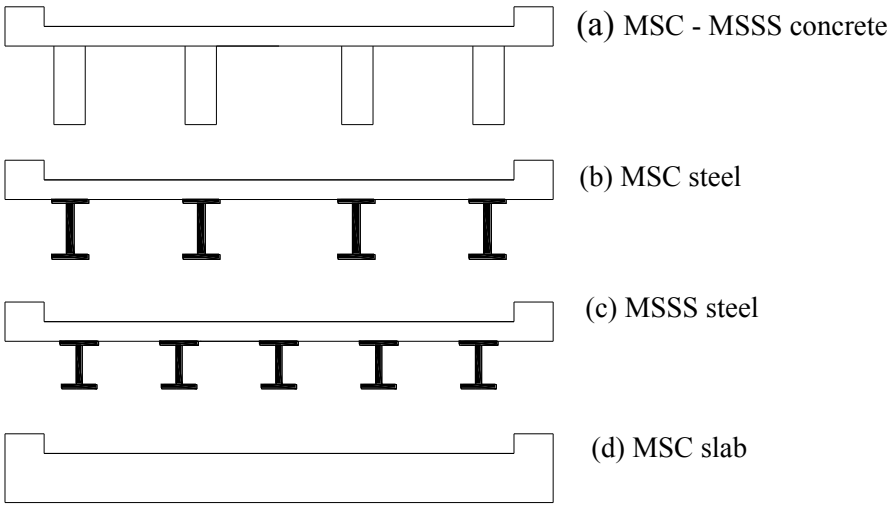

Figure 2.1 Typical bridge classes in Quebec (Adopted from Tavares et al. 2012).

superstructure of each type of bridges mentioned above is shown in Fig. 2.1. It is necessary to mention that seismic analysis is not required for one-span simply supported bridges according to CHBDC (2010) due to the fact that the seismic forces are resisted by abutments which have quite large lateral stiffness. Consequently, the superstructure of these bridges is not vulnerable to the seismic loads. Tavares et al. (2012) also found that most of the bridges in Quebec have three spans with seat-type abutments sitting on shallow foundations. In terms of the column bents, they reported that wall-type columns, circular columns, and rectangular columns are commonly used. Given these, two bridges located in Montreal were selected for this study. The first bridge is a three-span continuous concrete slab bridge, and the second one is a three-span continuous concrete girder-type bridge. For ease of discussion, these two bridges are referred to as Bridge #1 and Bridge #2 in the study, respectively. Figures 2.2 and 2.3 show the geometric configurations of two bridges. Detailed characteristics of the selected bridges are described hereafter.

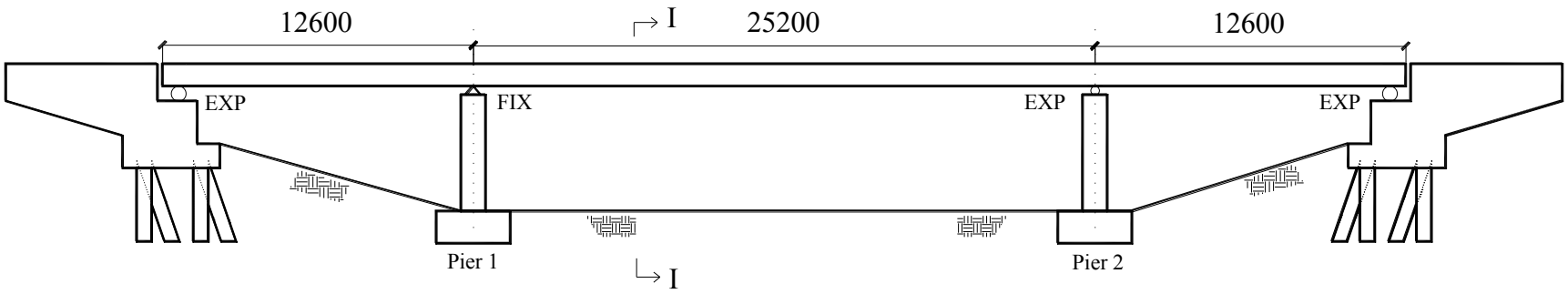

Elevation

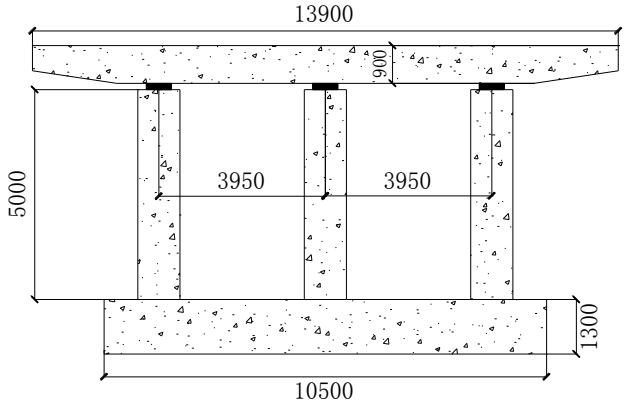

I-I section

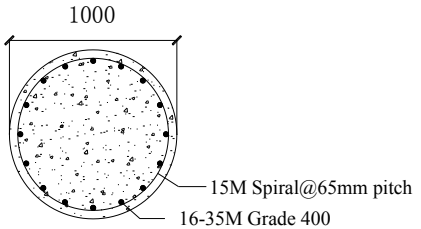

Column Section

Figure 2.2 Geometric configuration of Bridge #1.

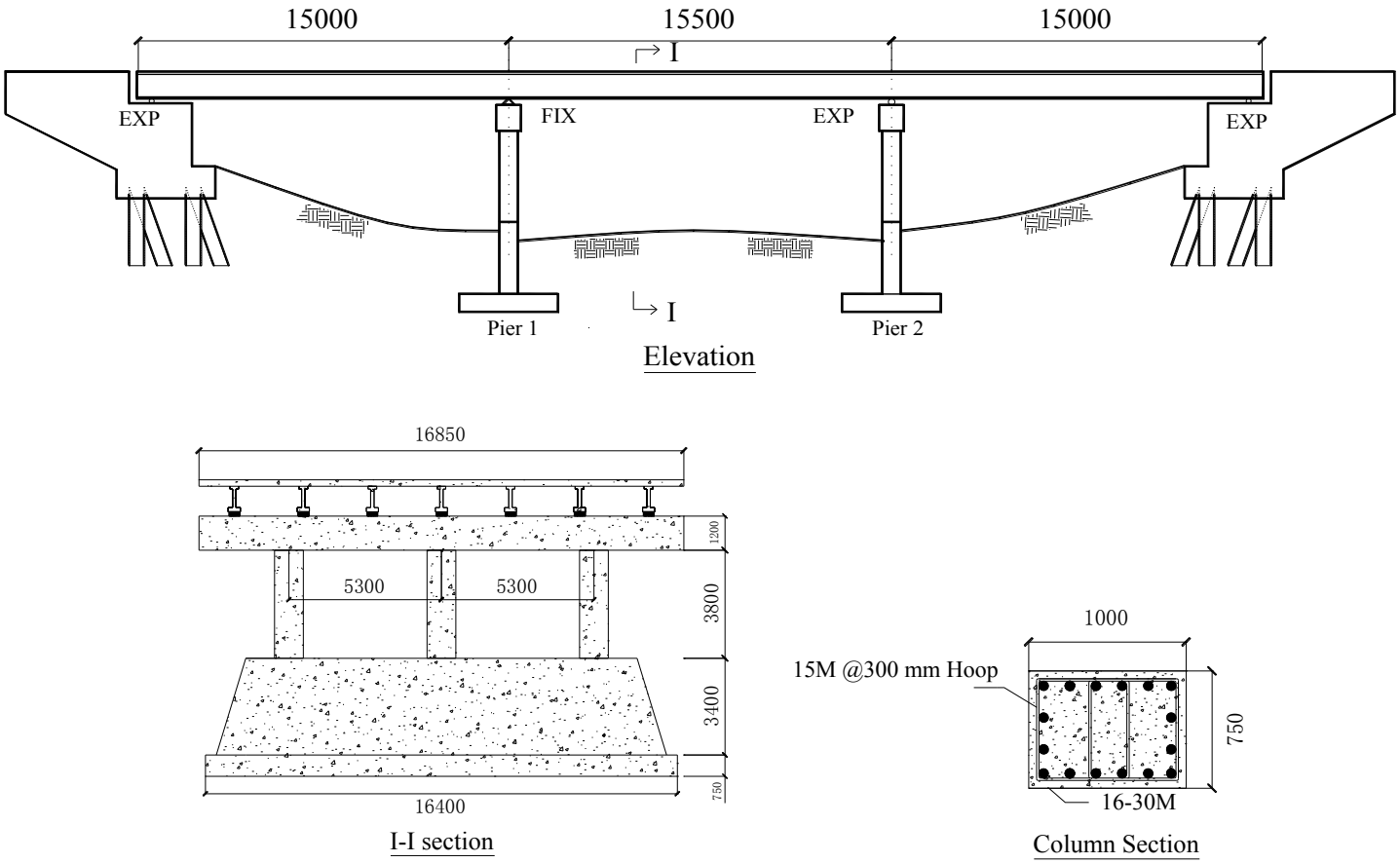

12

Figure 2.3 Geometric configuration of Bridge #2.

2.2 Description of Bridges

2.2.1 Bridge #1

Bridge #1 was built in the mid-1980s. It has three spans which are 12.6 m, 25.2 m, and 12.6 m, respectively for a total length of 50.4 m, as shown in Fig. 2.2. The bridge has no skewness (i.e., it is a straight bridge). The overall width of the bridge is 13.6 m. The superstructure consists of a continuous, voided prestressed concrete slab. The thickness of the slab is 90 cm. The prestressing force is provided by 14 parabolic cables in the longitudinal direction of the bridge, each cable consists of 19-0.5 inch diameter strands and 16-0.6 inch diameter strands. The slab is also prestressed in the transverse direction using 9 cables at the end span, and 20 cables at the middle span, in which each cable is composed of 4-0.5 inch diameter strands and 16-0.6 inch diameter strands. The jacking force of each cable at the final stage is 1100 kN.

The column bent has three circular columns. The diameter of each column is 1 m, and the average height of the column is 5 m. The distance between center to center of columns is 4.25 m. As illustrated in Fig. 2.2, the longitudinal reinforcement of the column consists of 16−35M (d_b = 35.7 mm) bars which provide a reinforcement ratio of 2.95%. The transverse reinforcement consists of a No. 15 (d_b = 16 mm) spiral with a pitch of 65 mm. The confinement steel ratio is 1.33%.

Seat-type abutments are used at the ends of the bridge. The width of the abutment back wall is 9.9 m and the height is 1.5 m. The length of the wing wall is 5.9 m. The foundations of both the column bents and abutments are strip footings on rock.

The compressive strength of the concrete used for the slab is 35 MPa, while for the

columns and foundations is 30 MPa. No information could be obtained from the original bridge drawings on the stress of the reinforcing steel used in the structure. Therefore, the yield strength of the reinforcement is assumed to be 400 MPa.

As shown in Fig. 2.2, expansion bearings, which allow both translation and rotation, are used on the abutments and Pier 2. Fixed bearings, which allow translation only (i.e., not rotation), are used on the Pier 1. Due to the lack of information on the type of bearings used in the bridge, elastomeric bearings are considered given their good performance against the seismic loads (Pan et al. 2010; Fu 2013), and they were designed according to CHDBC (2010). The requirements specified in AASHTO (2012) are also used to finalize the bearing design. More specifically, the bearings designed satisfy the following requirements:

- Maximum instantaneous compressive deflection,
- Bearing maximum rotation,
- Bearing combined compression and rotation including uplift requirement and shear deformation requirement,
- Bearing stability.

Rectangular elastomeric bearings with 600 mm x 600 mm x 130 mm are chosen to place on the top of each column at the abutments and piers. The bearing consists of 5 layers of the steel plate with the thickness of 2 mm each layer. The total thickness of the elastomer is 40 mm. It is necessary to mention that both fixed bearings and expansion bearings have the same size. As illustrated in Figs. 2.2 and 2.3, the fixed bearing and expansion bearing are drawn as triangle and circular shapes, respectively.

2.2.2 Bridge #2

Bridge #2 was also built in the 1980s and consists of three continuous spans without skew. As shown in Fig. 2.3, the two end spans of the bridge are 15 m, and the middle span is 15.5 m. The overall deck width is 16.85 m. The superstructure consists of a 0.225 m reinforced concrete slab and seven 0.9 m C.P.C.I (Canadian Precast Prestressed Concrete) prestressed girders at a spacing of 2.4 m. The concrete deck is reinforced with 15M bars on the top and the bottom. Each C.P.C.I girder consists of 6 straight tendons and 8 parabolic tendons on the bottom across each span. Each prestressing tendon is composed of 7 Grade-1860 wire strands. The jacking force per strand at the final stage is 145 kN.

The cross section of the cap beam is 1 m wide, 1.2 m deep. The multi-column bents consist of three rectangular columns. The center-to-center spacing between columns is 5.3 m. The dimensions of each column are 1 m (in the transverse direction) x 0.75 m (in the longitudinal direction). The average height of the column is 3.8 m. Each column is reinforced with 16-30M bars providing longitudinal reinforcement ratio of 1.49%. Ties with 15M at a spacing of 300 mm were used as transverse reinforcement. The transverse reinforcement ratio is about 0.24%. Strip footing is used for the column bents.

Seat-type abutments are on pile foundation as shown in Fig. 2.3. The width of the abutment back wall is 16.85 m, which is as wide as the superstructure. The height of the back wall is 1.5 m, and the length of the wing wall is 5 m.

For the deck and columns, the compressive strength of concrete is 30 MPa. For the girders, it is 35 MPa whereas it is 20 MPa for the cap beam. Like Bridge #1, the yield strength of the steel is assumed to be 400 MPa.

Rectangular elastomeric bearing (450 mm x 350 mm x 100 mm) is used on the bottom

of each girder at the abutments and piers. Each bearing consists of 4 layers of the steel plate and 6 layers of elastomer. The thickness of the steel plate is 2 mm, and the total thickness of the elastomer is 80 mm. Fixed bearings are used on the Pier 1, and expansion bearings are used on the abutments and Pier 2 (Fig. 2.3). The fixed bearings and the expansion bearings also have the same size like Bridge #1.

2.3 Modeling of Bridges

For the purpose of analyses, three-dimensional finite-element models were developed for the two bridges using the structural analysis software SAP2000 (CSI 2012). This program has been used in a number of studies on the investigation of the nonlinear behavior of bridges subjected to seismic loads (Shafiei-Tehrany 2008; Pan et al. 2010; Waller 2010; etc.). The advantage of SAP2000 is a number of elements (e.g., link element) are available which can be used to model the nonlinearity of different components of a bridge system including bearings and plastic hinges during seismic excitations. It is necessary to mention that another program OpenSees (McKenna and Feneves 2005) can also be used for the nonlinear analysis of bridges. However, a study conducted by Aviram et al. (2008a) showed that these two programs provide very similar results. SAP2000 was selected for this study due to its simplicity in modeling and less time-consuming in the analysis compared with OpenSees.

2.3.1 Superstructure

A spine model shown in Fig. 2.4 was used to model the superstructure of each bridge considered in this study. According to the capacity design method specified in AASHTO (2012) and CHBDC (2010), the superstructure of the bridge system should remain elastic during earthquake events. Therefore, the superstructure was modeled using elastic beam elements

located along the centroid of the superstructure. Each span of the bridge is discretized into 10 equal segments in order to achieve higher accuracy of the results. It is necessary to mention that a minimum number of four elements per span is required for modeling the superstructure according to ATC 32 (1996). The properties (such as, the cross-sectional area, moment inertia, shear area, torsional constant, etc.) of the cross section of the superstructure were determined using Section Designer incorporated in SAP2000. For illustration, Figures 2.5a and 2.5b show the typical geometric properties of Bridge #1 and Bridge #2 considered in this study, respectively. It is known that both the flexural moment of inertia and the torsional moment of inertia have significant effects on the bridge response. In this study, a factor of 0.75 was used to reduce the moment of inertia of the deck section, and no reduction factor was applied to the girder sections as recommended by Caltrans Seismic Design Criteria (SDC) (2013). Reduction of the torsional moment of inertia was not considered given the regularity of the bridge according to Caltrans SDC (2013).

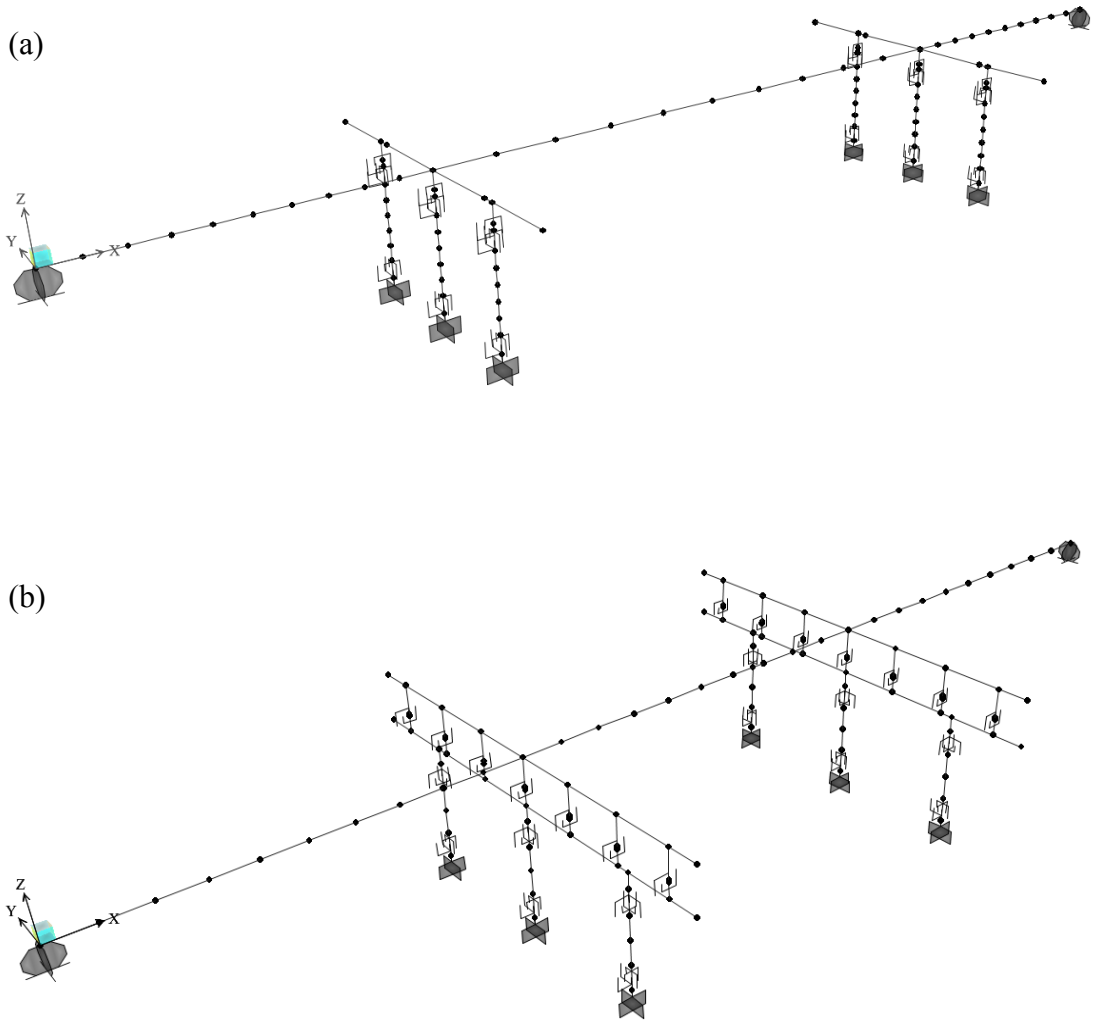

Figure 2.4 Scheme of the spine models in SAP2000, (a) Bridge #1; (b) Bridge #2.

(a)

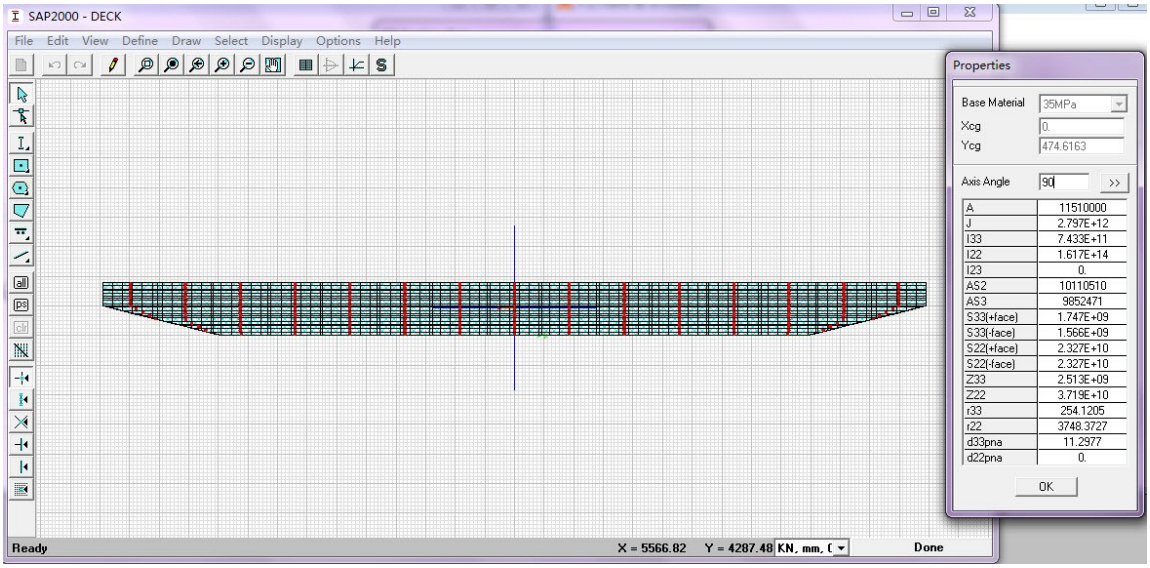

(b)

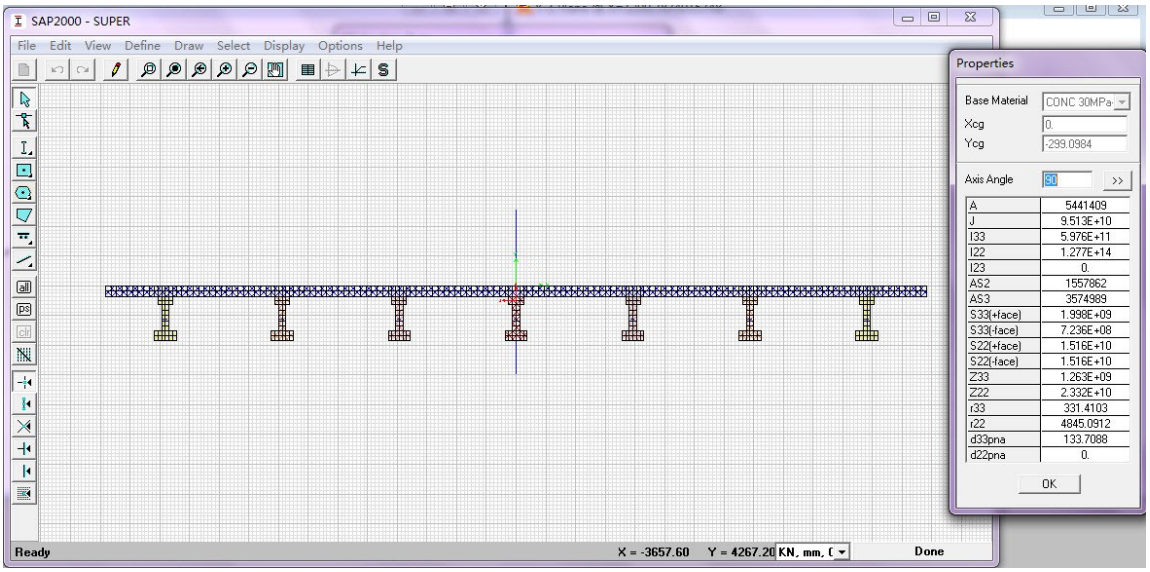

Figure 2.5 Determination of the geometric properties of the superstructure of bridge models using Section Designer in SAP2000 (a) Bridge #1; (b) Bridge #2.

The total mass of the bridge was lumped to the nodes of the superstructure. It is necessary to mention that the weight of the cap beams (for Bridge # 2) and the half weight of the column bents were lumped to the nodes of the superstructure (i.e., nodes in the longitudinal direction X-X, Fig. 2.4) at the Piers 1 and 2. Note that the translational mass lumped to each node can be calculated by the program itself, and it is assigned to each of the three global axes (X, Y, and Z as shown in Fig. 2.4). However, the rotational mass (i.e., the rotational mass moment of inertia) cannot be calculated by the program itself, i.e., it must be calculated manually. The rotational mass moment of inertia of the superstructure can be determined using Equation 2.1,

$$M_{xx} = (Md_w^2)/12 \tag{2.1}$$

Where

M_{xx} = mass of moment inertia of superstructure in the global X-X direction,

M = total tributary mass of the superstructure segment,

d_w = width of the superstructure.

2.3.2 Bearing

As given in the Section "Description of Bridges", two types of elastomeric bearings are used in the bridges, they are fixed bearings and expansion bearings. Fixed bearings only allow the rotation of the superstructure relative to the substructure, while expansion bearings allow both rotation and translation movements. In this study, the behavior of the bearing is represented by the Link Element in SAP2000. The initial lateral (K_H), vertical (Kv), and rotational (K_θ) stiffnesses of the elastomeric pads are determined using Equations 2.2, 2.3, and 2.4, respectively.

$$K_H = GA / H_r \tag{2.2}$$

$$K_V = EA / H \tag{2.3}$$

$$K_\theta = EI / H_r \tag{2.4}$$

Where

G = shear modulus, and it is taken as 0.80 MPa in this study following the recommendation of Caltrans SDC (2013),

E = modulus of elasticity of the rubber,

I = moment of inertia of the bearing,

A = plan area of the elastomeric pad,

H = thickness of the bearing,

H_r = total thickness of the rubber.

The nonlinear behavior of the elastomeric bearing in the longitudinal direction is modeled using bilinear hysteretic rule as shown in Fig. 2.6 following the recommendations made by Kelly (1997) and DesRoches et al. (2003). In Figure 2.6, K_1 and K_2 represent the initial lateral stiffness (i.e., elastic stiffness) and the plastic stiffness, respectively. Based on the experimental results given by DesRoches et al. (2003), the plastic stiffness K_2 is approximately one-third of the elastic stiffness K_1. In addition, the study conducted by Gao (2013) showed that the plastic stiffness K_2 did not have significant effect on the seismic response of bridges. Given this, the plastic stiffness K_2 is taken as 1/3 K_1 in this study. The notations D_y and D_u in Fig. 2.6 represent the yield displacement and the maximum displacement of the bearing, respectively. The values for the parameters used to model the bilinear behavior of the expansion bearings in Bridge #1 and Bridge # 2 are listed in Table 2.1. It is necessary to mention that the maximum displacement of the bearing (D_u) is assumed to be equal to the height

of the elastomer while the yield displacement of the bearing (D_y) is assumed to be 10% of its maximum displacement D_u following the recommendation by DesRoches et al. (2003). The stiffness of the bearing in transverse direction is assumed to be infinite, i.e., the stiffness is about 100 times larger than that in the longitudinal direction.

Table 2.1 Parameters used in the modeling the bilinear behavior of the expansion bearings.

Bridge No.	Bearing Size	D_y (mm)	F_y (kN)	D_u (mm)	F_u (kN)
#1	600 x 600 x 130 mm	5.0	15	50	60
#2	450 x 350 x 100 mm	7.5	12	75	47

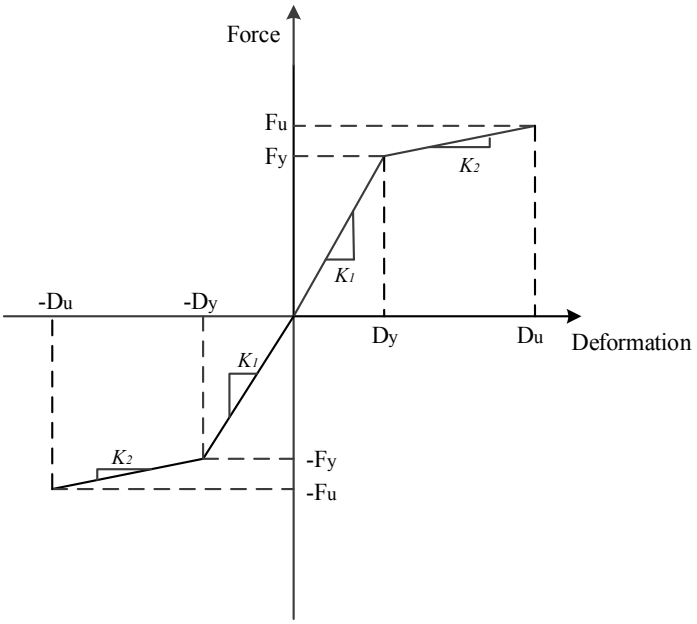

Figure 2.6 Bilinear behavior of elastomeric bearings in the longitudinal direction.

2.3.3 Columns and Cap Beams

It is expected that plastic hinges would form on the bottom and/or top of a column during larger earthquake events (Paulay and Priestley 1992). In this study, plastic hinges were assumed on both the bottom and top of the column in accordance with the seismic provisions of the New Zealand Code (TNZ 2003). It should be noted that the current edition of the

CHBDC (2010) does not specify the location of the plastic hinge. The plastic hinge zones are modeled with nonlinear elements while the rest part of the column is modeled by elastic elements. The detail description on the modeling of the columns and cap beams is given hereafter.

2.3.3.1 Modeling the plastic hinge zones

Plastic hinge length

According to CHBDC (2010), the plastic hinge length L_p shall be taken as the maximum dimension of the column. Therefore, the plastic hinge lengths of the columns of the Bridge #1 and Bridge #2 would be 1 m and 0.75 m (see Figs. 2.2 and 2.3.), respectively. In this study, the plastic hinge length of the column was also determined using the formula provided by Caltrans SDC (2013) as expressed in Equation 2.5,

$$L_p = 0.08L + 0.022 f_{ye} d_{bl} \geq 0.044 f_{ye} d_{bl} \tag{2.5}$$

Where

L = height of column, in mm

f_{ye} = expected yield strength of the steel bar, in MPa

d_{bl} = diameter of a longitudinal rebar, in mm

Using Equation 2.5, it was found that the plastic hinge length of the column of Bridge #1 was 720 mm while it was 610 mm for Bridge #2. Based on the calculation following the specifications of CHBDC and Caltrans, plastic hinge length of the column of 1.0 m was used in the model of Bridge #1, and 0.75 m was used in the model of Bridge #2.

Moment-curvature relationship for column section

For the purpose of defining the Link Element which is used to simulate the behavior of the column in the plastic hinge region during larger earthquakes, moment-curvature relationships for the end sections of the column were determined using fiber analyses of the cross sections. The concrete stress-strain relationship included the effect of confinement was determined based on the model proposed by Mander et al. (1988) as illustrated in Fig. 2.7. This model is also recommended by ATC 32 (1996), Caltrans SDC (2013) and FHWA (2012). As shown in Fig. 2.7, the major parameters that are used to define the confined concrete stress-strain relationship are, the compressive strength of confined concrete (f_c'), the compressive stress of confined concrete (ε_{cc}), and the ultimate compressive strain (ε_{cu}). The formulas for determining these parameters can be found in Paulay and Priestley (1992).

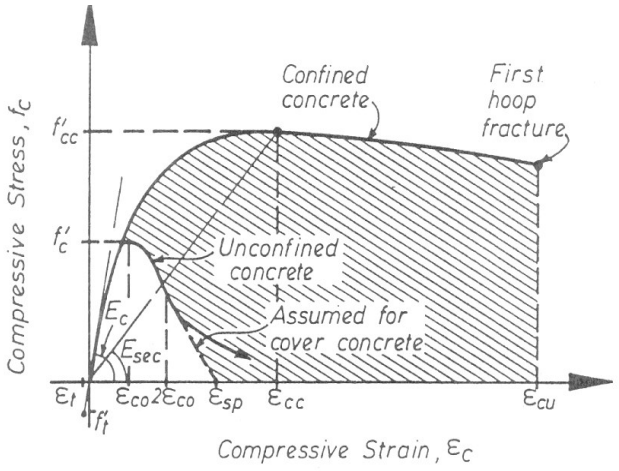

Figure 2.7. Mander Model for confined and unconfined concrete (Adopted from Paulay and Priestley 1992).

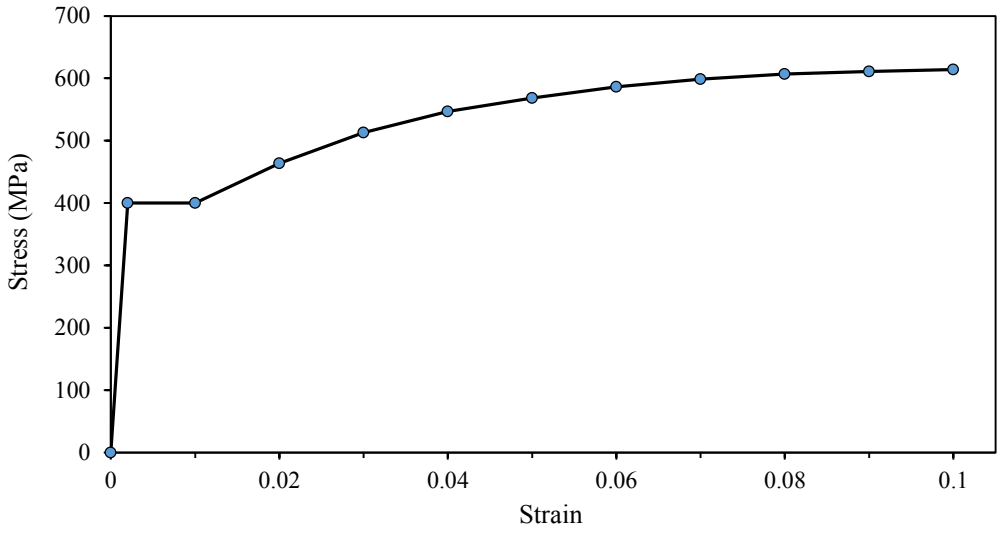

Figure 2.8 Stress-strain relationship for the steel (Adopted from Naumoski and Heidebrecht 1993).

Figure 2.8 shows a typical stress-strain relationship for steel bars reported in Naumoski and Heidebrecht (1993). As shown in the figure, behavior of the steel bar is characterized by an initial elastic portion of the stress-strain relationship with a modulus of elasticity of 200 GPa up to the yield stress f_y of 400 MPa followed by a yield plateau and a strain hardening.

Nominal values for the material strengths (i.e., concrete and reinforcement resistance factors $\Phi c = \Phi s = 1$) were used in the fiber analysis. The axial force used in the fiber analysis included the force resulting from the dead load only. For illustration, Figures 2.9a and 2.9b show the moment-curvature relationships for modeling the plastic hinges of the columns of the Bridge #1 and Bridge #2, respectively. The computed moment-curvature relationship was idealized by two linear segments representing the pre- and post-yielding ranges. Based on the shape of the moment-curvature relationship, a bilinear hysteretic model (i.e., Multi-linear Kinematic Plasticity model) was selected from a number of models available in SAP2000, as shown in Fig. 2.10.

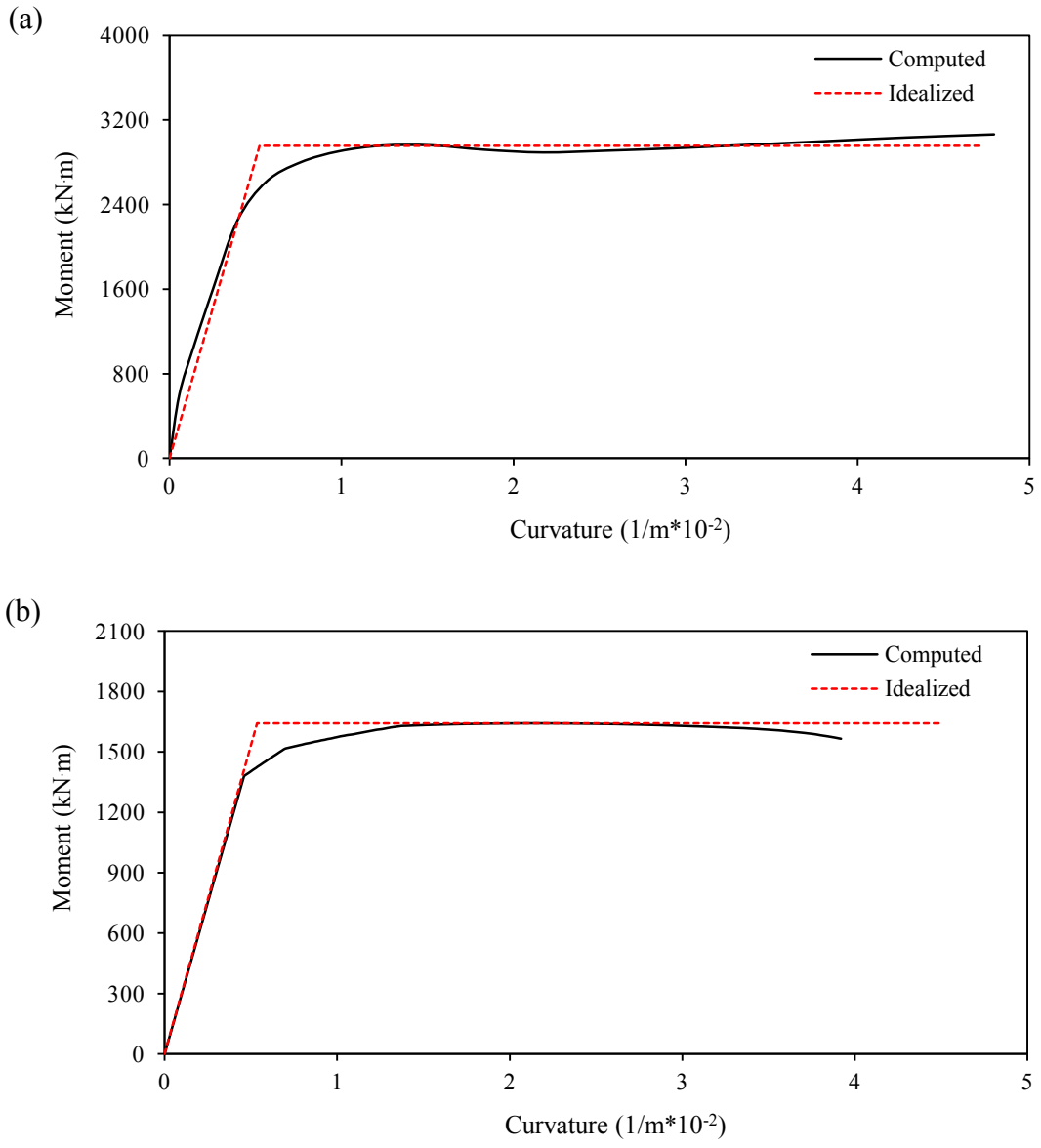

Figure 2.9 Moment-curvature curves of the column section, (a) Bridge #1; (b) Bridge #2.

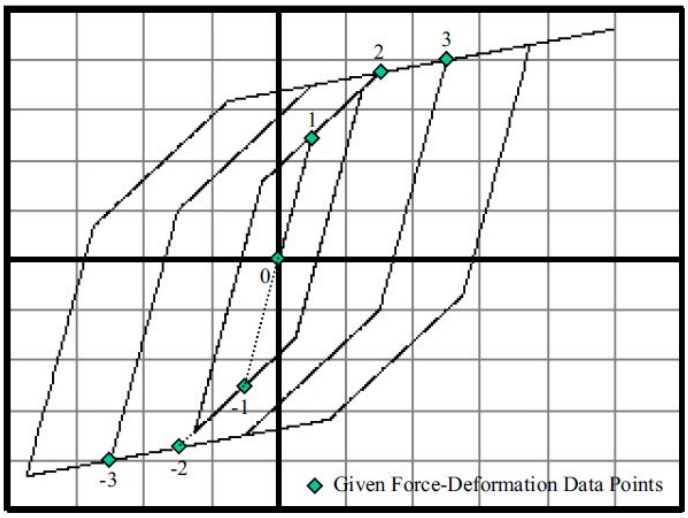

Figure 2.10 Multi-linear Kinematic Plasticity model (Adapted from CSI 2012).

2.3.3.2 Modeling columns and cap beams

The columns are assumed to behave elastically outside the plastic hinge regions. In total, each column was divided into 5 equal length segments. Cap beams (for Bridge #2) were modeled as elastic beam elements, and the connections between cap beams and bearings; cap beams and columns were modeled using rigid elements as shown in Fig. 2.11.

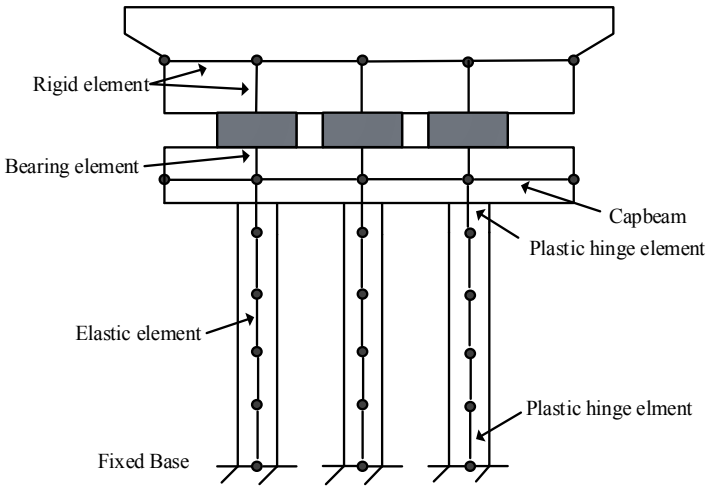

Figure 2.11 Detailed modeling of a column bent.

2.3.3.3 Material properties

In order to take into account the effect of the combined flexure and axial force, the effective shear area of the ductile concrete column was estimated by using a reduction factor of 0.8 to its gross shear area (i.e., $A_{v,\,eff} = 0.8\ A_{v,g}$) in accordance with Caltrans SDC (2013). In addition, the effective moment of inertia (I_{eff}) of column was calculated using Equation 2.6 to account for the effect of concrete cracking. The yield moment (M_y) can be determined based on the idealized moment-curvature curve as presented in Fig. 2.9. It was found that the effective moment inertias of the columns of the Bridge #1 and Bridge #2 are about $0.70I_g$ and $0.75I_g$, respectively. Moreover, Caltrans SDC (2013) recommends a factor of 0.2 shall be applied to the torsional stiffness of column members with respect to its gross area.

$$I_{eff} = \frac{M_y}{E_c \varphi_y} \tag{2.6}$$

Where

M_y = moment corresponds to the first steel bar yields,

φ_y = curvature corresponds to the first steel yields,

E_c = modulus of elasticity of concrete, it is calculated by $4500\sqrt{f_c'}$.

2.3.4 Abutment

Abutment modeling has a significant impact on the nonlinear response of bridges during earthquake events (Wilson and Tan 1990). Recently Aviram et al. (2008a) conduced a comprehension investigation of the effect of the abutment modeling on the seismic response of bridges. Three approaches for the modeling of the abutment were considered in their study, and they were designated as roller abutment model, simplified abutment model, and spring abutment model (Fig. 2.12). For the purpose of this study, a brief description of these models

is given hereafter, the detailed explanations for each of the modeling techniques can be found in Aviram et al. (2008a and 2008b).

As seen in Fig. 2.12a, the roller abutment model consists of a boundary condition that applies only constrains against the vertical displacement, i.e., the abutment is free for the translation in the longitudinal direction and rotation. Therefore, the response of this bridge model is dominated by the formation of the plastic hinges and the capacity of the columns. It is the simplest model among the three abutment models proposed by Aviram et al. (2008a).

Figure 2.12b illustrates a general scheme of the simplified abutment model. The model consists of a rigid element with its length equal to the width of the superstructure and a series of springs in the longitudinal, transverse, and vertical directions. The rigid element is connected to the centerline of the superstructure through a rigid joint. In the longitudinal direction, the simplified abutment model consists of three elements, i.e., a rigid element in which both shear and moment are released at the end, a gap element which is used to represent the gap between the superstructure and the abutment in the longitudinal direction, and a zero-length element used to represent the response of the embankment fill. The nonlinear behavior of the embankment fill is modeled using an elastic-perfectly-plastic curve, which can be defined according to Caltrans SDC (2013). In the transverse direction, a zero-length element is defined at each end of the rigid element (see Fig. 2.12b), and it is used to present the response of the backfill and wing wall. Generally speaking, the nonlinear response curve of the zero-length element is similar to that defined in the longitudinal direction, however, the stiffness of abutment is modified due to the different behavior of the abutment in the longitudinal and transverse directions. In the vertical direction, elastic spring is defined at each end of the rigid element. The stiffness of the spring is equal to the stiffness of the total bearing pads.

(a)

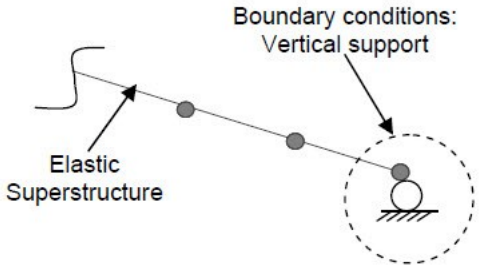

(b)

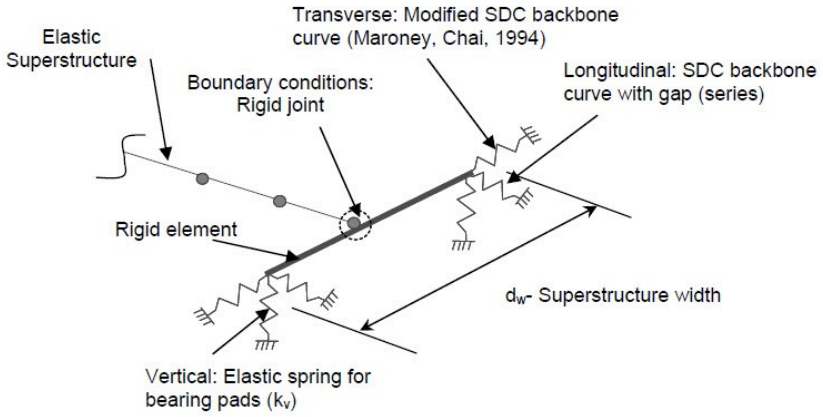

(c)

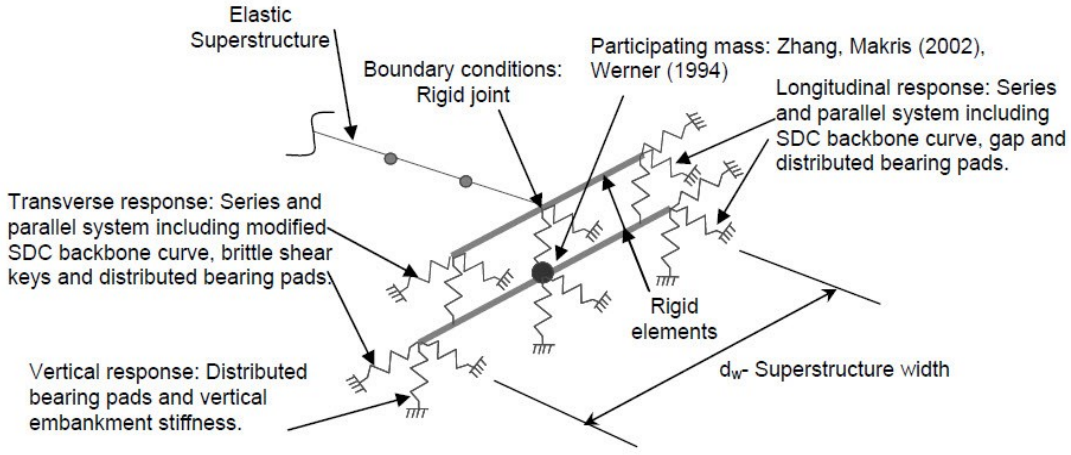

Figure 2.12 Abutment models, (a) Roller model; (2) Simplified model; (3) Spring model (Adopted from Aviram et al. 2008a)

The spring abutment model is an improved model based on the simplified abutment model, and a general scheme of the model is presented in Fig. 2.12c. The spring model considers the nonlinear response of the abutment in the longitudinal, transverse, and vertical directions while the simplified abutment model considers the nonlinear response of the abutment in the longitudinal and transverse directions (i.e., the simplified model assumes the response of the abutment in the vertical direction is linear). As shown in Fig. 2.12c, the responses of both bearing pads and embankments are considered in the modeling.

Aviram et al. (2008a) used six different types of bridges for the investigation. Nonlinear time-history analyses were conducted on each bridge by using the three abutment models described above. They concluded that the roller model provided relatively conservative results while simplified model and the spring model provided very similar longitudinal displacement. The dominat periods of the bridge obtained from these three abutment models are relatively close except that the first mode period of the bridge from the spring model is significantly smaller than that from the roller model and the simplified model. Given these and the objective of this study (i.e., selection appropriate records for use for the nonlinear time-history analysis of bridges), the roller abutment model was selected due to its lowest model complexity.

2.4 Dynamic Characteristics of the Bridge Models

In this study, modal analysis was conducted first on the bridge models in order to understand the dynamic characteristics of the two bridges. In total, 50 modes were considered in the modal analysis. Rayleigh damping of 5% of critical was assigned to all 50 modes of the bridges models. The damping was specified to be proportional to the initial stiffness of the models.

Table 2.2 shows the natural periods of the first three vibration modes of the Bridge #1

model and Bridge #2 model, respectively. The mass participation factor and the modal participation factor resulting from the modal analysis are also included in the table. It can be seen in the table that the first mode period of the Bridge # 1 is about 0.81 s and that of the Bridge #2 is about 0.71 s, which are very close. This is because the substructure system of the two bridges is very similar, i.e., both have two column bents in the longitudinal direction, and each column bent has three columns in the transverse direction. The results in Table 2.2 indicate that the response of the two bridges is dominated by the first mode. Moreover, it can be seen in Table 2.2 that the mass participation factor of both bridge models (98% for Bridge #1 and 91% for Bridge #2) is larger than 90% which satisfies the requirement for the dynamic analysis (CHBDC 2010).

Table 2.2 Dynamic characteristics of the bridge models from modal analysis.

	Bridge #1					Bridge #2				
Mode	Period (sec)	MPR UX	MPR UY	MPF UX	MPF UY	Period (sec)	MPR UX	MPR UY	MPF UX	MPF UY
1	0.81	0.98	0	1.19	0	0.71	0.91	0	8.69	0
2	0.52	0	0	0	0	0.34	0	0	0	0.03
3	0.45	0	0.99	0	1.19	0.22	0	0.96	0	8.94

Note: MPR-Mass participation ratio; MPF-Modal participation factor.

Figure 2.13 illustrates the mode shapes of the first three modes of the Bridge #1 and Bridge #2. It can be seen clearly in Fig. 2.13 that the first mode shape is dominated by the vibration in the longitudinal direction for both bridges. In terms of the second mode shape, the vibration of the model of the Bridge #1 is in the transverse direction with the period of 0.52 s. It is interesting to notice that the second mode shape for the Bridge #2 corresponds to the torsion in which the vibration period is about 0.34 s. The third mode shape of the Bridge #1 corresponds to torsion with the period of about 0.45 s while that for Bridge #2 corresponds to the vibration in the transverse direction, and the period is about 0.22 s.

(a)

Mode 1:
Longitudinal T_1=0.81 s

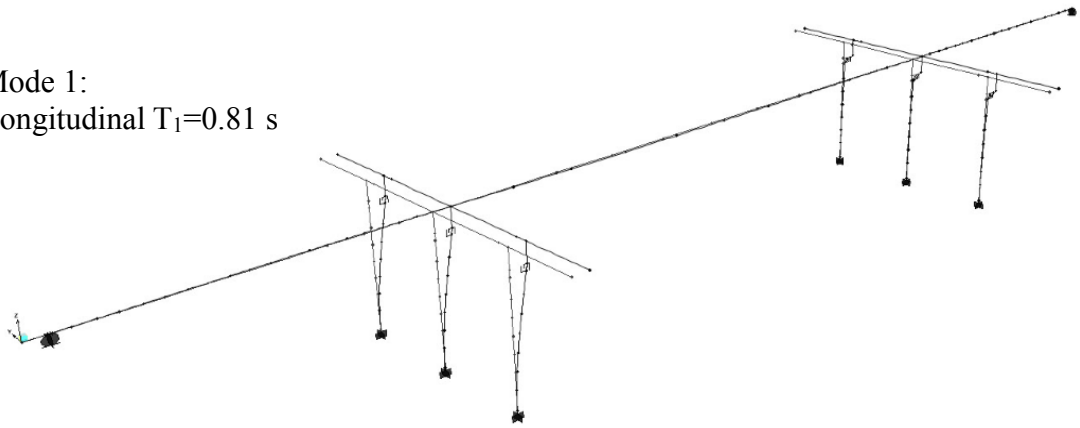

Mode 2:
Transverse T_3=0.52 s

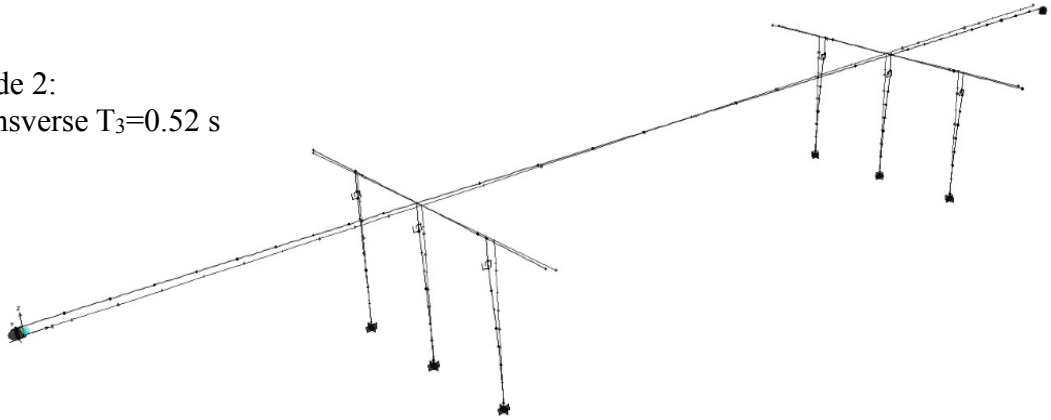

Mode 3:
Torsional T_2=0.45 s

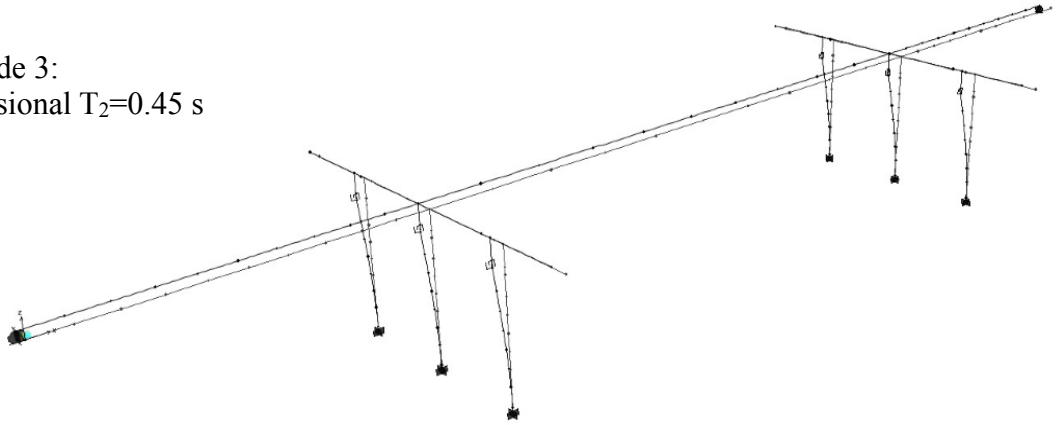

(b)

Mode 1:
Longitudinal T_1=0.71 s

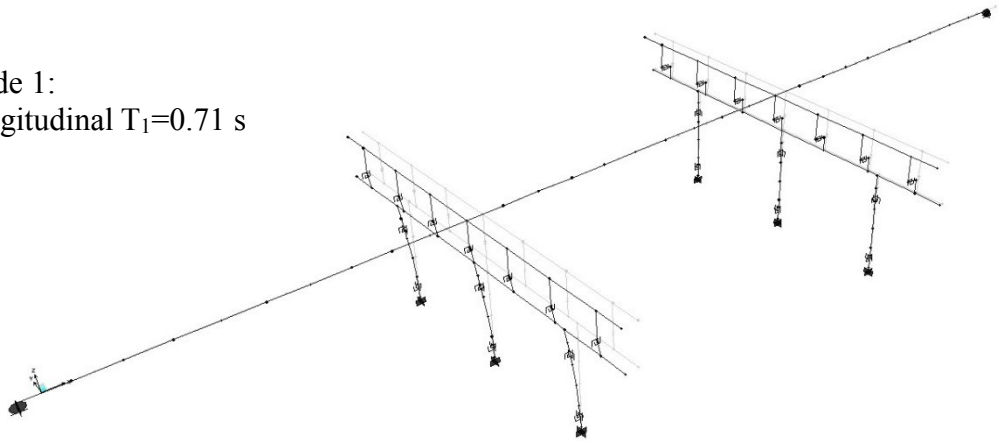

Model 2:
Torsional T_2=0.34 s

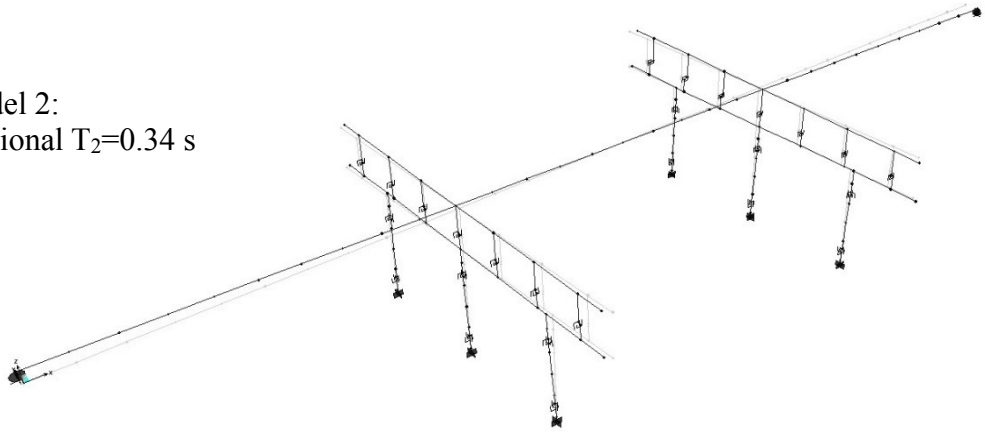

Mode 3:
Transverse T_3=0.22 s

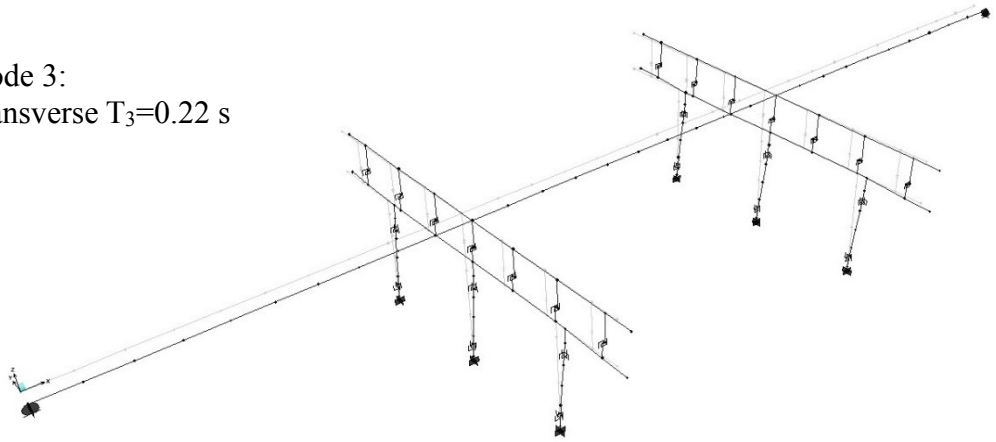

Figure 2.13 Mode shapes of the first three modes from the modal analysis, (a) Bridge #1; (b) Bridge #2.

2.5 Seismic Analysis

The seismic response of the bridge models is illustrated by using one of the ground motion records selected for this study. The record was obtained from M_w 6.6 San Fernando earthquake occurred on 9 February, 1971, the epicenter distance of the earthquake was about 31 km (see Table 3.2, Chapter 3). Figure 2.14 shows the acceleration time history of the record, and Fig. 2.15 shows the 5% damped acceleration response spectrum of that record. The ratio of the peak acceleration (in g) to the peak velocity (in m/s) of the record is about 0.88, which is considered to be representative of the characteristics of the ground motions in eastern Canada according to Naumoski et al. (1993). The detailed discussion on the selection of earthquake records for use in this study is given in Chapter 3.

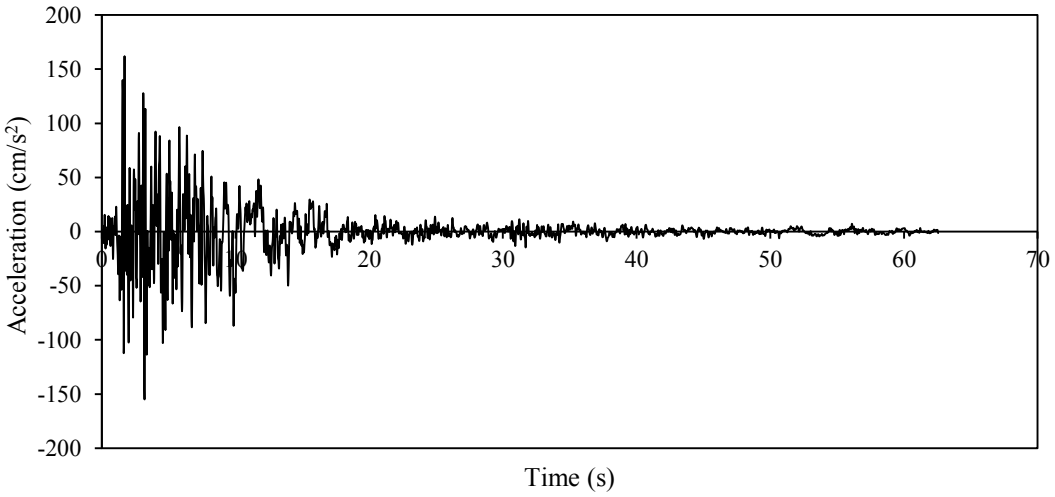

Figure 2.14 Acceleration time-history of one sample record.

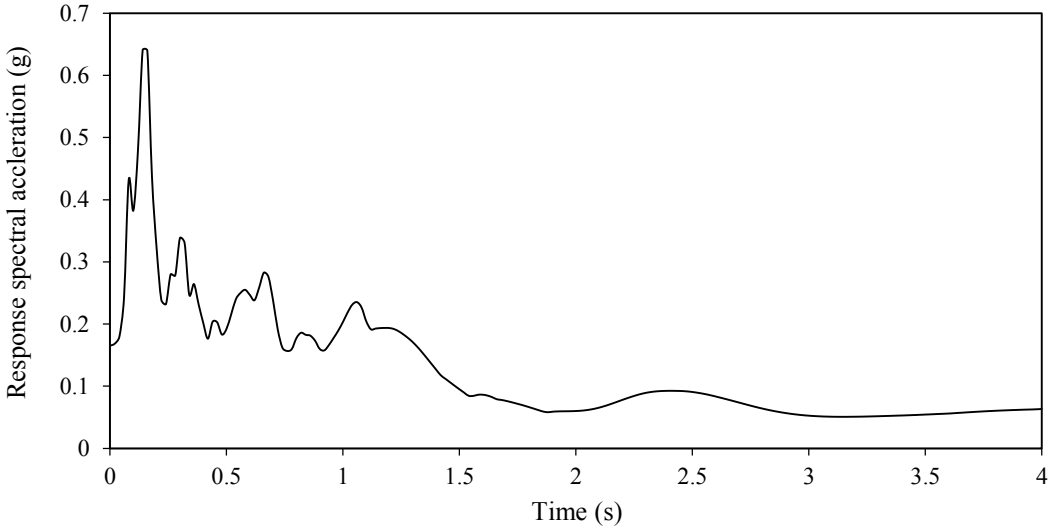

Figure 2.15 Acceleration response spectrum of the sample record, 5% damping.

Among a number of response parameters, the deck displacement, expansion bearing displacement, column displacement, and column curvature were selected to represent the bridge response. In this study, the seismic loading is only applied in the longitudinal direction of the bridge model. This is because studies have reported that the longitudinal direction of bridge is more critical than the transverse direction under seismic loads (e.g., Choi, 2002; Shinozuka, 1998). For the purpose of illustration, only the results from Bridge #1, which is a 3-span reinforced concrete slab bridge, are presented.

2.5.1 Deck displacement

Figures 2.16a and 2.16b show the deck displacement time histories corresponding to the seismic excitations scaled to two intensity levels, i.e., $0.5Sa(T_1)$ and $2.0Sa(T_1)$, in which $Sa(T_1)$ represents the spectral acceleration at the first mode period (T_1) of the bridge model and it was determined based on the design spectrum for Montreal (Fig. 3.4 in Chapter 3). These two scaling levels were selected to represent the elastic and inelastic responses of the bridge, respectively. The dominant period T_1 for Bridge #1 is about 0.81 s, and the target $Sa(T_1)$ based

on Fig. 3.4 in Chapter 3 is about 0.28 g.

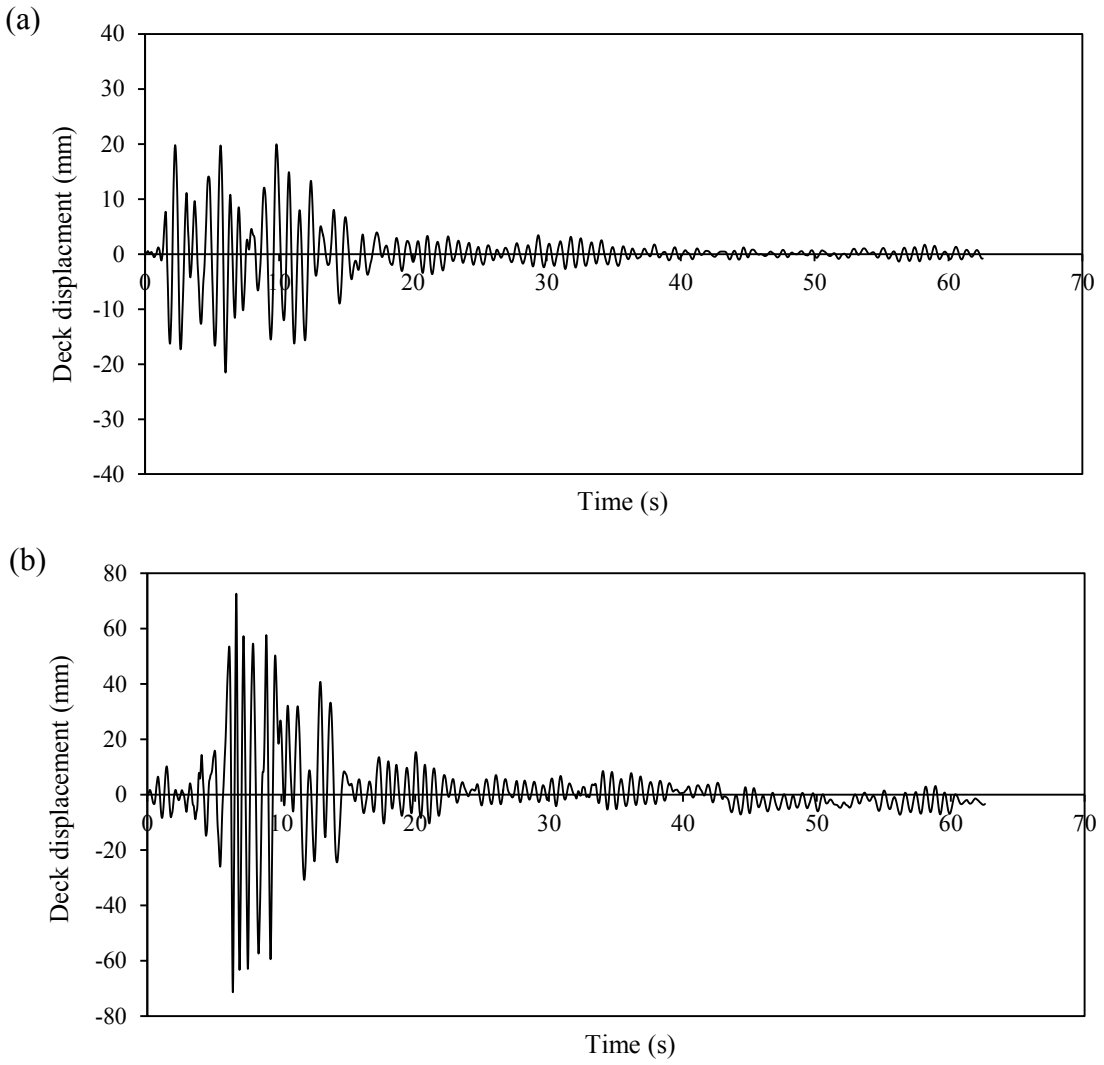

Figure 2.16 Deck displacement time histories of Bridge #1 for a record scaled to (a) 0.5Sa(T_1); (b) 2.0 Sa(T_1).

It can be seen in Fig. 2.16 that the maximum deck displacement is about 22 mm for the record scaled to 0.5Sa(T_1) of 0.14 g while it is about 70 mm for the record scaled to 2.0Sa(T_1) of 0.56 g. These results indicate that significant inelastic deformations occurred in both bearings and columns. In addition, the comparison between the deck displacement and the bearing displacement (see discussion below) shows that the deformation of the expansion bearing contributes to a large amount of the displacement to the deck. Please take note that the

residual displacements of the deck corresponding to the intensity levels of 0.5Sa(T_1) and 2.0Sa(T_1) for this specific record are very small which can be seen in the figure. In this study, it was found that the maximum residual displacement of the deck was about 20 mm from some of the records scaled to 2.0Sa(T_1).

2.5.2 Expansion bearing displacement

As mentioned in the Section2.2 "Description of Bridges", both fixed bearings and expansion bearings are used in the two bridges. Since the fixed bearing does not allow translation (strictly speaking, it allows very small translation), only the results for the displacement of the expansion bearing from the analysis are shown here. Figure 2.17 illustrates the displacements of an expansion bearing on Pier 2 of Bridge #1 (see Fig. 2.3) when the ground motion is scaled to 0.5Sa(T_1) and 2.0Sa(T_1), respectively. The vertical axis of the figure represents the lateral force on the bearing due to the seismic excitation applied in the longitudinal direction of the bridge, and the horizontal axis represents the corresponding lateral displacement. As expected, the behavior of the bearing under the lateral loads follows the bilinear curve as defined in Fig. 2.6 for both scaling levels considered in the time-history analysis. It can be seen in Fig. 2.17 that the maximum lateral displacement is about 19 mm at the intensity of 0.5Sa(T_1) of 0.14 g while is about 51 mm at the intensity of 2.0Sa(T_1) of 0.56 g. It should be noted that the lateral force-displacement response curve of the fixed bearing is very similar to that of the expansion bearing. However, the number of cycles of the hysteretic behavior of the fixed bearing is much smaller than that of the expansion bearing due to the mechanism of the fixed bearing.

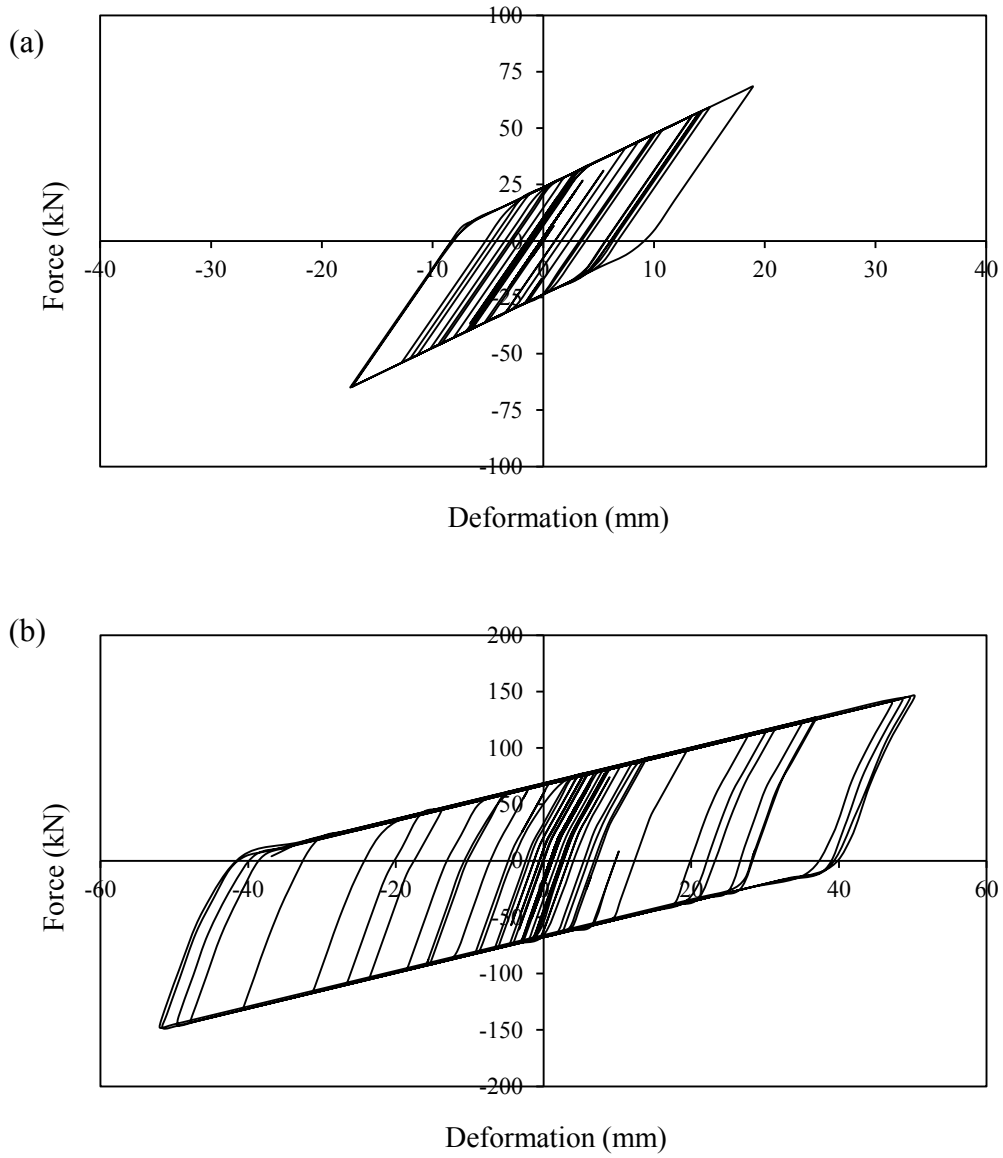

Figure 2.17 Expansion bearing force-displacement curves of Bridge #1 for a record scaled to (a) 0.5Sa(T_1); (b) 2.0Sa(T_1).

2.5.3 Response of the column

Two response parameters were considered in the preliminary time-history analysis in this study in order to evaluate the performance of the columns, which are displacement and curvature. The displacement is used as a "global" response parameter while the curvature is used as a "local" response parameter.

Displacement of the column under the expansion bearing

The displacement time histories of the columns of the Pier 2, in which the expansion bearings were installed, for the seismic excitations scaled to $0.5Sa(T_1)$ and $2.0Sa(T_1)$ of the Bridge #1 are presented in Fig. 2.18. It can be seen in the figure that the maximum displacements of the column corresponding to the two intensity levels of $0.5Sa(T_1)$ and $2.0Sa(T_1)$ are about 2.9 mm and 6.0 mm. These displacements are significantly smaller than those of the expansion bearings (see Fig. 2.17). This is because the lateral stiffness of the column is much larger than that of the expansion bearing. As expected, relatively larger residual displacement of the column was observed at the intensity level of $2.0Sa(T_1)$ due to the form of the plastic hinges on the top and bottom of the column considered in the modeling.

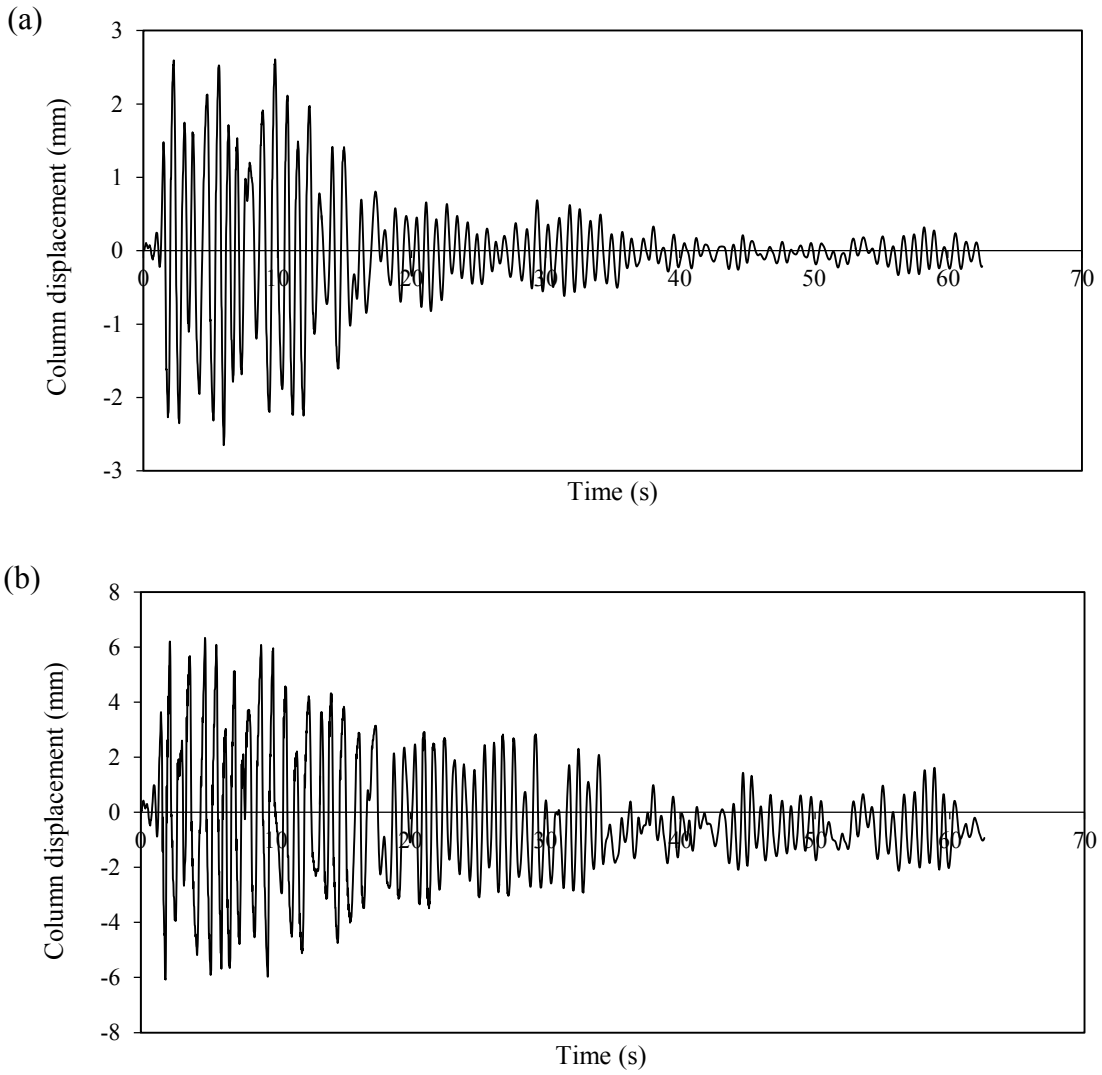

Figure 2.18 Column (of Pier 2) displacement time histories of Bridge #1 for a record scaled to (a) 0.5Sa(T_1); (b) 2.0Sa(T_1).

Displacement of the column under fixed bearing

For purpose of comparison, Figure 2.19 shows the displacement time histories of the column under the fixed bearing on Pier 1. It can be seen in the figure, the maximum column displacements for the record scaled to 0.5Sa(T_1) and 2.0Sa(T_1) are about 20 mm and 60 mm, respectively. The displacements of Pier 1 are significantly larger than that of the Pier 2. This is because the fixed bearings are used on the top of the columns of the Pier 1 which result in

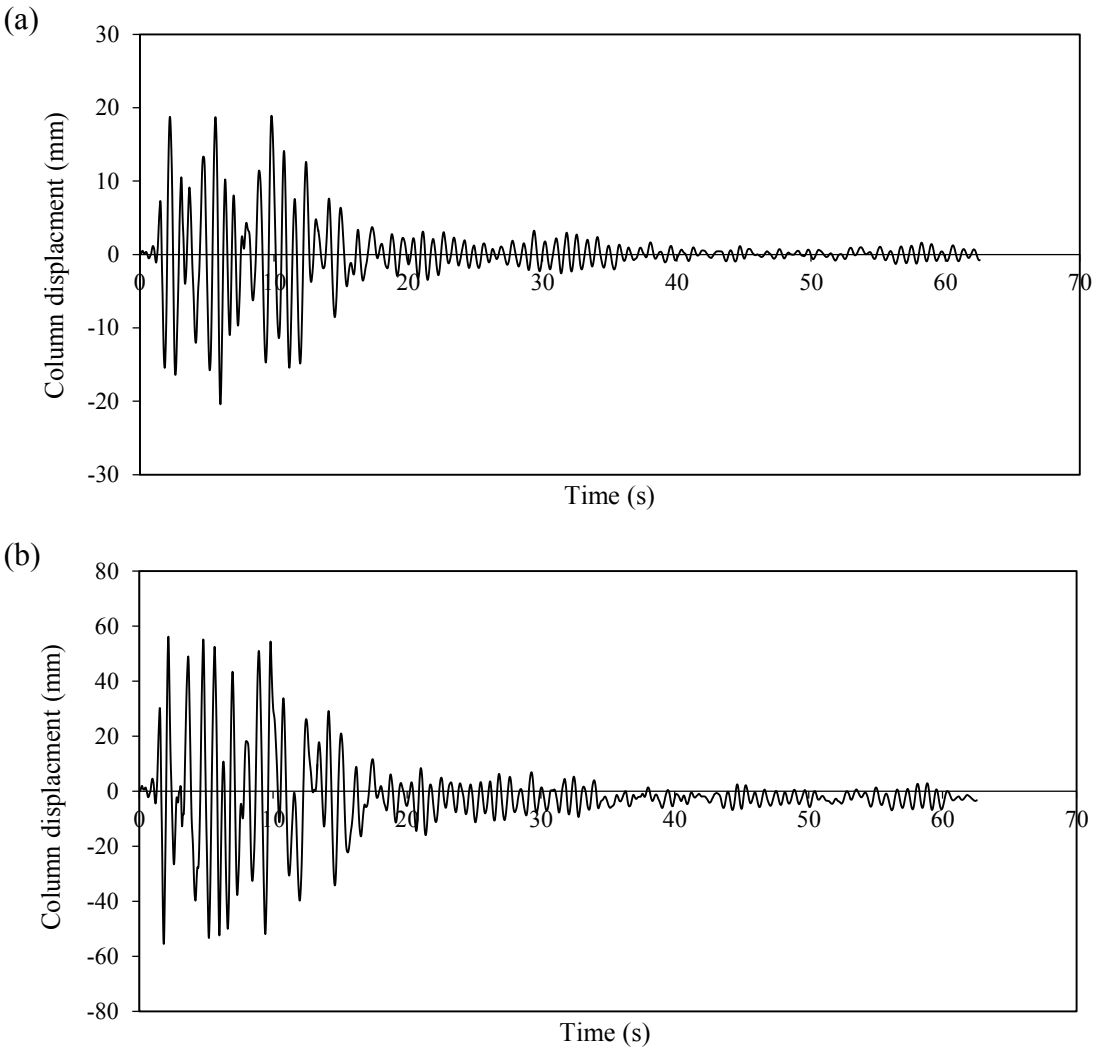

Figure 2.19 Column (of Pier 1) displacement time histories of Bridge #1 for a record scaled to (a) 0.5Sa(T_1); (b) 2.0Sa(T_1).

relatively larger combined lateral stiffness of bearings and columns of the Pier 1 due to the extremely larger lateral stiffness of the fixed bearing to limit the translation of the fixed bearing. More specifically, the maximum lateral deflection of a column of a bridge occurs on the column on which the fixed bearing is installed, i.e., the maximum displacement of the column of the Bridge 1 is dominated by the column of the Pier 1 (fixed bearings were installed) not Pier 2 (expansion bearings were installed).

Curvature of the column under the expansion bearing

Figure 2.20 shows the moment-curvature response curves for the end section of column, which was used to model the plastic hinge of the column in this study, under the expansion bearing (Pier 2) for the sample record scaled to 0.5Sa(T_1) and 2.0Sa(T_1), respectively. The

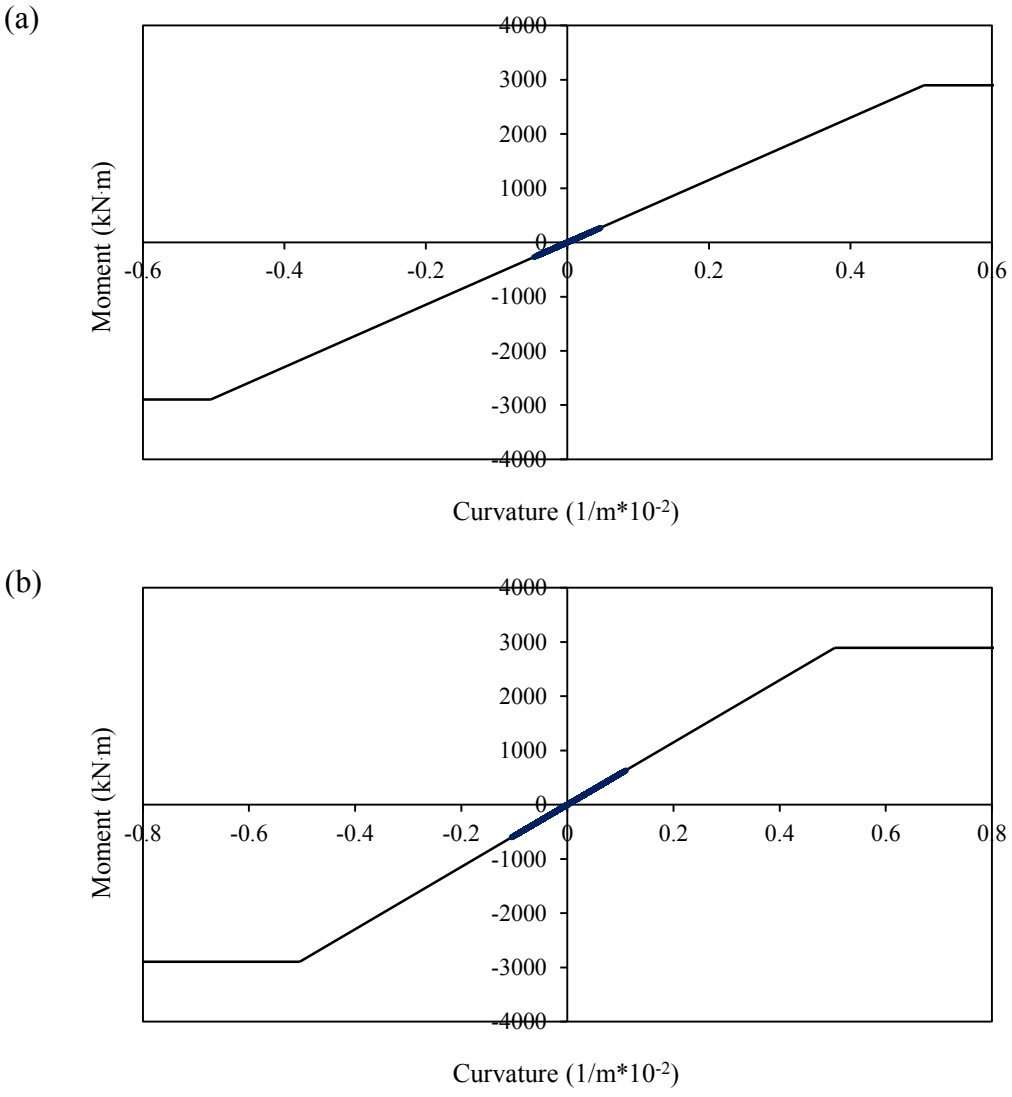

Figure 2.20 Column (of Pier 2) moment-curvature curves of Bridge #1 for a record scaled to (a) 0.5Sa(T_1); (b) 2.0 Sa(T_1).

results in the figure clearly show that the columns of Pier 2 behave elastically for the both levels of the seismic excitations used in the analysis. In addition, the curvature of the section is quite small due to the relatively small lateral force distributed to the Pier 2 compared to the Pier 1.

Curvature of the column under the fixed bearing

The results for the moment-curvature curve for the end section of column under the fixed bearing (Pier 1) for the record scaled to $0.5Sa(T_1)$ and $2.0Sa(T_1)$, are presented in Fig. 2.21. As illustrated in the figure, the response of the plastic hinge follows exactly the bilinear curve used to define the behavior of the plastic hinge in the modeling. It is also seen in the figure that the plastic hinge behaves elastically at the intensity level of $0.5Sa(T_1)$ while it undergoes a number of cycles showing significant inelasticity of the column at the intensity level of $2.0Sa(T_1)$. In this study, it was found the maximum curvature ductility of the column was about 4.

(a)

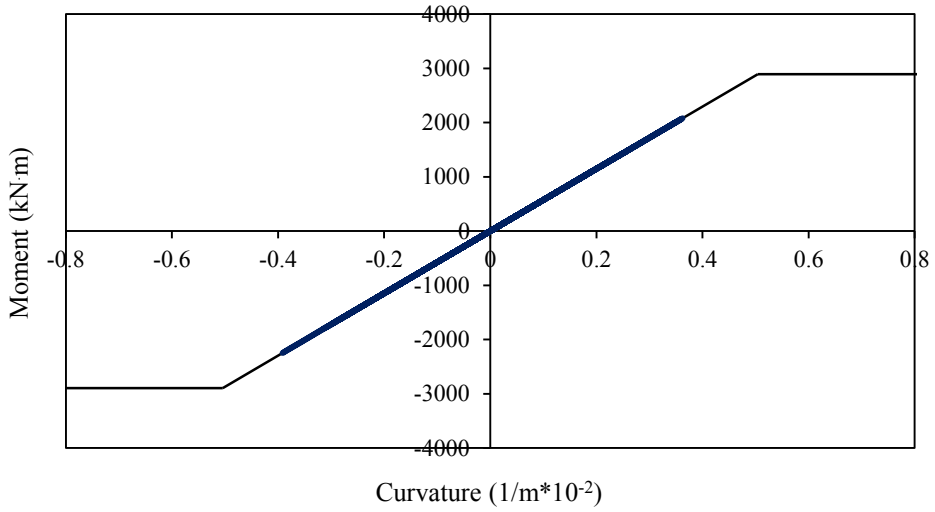

(b)

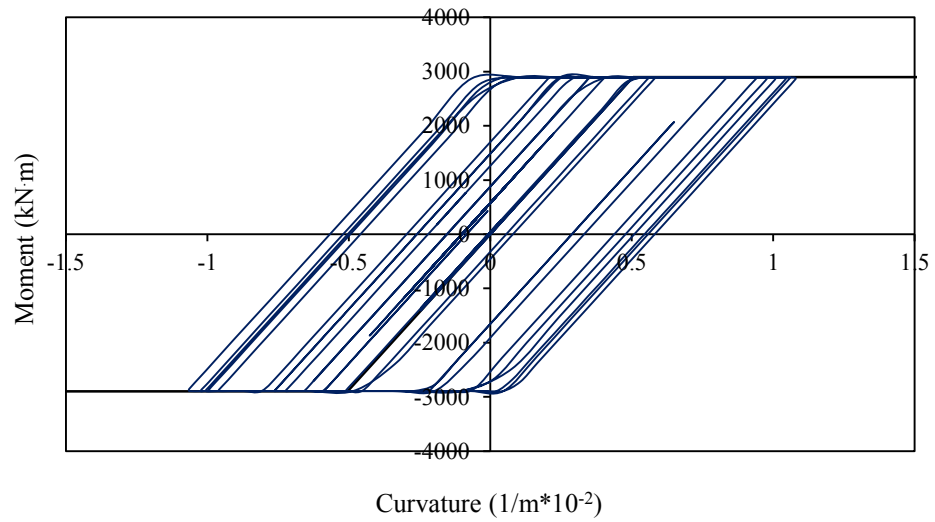

Figure 2.21 Column (of Pier 1) moment-curvature curves of Bridge #1 for a record scaled to (a) 0.5Sa(T_1); (b) 2.0 Sa(T_1).

Chapter 3

Selection of Earthquake Records

3.1 Seismic Hazard for Montreal

There have been significant advances in the understanding of the seismic hazard in Canada since 1980s. New source models, and most updated software have been used for the assessment of the seismic hazard. It should be mentioned, however, that there are still significant uncertainties in the estimation of seismic hazard. As pointed out by Adams (2011); Adams and Atkinson (2003), the ground motion attenuation relations for eastern Canada are the major source of uncertainty in the seismic hazard estimations. This is because of the lack of recordings of ground motions from strong earthquakes in eastern Canada for use in the calibration of the attenuation relations. Given this, Adams (2011) reported that the ground motion attenuation relations for eastern Canada may change significantly as new events are recorded.

The seismic hazard is currently represented by uniform hazard spectra rather than by peak ground motions. A uniform hazard spectrum represents an acceleration spectrum with spectral ordinates that have the same probability of exceedance. Uniform hazard spectra can be computed for different probabilities and confidence levels. Confidence levels of 50% (median) and 84% are typically used for uniform hazard spectra. These levels represent the confidence (in %) that the spectral values will not be exceeded for the specified probability. Figure 3.1 shows the 50% level uniform hazard spectrum (UHS) for the probability of

exceedance of 10% in 50 years (i.e., annual probability of exceedance of 0.002) for 5% damping for soil class C. The spectral values for periods below 2.0 s were provided by Geological Survey of Canada. For periods between 2.0 s and 4.0 s, the spectrum was extended assuming a constant spectral velocity with the same value as that at 2.0 s. This is the same as assumed in the defining of the spectral values in the intermediate period range of the design spectrum.

The seismic response coefficient (i.e., seismic design spectrum) for Montreal was determined using Equation 3.1 in accordance with CHBDC (2010),

$$C_{sm} = \frac{1.2AIS}{T_m^{2/3}} \leq 2.5AI \tag{3.1}$$

Where

A = zonal acceleration ratio,

I = importance factor,

S = site coefficient,

T_m = period of vibration of the m^{th} mode.

The zonal acceleration ratio A for Montreal is 0.2 for probability of exceedance of 10% in 50 years. The importance factor I is taken as 1.0 (normal importance) for the two bridges. In this study, Reference ground conditions, represented by soil profile type I (rock or stiff soil) in CHBDC, were assumed at the bridge location. It is necessary to mention that soil class C used to develop UHS is referred to firm soil according to 2010 edition of the National Building Code of Canada, and it is equivalent to the Soil Profile Type I in CHBDC.

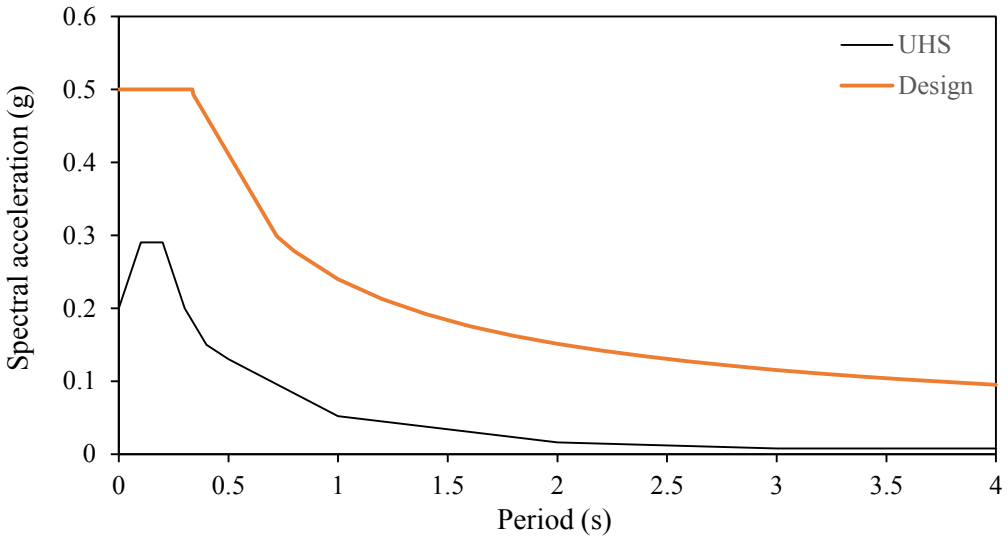

Figure 3.1 Uniform hazard spectrum and design spectrum for Montreal, 5% damping.

It can be seen in Fig. 3.1 that design spectrum is much higher than the uniform hazard spectrum which indicates the response spectra defined in CHBDC is quite conservative.

3.2 Scenario Earthquakes for Montreal

The seismic hazard at a given site represents the sum of the hazard contributions of different earthquakes at different distances from the site. For each site, however, there are a few earthquakes that have dominant contributions to the hazard. These earthquakes are normally referred to as scenario or predominant earthquakes. The shape of the uniform hazard spectrum for a given site, represents the seismic hazard for the site, and it depends on the magnitudes of the scenario earthquakes and the distances of these earthquakes from the site. In general, the dominant contribution to the short period ground motion hazard is from small to moderate earthquakes at small distances, whereas larger earthquakes at greater distance contribute most to the long period ground motion hazard.

For the purpose of the selection of earthquake ground motions for use in the seismic analysis, it is necessary to know the magnitude (M) and the distance (R) of the earthquakes that have the largest contributions to the seismic hazard. This can be done by computing the seismic hazard contributions of selected M-R ranges that cover all possible magnitude-distance combinations, which is also called seismic hazard deaggregation analysis. Figure 3.2 provided by Geological Survey of Canada shows the M-R contributions for Montreal for probability of exceedance of 10% in 50 years.

Figure 3.2a shows the contributions to the seismic hazard for period of 0.2 s, representing the short period ground motion hazard. Similarly, Figure 3.2b shows the contributions for period of 1.0 s, representing the long period ground motion hazard. The contributions were computed for magnitude intervals of 0.25, and distance intervals of 20 km. It can be seen in Fig. 3.2a that the dominant M-R values corresponding to the seismic hazard of 10% in 50 years probability of exceedance are $M_w = 5.65$ and R = 55 km for period of 0.2 s, and $M_w = 6.5$ and R = 134 km for period of 1.0 s. Note that these M and R values are the *mean* (or weighted average) values for each period.

(a)

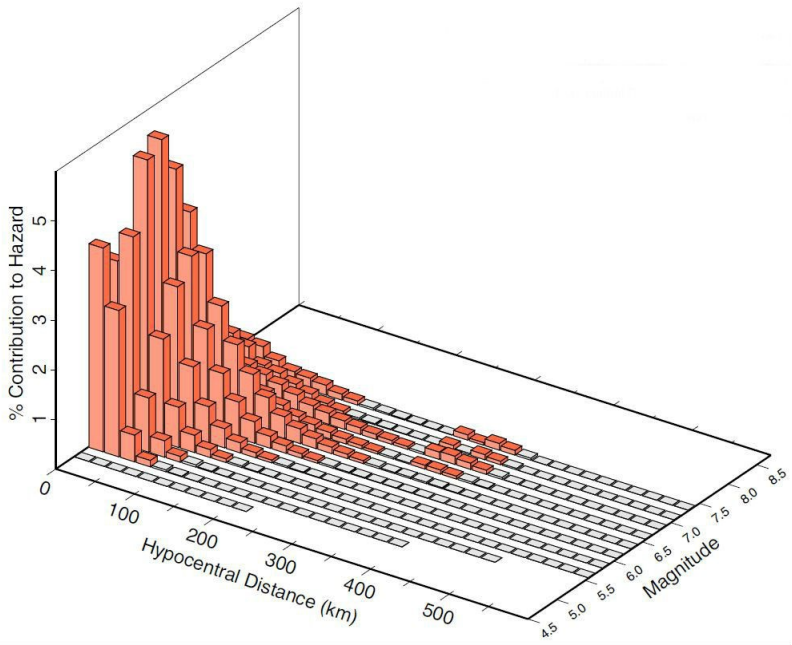

(b)

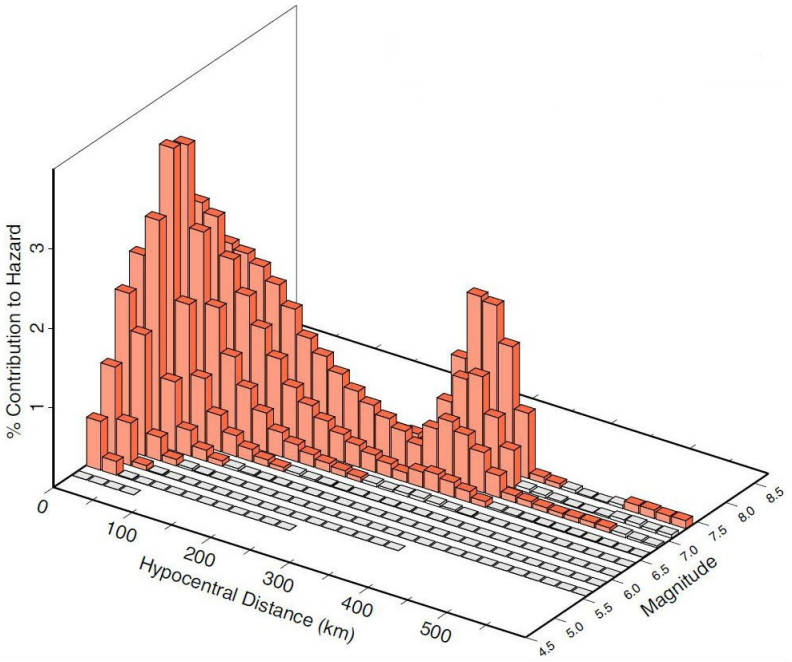

Figure 3.2 Seismic hazard deaggregation results for Montreal for probability of exceedance of 10% in 50 years: (a) Sa(0.2s); (b) Sa(1.0s).

3.3 Selection of records

The nonlinear time-history analysis is the most reliable method for the assessment of the behavior of building subjected to seismic loads. To perform nonlinear dynamic analysis, acceleration time histories (i.e., accelerograms) of the seismic excitations are needed. The code requires that these accelerograms be compatible with the design spectrum (CHDBC 2010; AASHTO 2012; Caltrans SDC 2013). For the purpose of this study, four sets of seismic excitations were considered, which include:

Set 1: Scaled real accelerograms,

Set 2: Modified real accelerograms,

Set 3: Simulated accelerograms, and

Set 4: Artificial accelerograms.

While Set 1 consists of actual accelerograms recorded during earthquakes, Sets 2 to 4 can all be considered as synthetic. The names "Modified real", "Simulated" and "Artificial" refer to the method for deriving the accelerograms of these sets. Each set consists of 30 accelerograms.

It is necessary to mention that there is no guidance on how to achieve spectrum-compatible accelerograms for the time-history analysis in the current bridge code, such as, CHBDC, AASHTO, and Caltrans SDC. Given this, the specifications prescribed in the U.S. Standard ASCE/SEI 7-10 (ASCE 2010) are used in this study. According to ASCE (2010), the selected accelerograms should be properly scaled such that the 5% damped mean spectrum of the set is above the design spectrum for all periods between 0.2T and 1.5T, where T is the fundamental period of the building for the direction of the response being analysed.

Following the requirements in ASCE (2010), the accelerograms of each set are scaled such that the mean acceleration spectrum of the set is above the design spectrum for Montreal

within the period range between 0.14 s and 1.2 s. The value of 0.14 s corresponds approximately to $0.2T_{1\text{-Bridge \#2}}$ (where $T_{1\text{-Bridge \#2}}$ is the first mode period of the Bridge #2, and it is 0.71 s), and the value of 1.2 s is close to $1.5T_{1\text{-Bridge \#1}}$ (where $T_{1\text{-Bridge \#1}}$ is the first mode period of the Bridge #1, and it is 0.81 s). In addition, this period range was selected in order to take into account the effects of higher modes through the use of the period of $0.2T_1$ and the period elongation which is represented by $1.5T_1$ in which T_1 is the predominant period of the bridge. Gao et al. (2013) investigated the period elongation of typical highway bridges and reported that the dominant period of bridge was approximately elongated about 1.5 times than its first mode period during nonlinear response. On the other hand, the threshold of $0.2T_1$ roughly corresponds to the period of the higher mode of the two bridge models considered in this study.

3.3.1 Set 1 - Scaled real accelerograms

Because of the lack of strong seismic motion records in eastern Canada, a set of ground motion records obtained from strong earthquakes around the world was used in this study. The set consists of two subsets of accelerograms, which are described in Naumoski et al. (1988, 1993) and are characterized by different peak ground acceleration to peak ground velocity ratios (A/V ratios). The average A/V ratio (A in g, and V in m/s) of the records of one of the subsets is 2.12, and that of the other subset is 1.03. Based on the A/V ratios of the records, the subsets are referred to as the high and intermediate A/V subsets. In general, high A/V ratios are characteristics of seismic motions from small to moderate earthquakes at short distances, and intermediate A/V ratios are characteristics of seismic motions from moderate to large earthquakes at moderate distances. Regarding the frequency content, high A/V motions normally have a high frequency content, and intermediate A/V motions have an intermediate

frequency content compared to a low frequency content. Seismic motions with a high frequency content are characterized by predominant frequencies higher than approximately 2 Hz (i.e. periods lower than 0.5 s), and seismic motions with a low frequency content are characterized by predominant frequencies lower than 2 Hz (i.e. periods longer than 0.5 s).

3.3.1.1 High A/V accelerograms

It is well known that seismic ground motions in eastern Canada are characterized by high frequency content and high A/V ratios (Adams and Halchuk 2003; Naumoski et al. 1988). As discussed above, a set of records with high A/V ratios from strong earthquakes around the world (Naumoski et al. 1988) was adopted for the analysis. The set consisted of 15 pairs of horizontal and vertical records. The characteristics of the earthquakes and the horizontal records are shown in Table 3.1. It can be seen in the table that the magnitudes of the earthquakes are between 5.25 and 6.9. The records were taken at distances ranging from 4 km to 33 km, and have A/V ratios (A in g, and V in m/s) between 1.67 and 2.63, with an average A/V of 2.12. The magnitudes of these earthquakes cover dominant magnitude of the scenario earthquakes for the short period ground motion hazard for the bridge location (see Section 3.2).

Table 3.1 High A/V records included in the accelerograms of Set 1(Naumoski, 1988).

Earthquake	Date	M_w	Site	Epic. Dist. (km)	Comp.	Max. Acc. A(g)	Max. Vel. V(m/s)	A/V	Soil Cond.
Parkfield California	June 27 1966	5.6	Temblor No. 2	7	N65W	0.269	0.145	1.86	Rock
Parkfield California	June 27 1966	5.6	Cholame Shandon No. 5	5	N85W	0.434	0.255	1.7	Rock
San Francisco California	Mar. 22 1957	5.25	Golden Gate Park	11	S80E	0.105	0.046	2.28	Rock
San Francisco California	Mar. 22 1957	5.25	State Bldg., S.F.	17	S09E	0.085	0.051	1.67	Stiff Soil
Helena Montana	Oct. 31 1935	6	Carroll College	8	N00E	0.146	0.072	2.03	Rock
Lytle Creek	Sep. 12 1970	5.4	Wrightwood, California	15	S25W	0.198	0.096	2.06	Rock
Oroville California	Aug. 1 1975	5.7	Seismogr, Station Oroville	13	N53W	0.084	0.044	1.91	Rock
San Fernando California	Feb. 9 1971	6.4	Pacomia Dam	4	S74W	1.075	0.577	1.86	Rock
San Fernando California	Feb. 9 1971	6.4	Lake Hughes, Station 4	26	S21W	0.146	0.085	1.72	Rock
NahanniN.W.T. Canada	Dec. 23 1985	6.9	Site 1, Iverson	7.5	LONG	1.101	0.462	2.38	Rock
Central Honshu, Japan	Feb. 26 1971	5.5	Yoneyama Bridge	27	TRANS	0.151	0.059	2.56	Stiff Soil
Near E. Coast of Honshu, Japan	May. 11 1972	5.8	Kushiro Central, Wharf	33	N00E	0.146	0.06	2.43	Stiff Soil
Honshu, Japan	Apr. 5 1966	5.4	Hoshina–A	4	N00E	0.27	0.111	2.43	Stiff Soil
Monte Negro Yugoslavia	Apr. 9 1979	5.4	Albatros Hotel, Ulcinj	12.5	N00E	0.042	0.016	2.63	Rock
Banja Luka Yugoslavia	Aug. 13 1981	6.1	Seism. Station, Banja Luka	8.5	N90W	0.074	0.032	2.31	Rock

Table 3.2 Intermediate A/V records included in the accelerograms of Set 1 (Naumoski 1988).

Earthquake	Date	M_w	Site	Epic. Dist. (km)	Comp.	Max. Acc. A(g)	Max. Vel. V(m/s)	A/V	Soil Cond.
Imperial Valley California	May 18 1940	6.6	El Centro	8	S00E	0.348	0.334	1.04	Stiff Soil
Kern County California	July 21 1952	7.6	Taft Lincoln School Tunnel	56	S69E	0.179	0.177	1.01	Rock
Kern County California	July 21 1952	7.6	Taft Lincoln School Tunnel	56	N21E	0.156	0.157	0.99	Rock
Borrego Mtn. California	April 8 1968	6.5	San Onofre SCE Power Plant	122	N57W	0.046	0.042	1.1	Stiff Soil
Borrego Mtn. California	April 8 1968	6.5	San Onofre SCE Power Plant	122	N33E	0.041	0.037	1.11	Stiff Soil
San Fernando California	Feb. 9 1971	6.4	3838 Lankershim Blvd., L.A.	24	S90W	0.15	0.149	1.01	Rock
San Fernando California	Feb. 9 1971	6.4	Hollywood Storage P.E. Lot, L.A.	35	N90E	0.211	0.211	1	Stiff Soil
San Fernando California	Feb. 9 1971	6.4	3407 6^{th} Street, L.A.	39	N90E	0.165	0.166	0.99	Stiff Soil
San Fernando California	Feb. 9 1971	6.4	Griffith Park Observatory, L.A.	31	S00W	0.18	0.205	0.88	Rock
San Fernando California	Feb. 9 1971	6.4	234 Figueroa St., L.A.	41	N37E	0.199	0.167	1.19	Stiff Soil
Near East Coast of Honshu,Japan	Nov. 16 1974	6.1	Kashima Harbor Works	38	N00E	0.07	0.072	0.97	Stiff Soil
Near East Coast of Honshu,Japan	Aug. 2 1971	7	Kushiro Central Wharf	196	N90E	0.078	0.068	1.15	Stiff Soil
Monte Negro Yugoslavia	Apr. 15 1979	7	Albatros Hotel, Ulcinj	17	N00E	0.171	0.194	0.88	Rock
Mexico Earthq.	Sept. 19 1985	8.1	El Suchil, Guerrero Array	230	S00E	0.105	0.116	0.91	Rock
Mexico Earthq.	Sept. 19 1985	8.1	La Villita, Guerrero Array	44	N90E	0.123	0.105	1.17	Rock

3.3.1.2 Intermediate A/V accelerograms

The intermediate A/V set consisted of 15 pairs of horizontal and vertical records of seismic ground motions (Naumoski et al. 1993). The characteristics of the horizontal records of the set are given in Table 3.2. The A/V ratios of the records are between 0.88 and 1.17. The

records were obtained from strong earthquakes with magnitudes ranging from 6.1 to 8.1, distances between 8 km and 230 km. Both magnitudes and the distances cover the magnitude and distance ranges of the scenario earthquakes for short and long period ground motion hazards for the bridge location determined from the seismic hazard analysis (see Section 3.2).

3.3.1.3 Scaling of ground motions

To achieve spectral compatibility with the design spectrum, the records were scaled in two steps to satisfy the requirements specified in ASCE (2010). Note that there is no specification of the scaling of records for time-history analysis in CHDBC (2010), AASHTO (2012), and Caltans SDC (2013). In the first step, the method known as "scaling to partial spectral area" was used (Amiri-Hormozaki 2003). In this method, each record was scaled such that the area of the 5% damped acceleration spectrum of the record within the period range between 0.14 s and 1.20 s is equal to the area under the design spectrum within the same period range. The mean spectrum of the scaled accelerograms resulting from this method was close to the design spectrum, with some parts being above and some parts below the design spectrum. In order to have a mean spectrum above the design spectrum for the periods between 0.14 s and 1.20 s, additional scaling was conducted by multiplying the accelerograms (already scaled in the first step) by a factor of 1.25. This value was determined by several trials using different factors. The spectra of the scaled accelerograms, the mean spectrum of the set, and the design spectrum for Montreal are shown in Fig. 3.3. It is seen in the figure that the mean spectrum of the set is above the design spectrum as required by ASCE (2010).

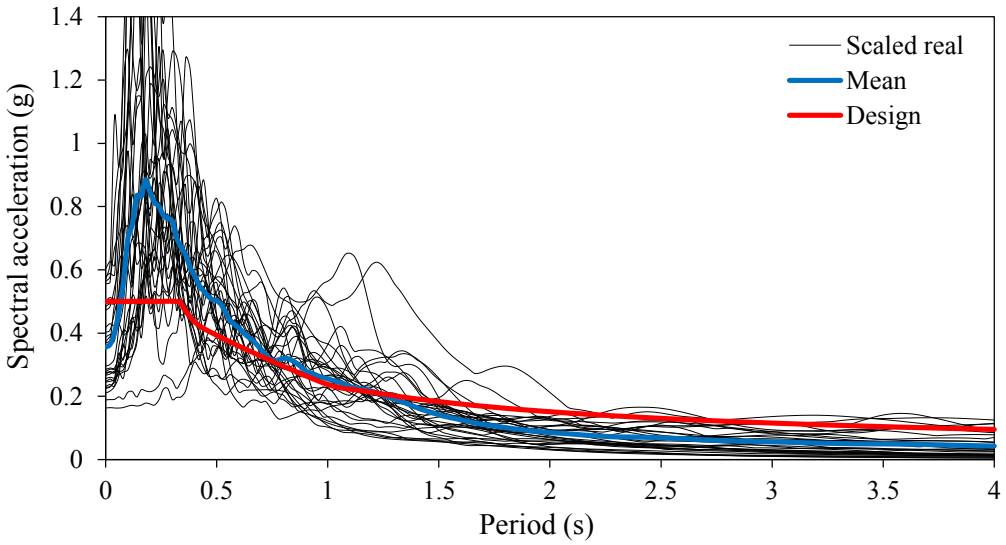

Figure 3.3 Scaled response spectra of the accelerograms of Set 1, 5% damping.

3.3.2 Set 2 - Modified real accelerograms

A method described by Naumoski (2001) was used for the generation of spectrum compatible accelerograms by modifying real accelerograms. In this method, a selected (i.e., initial) accelerogram is modified iteratively until its spectrum matches the prescribed design spectrum. The initial accelerogram can be any ground motion record (i.e., real or synthetic). In this study, the originally selected earthquake records for Set 1 (listed in Tables 3.1 and 3.2) were used as initial accelerograms. The spectrum to be matched was the design spectrum for Montreal for soil profile type I (Fig. 3.1). However, the portion of the spectrum for the periods shorter than 0.15s was modified for the purpose of generation of accelerograms as required by Naumoski (2001). The modified design spectrum is designated as target spectrum, and it is shown in Fig. 3.4.

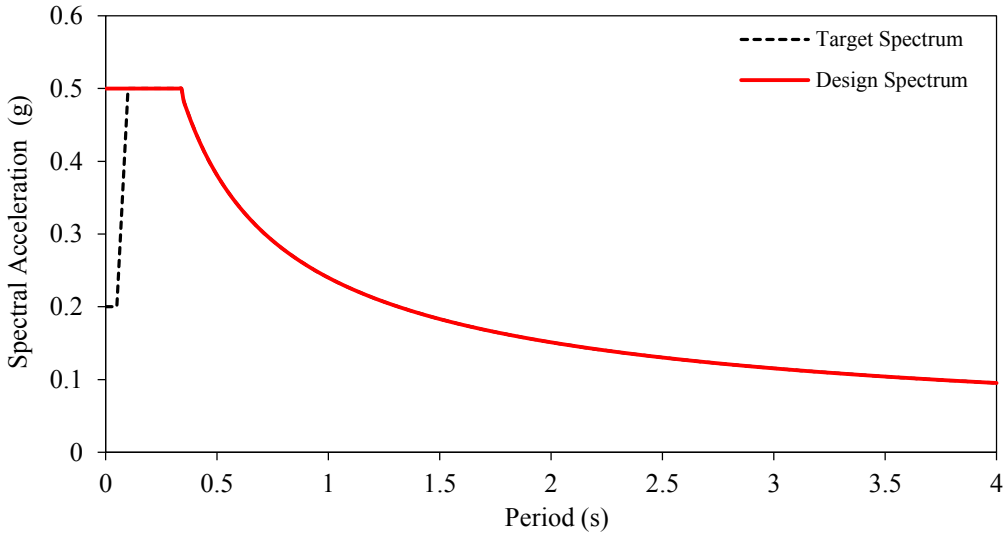

Figure 3.4 Target spectrum used to generate the accelerograms of Set 2 (modified real accelerograms).

The modifications of the initial accelerogram are conducted in the frequency domain. In the first iteration, the ratios of the spectral ordinates of the design spectrum to those of the acceleration spectrum of the initial accelerogram are computed for all the periods considered Based on these ratios, the frequency content and the amplitudes of the initial accelerograms are modified such that the spectrum of the modified accelerogram becomes closer to the target spectrum. The modified accelerogram is used in the next iteration, and the iterative process continues until the spectrum of the accelerogram matches the target spectrum throughout the period range of interest. An important feature of the method is that it preserves the phases of the Fourier components (sinusoids) of the initial accelerogram, i.e., the phases in the generated accelerogram are the same as those in the initial accelerogram. Detailed explanations for the method can be found in Naumoski (2001). Figure 3.5 shows the spectra of the accelerograms generated for use in this study. In order to rise the mean spectrum to be above the design spectrum, the accelerograms generated as described above were scaled by 1.10.

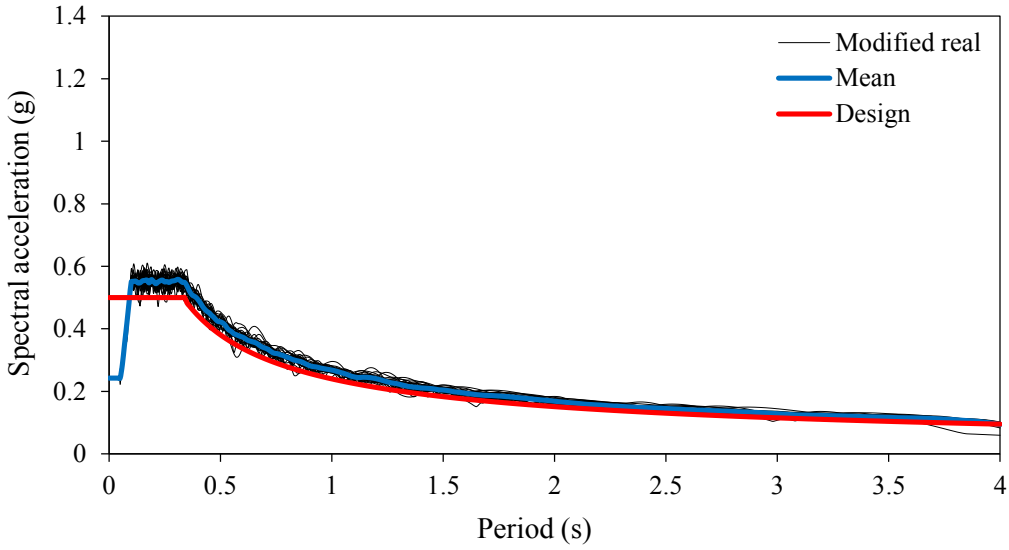

Figure 3.5 Scaled response spectra of the accelerograms of Set 2, 5% damping.

3.3.3 Set 3 - Simulated accelerograms

Due to the lack of earthquake records in eastern Canada, a comprehensive library of simulated accelerograms compatible with the 2005 NBCC uniform hazard spectra is established by Atkinson (2009). A stochastic finite-fault method is used for the simulation of the accelerograms. This method was first introduced by Hartzell (1978). In this method, a large fault is divided into a number of subfaults and each subfault is considered as a point source. Ground motions of the point sources are simulated using the stochastic point-source approach. The simulation is based on a specified Fourier spectrum of ground motion as a function of magnitude and distance. The simulation model also includes the source parameters characteristic for the geographic region considered, and takes into account the effects of the magnitude and distance on the duration of the ground motion. The accelerograms simulated for the point (i.e., subfault) sources along the fault are summed (with a proper time delay) in the time domain to obtain the ground motion from the entire fault.

Using this method, Atkinson (2009) simulated accelerograms for eastern Canada for earthquake magnitudes of 6.0 and 7.0, and for a wide range of source-to-site distances. These accelerograms are available on the website of Engineering Seismology Toolbox (www.seismotoolbox.ca). Among these accelerograms, a set of 30 accelerograms was selected for this study. The selected accelerograms correspond to earthquake magnitudes of 6.0 and 7.0, distances between 10 km to 100 km, and soil class C (equivalent to soil profile type I of CHBDC). The accelerograms were scaled such that the mean spectrum of the set is above the design spectrum (Fig. 3.6).

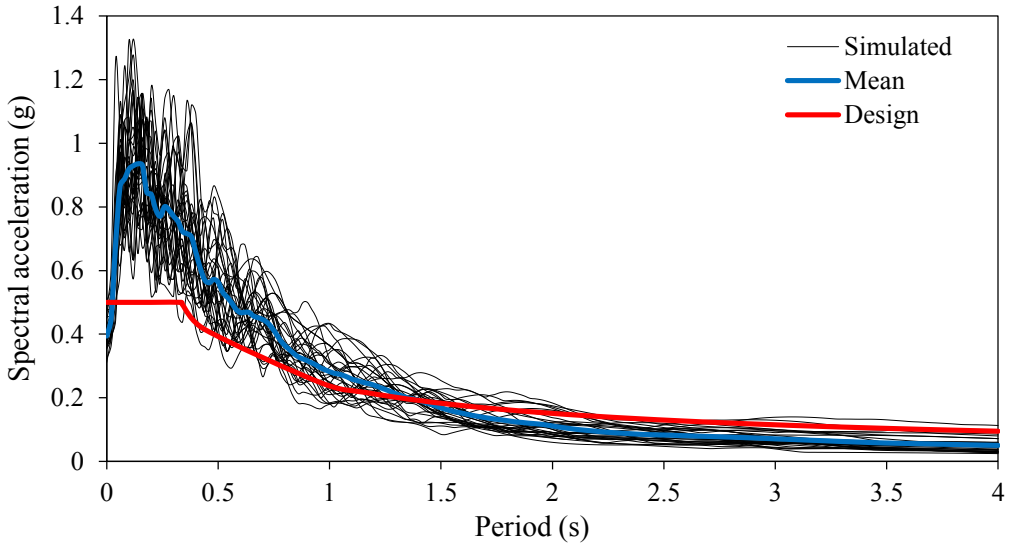

Figure 3.6 Scaled response spectra of the accelerograms of Set 3, 5% damping.

3.3.4 Set 4 - Artificial accelerograms

Artificial accelerograms compatible with the design spectrum for Montreal were generated using the method proposed by Gasparini and Vanmarcke (1976) which has been incorporated in the computer program SeismoArtif (Seismosoft 2013). The method is based on the well-known principle that each accelerogram can be represented by a sum of sinusoids. As the first step, sinusoids are generated at a specified number of frequencies within the frequency range of the design spectrum. The phase angles of the sinusoids are produced using random number generation software. The amplitudes of the sinusoids are determined from the spectrum density function, which is derived based on the design spectrum. Then, an accelerogram is obtained by summation of the sinusoids. The accelerogram is multiplied by a specified shape function (i.e., intensity envelope function) in order to simulate the shape of a real earthquake motion. The mathematical expression for the accelerogram generated is shown in Equation 3.2.

$$Z(t) = I(t) * \sum A_n \sin(\omega_n t + \varphi_n) \tag{3.2}$$

Where

I_t = shape function of an artificial accelerogram,

A_n = amplitude of n^{th} sinusoid wave,

φ_n = phase angle of n^{th} sinusoid wave.

The response spectrum of the resulting accelerogram is computed and compared with the design spectrum. Based on the ratios of the ordinates of the computed spectrum and those of the design spectrum, the spectrum density function is modified for use in the calculation of the amplitudes of the sinusoids for the next iteration. The iterative process continues until the spectrum of the accelerogram is close to the design spectrum.

The shape function used for the generation of the accelerograms in this study is illustrated in Fig. 3.7. The maximum intensity of the shape function is 0.20 g which corresponds to the peak ground acceleration for Montreal for the probability of exceedance of 10% in 50 years. In total, 30 accelerograms were generated using SeismoArtif (Seismosoft 2013). The matching of the spectra of the artificial accelerograms and the design spectrum is shown in Fig. 3.8. It is necessary to point out that no additional scaling factor is applied to the accelerograms.

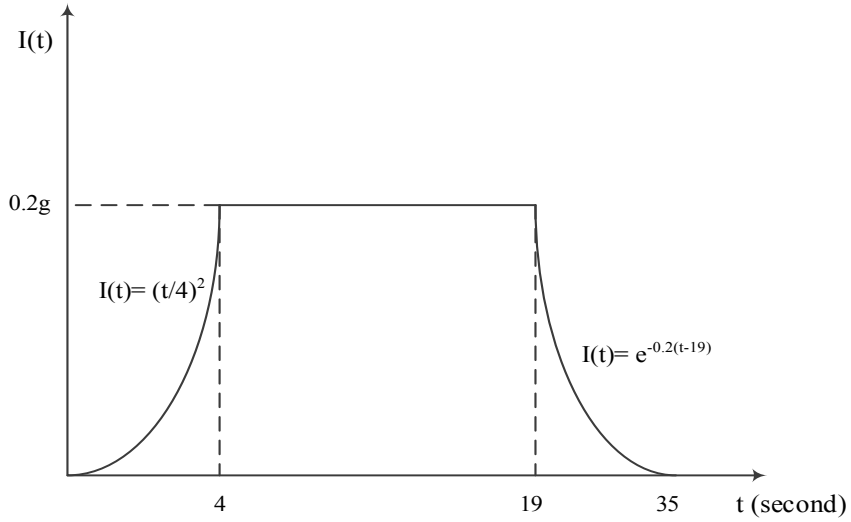

Figure 3.7 Shape function used to generate artificial accelerograms of Set 4.

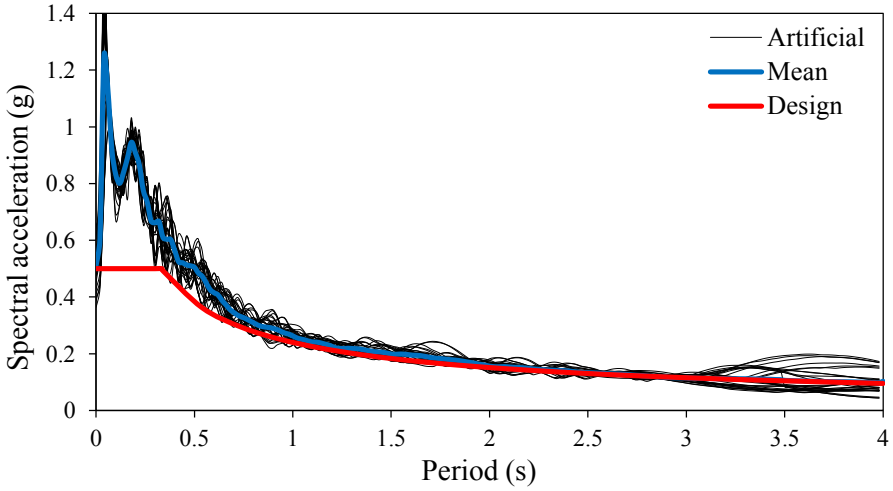

Figure 3.8 Scaled response spectra of the accelerograms of Set 4, 5% damping.

Chapter 4

Selection of Spectrum-compatible Accelerograms for Nonlinear Time-history Analysis

4.1 Introduction

As described in Chapter 3, four sets of accelerograms were selected for use in the time-history analysis in this study. They are, Set 1 - Scaled real accelerograms; Set 2 - Modified real accelerogram; Set 3 - Simulated accelerograms; and Set 4 - Artificial accelerograms. As required by ASCE/SEI (2010), the selected accelerograms for the time-history analysis should be properly scaled such that the 5% damped mean spectrum of the set is above the design spectrum for all the periods between 0.2T - 1.5T, where T is the fundamental period of the bridge for the direction of the response being analyzed. In this study, the scaling method proposed by Amiri-Hormozaki (2003) was used. According to this method, first, the set of the accelerograms was scaled such that the area under the 5% damped response spectrum for each accelerogram within the period range of 0.14 s and 1.20 s is equal to the area under the design spectrum within the same period range. Then, additional scaling factor was applied to each accelerogram of the set in order to make the mean spectrum of the set above the design spectrum. It should be noted that the additional scaling factors for the four sets of the accelerograms are different. They were determined by trial and error, and these factors were discussed in Chapter 3. For ease of discussion, the seismic intensity corresponding to the scaling procedure described above is referred to as $1.0Sa_{Area}$. In this study, two additional

intensity levels were also considered in the analysis which are $0.5Sa_{Area}$ and $2.0Sa_{Area}$. The highest intensity level ($2.0Sa_{Area}$) was selected based on the finding given in Heidebrecht (1995) that seismic ground motions about two to three times the design level might occur at the location of the structure. Furthurmore, the three intensity levels, i.e., $0.5Sa_{Area}$, $1.0Sa_{Area}$, and $2.0Sa_{Area}$, were used in this study in order to cover the responses of the two bridges from elastic to inelastic.

Nonlinear time-history analyses were conducted by subjecting the two bridge models to the selected sets of accelerograms. Among a number of response parameters from the analyses, deck displacements, expansion bearing displacements, curvature ductilities at the end sections of the columns which are under the fixed bearing and the expansion bearing, and the base shear, were used in this study. The base shear represents a global force demand on a bridge structure subjected to seismic motions. It is also an indicator of the seismic moments in the columns. The deck displacement is a global deformation parameter, and it represents the sum of the displacements of both bearing and column. The curvature ductility, on the other hand, is a local deformation parameter and represents the extent of inelastic deformations at a specified section of a structural member. The curvature ductility for a given section of a member represents the ratio of the maximum curvature experienced during the response to the yield curvature of the section.

Please take note that the column displacement was not considered in the investigation. This is because the column displacement can be determined by using the deck displacement subtracted the expansion bearing displacement as discussed in Chapter 2. More specifically, the observations of the results for the deck displacement and the expansion bearing displacement will be similar to those of the column displacement.

For each excitation motion, maximum values for the response parameters mentioned above were computed. These maximum values are the peak values (i.e., absolute values) for the response parameters considered from a single time-history analysis. Given the large number of time-history analyses, and the large number of structural members in bridge models, the consideration of the results from each time-history analysis was impractical. Therefore, deck displacements, expansion bearing displacements, curvature ductilities at the end sections of the columns, and the base shear resulting from the sets of excitations were statistically analyzed to compute the mean (M) and the mean plus one standard deviation (M + SD) values. The coefficient of variation (COV) was also computed for the response parameters mentioned above in order to evaluate the dispersion of the response resulting from each set of accelerograms.

4.2 Analysis Results of the Bridge #1

4.2.1 Statistics results

The results from the dynamic analysis of the Bridge #1 are presented in Figs. 4.1 to 4.5. While it is normal practice to present forces first and then deformations, in this chapter the deformations (e.g., deck displacement, expansion bearing displacement, and curvature ductilities of columns) are discussed first followed by a discussion of the shear forces. This is for better understanding of the results, i.e., some characteristics of the shear forces can be explained based on the curvature ductilities. Figure 4.1 shows the results for deck displacements, the displacements of expansion bearing are described in Fig. 4.2, and Figs. 4.3 and 4.4 show the curvature ductilities for the columns of Pier 1 (fixed bearings were installed) and Pier 2 (expansion bearings were installed), respectively. Figure 4.5 presents the total shear

forces at the base of Piers 1 and 2. The vertical bars in these figures represent the mean response values, and the line extensions to the bars show the M + SD response values.

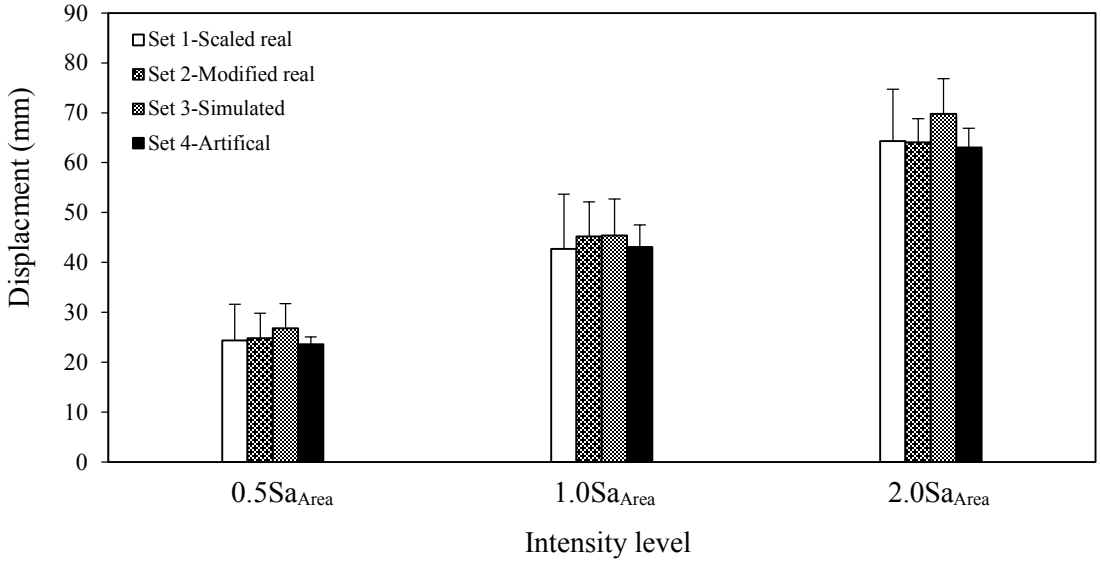

Figure 4.1 Deck displacements of Bridge #1.

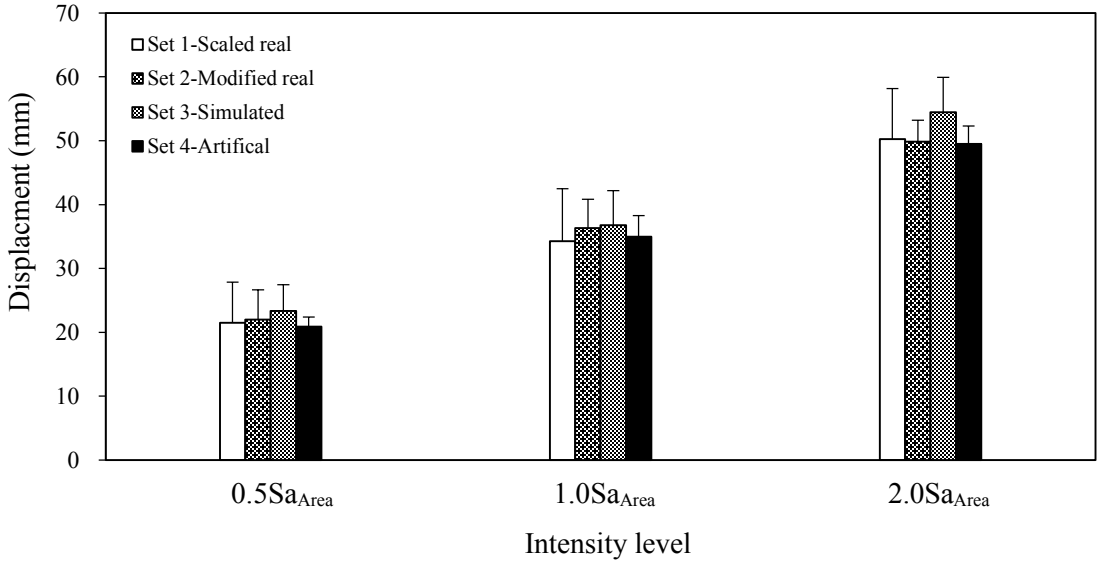

Figure 4.2 Expansion bearing displacements of Bridge #1.

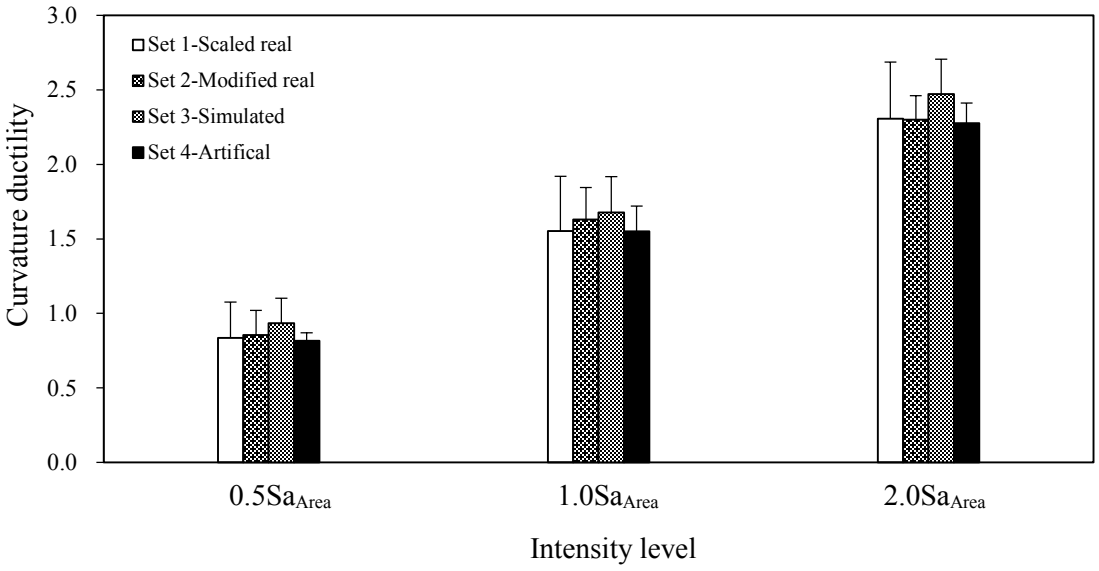

Figure 4.3 Column curvature ductilities of Bridge #1 (Pier 1).

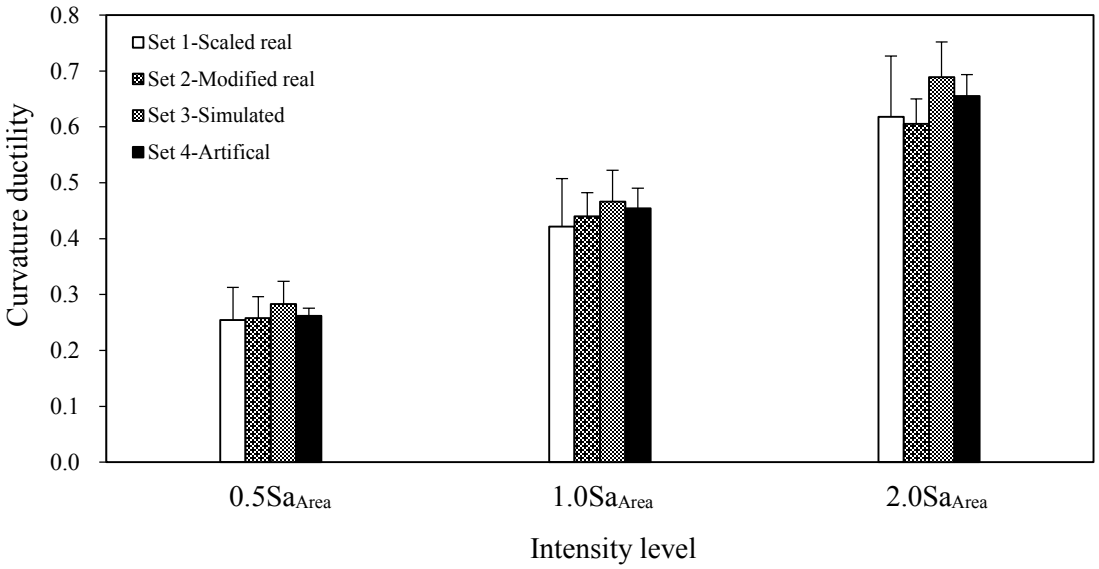

Figure 4.4 Column curvature ductilities of Bridge #1 (Pier 2).

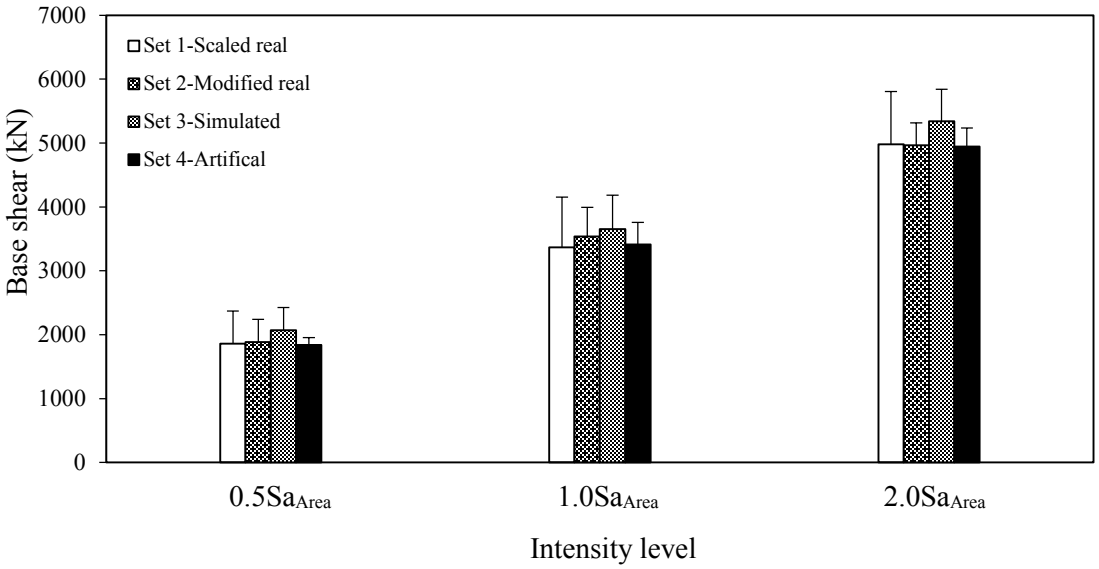

Figure 4.5 Base shears of Bridge #1.

The variations of the responses from the sets are quantified by considering the differences between the largest and the smallest mean response values from the sets. For simplicity, these differences are expressed in percentages relative to the smallest mean responses. The use of the mean values is considered appropriate because these values are more "stable" (i.e., they have smaller variations) than the M + SD values. In addition, the use of mean responses is recommended by ASCE (2010) when seven or more excitations are included in the set of the accelerograms for the analysis. Table 4.1 shows the differences of the largest and smallest mean responses values from the selected sets of excitations for Bridge #1.

Table 4.1 Ranges of the difference (in percentage) between the largest and smallest mean responses values from the selected sets of excitations for Bridge #1.

Intensity level	Deck displ.	Exp. displ.	Column curvature ductility@ Pier1	Column curvature ductility@ Pier2	Base shear
$0.5Sa_{Area}$	3 to 14	3 to 12	3 to 15	3 to 14	3 to 13
$1.0Sa_{Area}$	1 to 6	2 to 7	3 to 7	2 to 7	2 to 7
$2.0Sa_{Area}$	2 to 11	2 to 10	2 to 11	1 to 10	1 to 8

The results in Figs. 4.1 to 4.5 show that the excitations of Set 3 (Simulated accelerograms) produce the largest responses. Note that the deformation responses from Set 2 (Modified real accelerograms) are very close to those from Set 1 when the accelerograms scaled to the intensity level of $1.0Sa_{Area}$, which can be considered representative of the ground motions for the design earthquake according to CHBDC (2010). This gives a great advantage of using either of these two sets of accelerograms for the time-history analysis of bridges in eastern Canada due to the fact that few strong-motion records are available from earthquakes occurred in eastern Canada. Among the four sets of accelerograms considered in this study, the accelerograms of Set 4 (Artificial accelerogram) provide the smallest responses except for the curvature ductility of the column of Pier 2 in which the expansion bearings were installed. In terms of the standard deviation of the response parameter, the results in Figs. 4.1 to 4.5 show that the accelerograms of Set 1 (Scaled real accelerograms) produce the largest standard deviation, while the accelerograms of Set 4 (Artificial accelerograms) produce the smallest standard deviation.

For better understanding the dispersion of the response from each set of the accelerograms, Figures. 4.6 to 4.10 show the results for coefficients of variation (COV) in terms of the deck displacement, expansion bearing displacement, curvature ductilities of columns of Pier 1 (fixed bearings were installed) and Pier 2 (expansion bearings were installed), and base shear, respectively. It can be seen in the figures that seismic excitations of Set 4 (Artificial accelerograms) give the smallest COV of the response, and those of Set 1 (Scaled real accelerograms) give the largest COV. It was found that at the intensity level of $0.5Sa_{Area}$, the COV of the response using the accelerograms of Set 1 was about 6 times than that using the accelerograms of Set 4 while at the intensity level of $2.0Sa_{Area}$, the COV of the response

based on the accelerograms of Set 1 was about 3 times than that based on the accelerograms of Set 4. The larger difference for the COV between the accelerograms of Set 1 and Set 4 was due to the characteristics of the accelerograms of each set. As described in Chapter 3, the accelerograms of Set 1 were selected from earthquakes around world. Even though the characteristics of ground motions of the accelerograms are representative of ground motions in eastern Canada according to Naumoski et al. (1988, 1993), it can be reasonably assumed that the response of the bridge would be quite different from accelerogram to accelerogram because the accelerograms were collected from different sources.

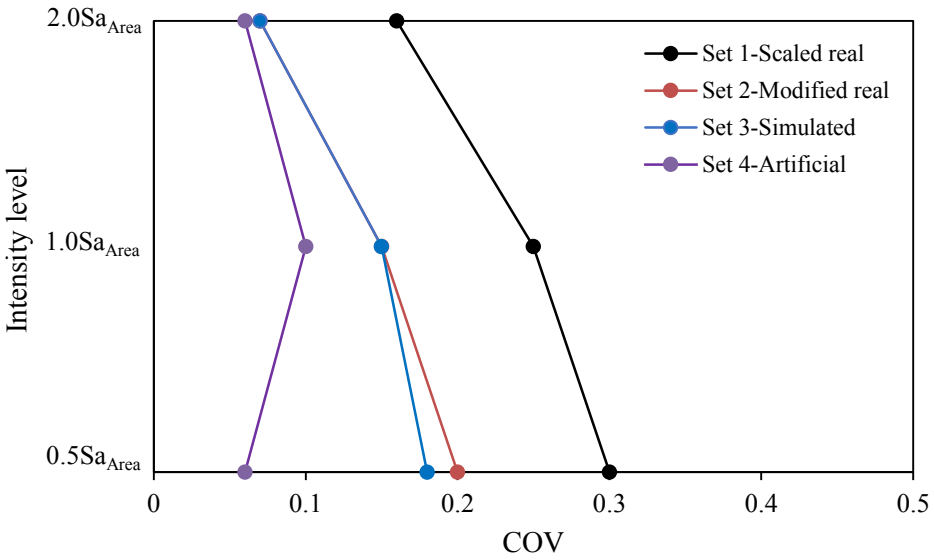

Figure 4.6 Coefficients of variation (COV) of deck displacements of Bridge #1.

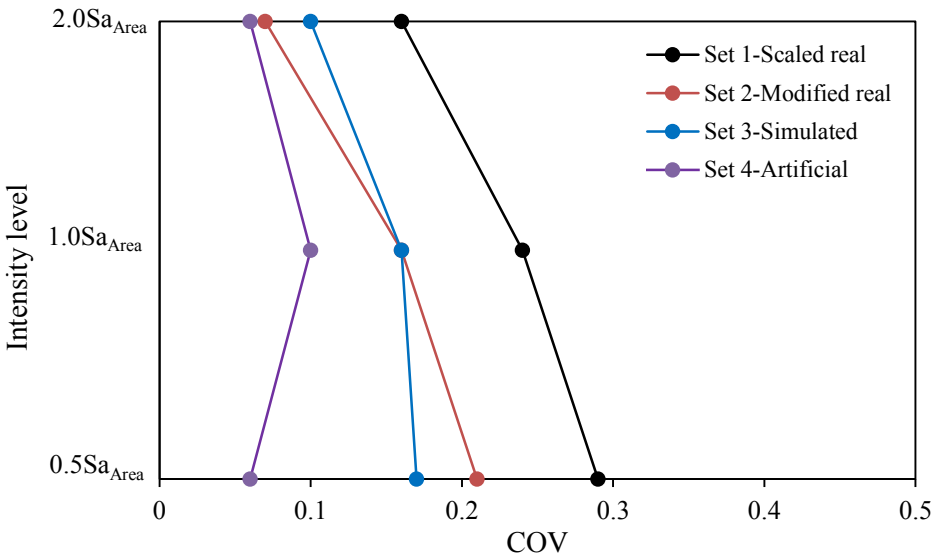

Figure 4.7 Coefficients of variation (COV) of expansion bearing displacements of Bridge #1.

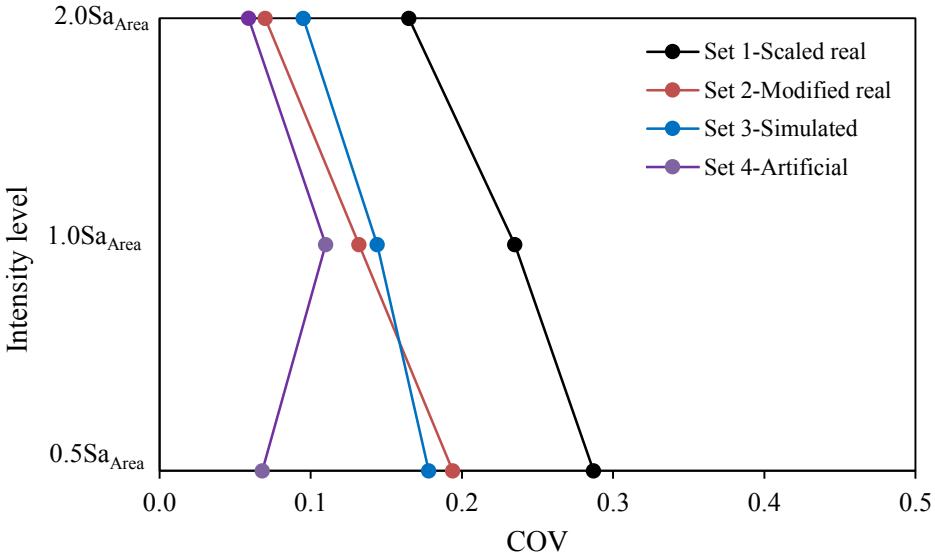

Figure 4.8 Coefficients of variation (COV) of column curvature ductilities of Bridge #1 (Pier 1).

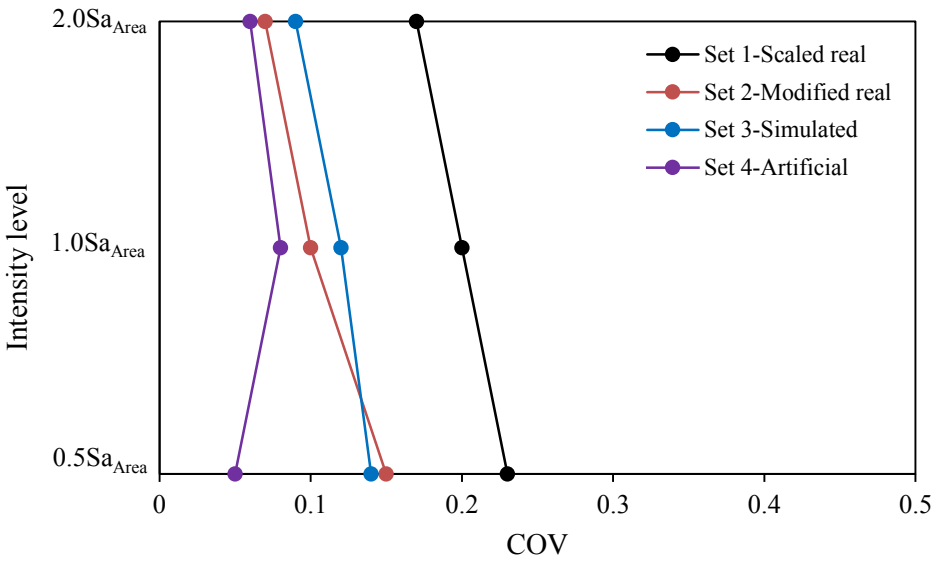

Figure 4.9 Coefficients of variation (COV) of column curvature ductilities of Bridge #1 (Pier 2).

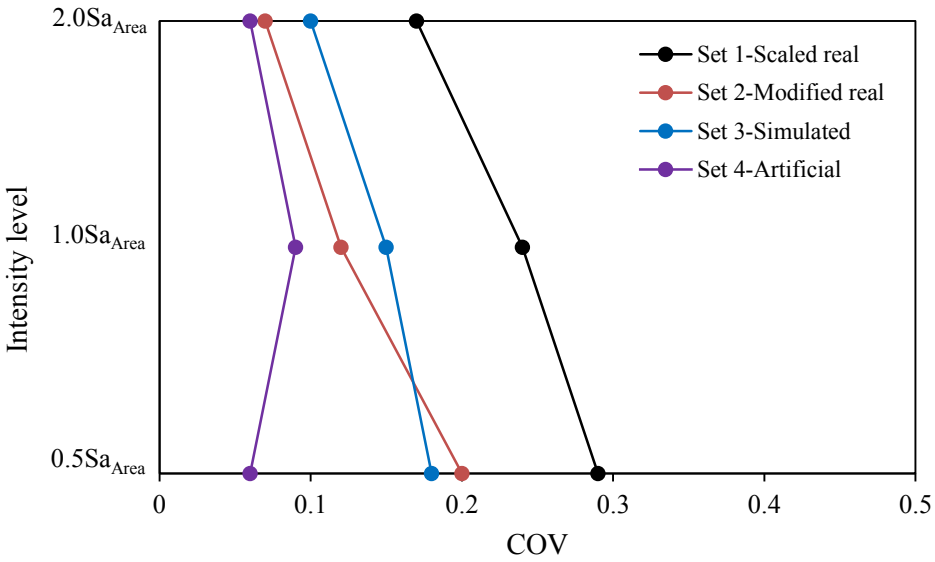

Figure 4.10 Coefficients of variation (COV) of base shears of Bridge #1.

Therefore, larger COV was observed of the results using the accelerograms of Set 1. The relatively small COV of the response obtained from the seismic excitations of Set 4 was because of the method used to generate the accelerograms as discussed in Chapter 3. In general,

the artificial accelerograms were generated to match the shape function as illustrated in Fig. 3.7, Chapter 3. The maximum intensity of the shape function corresponds to the peak ground acceleration (PGA) of the location of the structure. For this study, it is equal to PGA of 0.20 g for Montreal for the probability of exceedance of 10% in 50 years. As a result, the PGA of each accelerogram of Set 4 is approximately equal to 0.20 g. Given the relatively short period of the first mode of the bridge, the response of the bridge is dominated by PGA not Sa. Therefore, it is not surprise that each accelerogram gives will similar response. Another reason of the smaller COV for the response using records of Set 4 can be explained by the smaller deviation of the response spectra for the accelerograms of the set (see Fig. 3.8, Chapter 3). It also can be seen in Figs. 4.6 to 4.10 that the COV for the responses from the accelerograms of Sets 2 and 3 are very close. The results in Figs. 4.6 to 4.10 also show that the COV of the response corresponding to lower excitations is much smaller than that to the higher excitations. For example, for the deck displacement, at the intensity level of $0.5Sa_{Area}$, COV of the response was about 0.2 from the accelerograms of Set 2; while it was about 0.1 when the accelerograms were scaled to $2.0Sa_{Area}$.

4.2.2 Behavior of the Bridge #1

While the focus of this section is to discuss the effects of different types of spectrum-compatible excitations on the responses of two bridges, it is useful to discuss briefly the behavior of the bridge under different levels of the seismic excitations. The results in Fig. 4.1 show that the deck displacements from the ground motions scaled to $0.5Sa_{Area}$, $1.0Sa_{Area}$, and $2.0Sa_{Area}$ are about 25 mm, 45 mm, and 65 mm. Since the displacement is not proportional to the intensity level, it indicates nonlinear deformations occurred in the substructure, i.e., either

on the bearings or on the columns, or both of them. For Bridge #1 in this study, both expansion bearings and the columns of Pier 1 behave inelastically during the response. Detailed discussion of this issue is given in the section below.

The displacements of expansion bearings (shown in Fig. 4.2) at the three intensity levels $0.5Sa_{Area}$, $1.0Sa_{Area}$, and $2.0Sa_{Area}$ are very close to those of the deck. This is because the displacement of the column under the expansion bearing was very small as explained in Section 2.5.3, Chapter 2. It is necessary to mention that the expansion bearing behaves inelastically at all the three intensity levels considered in the study. This is because the displacement is larger than the yield displacement (i.e., 5 mm, see Table 2.1, Chapter 2) used to define the response curve for the bearing. The bearing displacement at the intensity level of $2.0Sa_{Area}$ almost reached its maximum displacement (i.e., 50 mm see Table 2.1, Chapter 2) before it fails. It indicates the expansion bearing might fail when the seismic intensity is larger than $2.0Sa_{Area}$ which is about twice the design earthquake.

The results for the curvature ductilities of columns of Pier 1 (fixed bearings were installed) and Pier 2 (expansion bearings were installed) indicate the Pier 1 and Pier 2 of Bridge #1 behaved differently during the seismic response. The column of Pier 1, in which fixed bearings were installed, behaves elastically (ductility is less than 1.0) at the seismic excitation of $0.5Sa_{Area}$. However, it behaves inelastically because the curvature ductility at the seismic excitations of $1.0Sa_{Area}$ and $2.0Sa_{Area}$ is larger than 1.0. More specifically, the curvature ductility at the highest intensity level considered in this study, i.e., $2.0Sa_{Area}$ was about 2.5. Such result indicates that the nonlinear deformation was not significant in the column of this bridge. Nielson (2005) conducted a study on the seismic fragility of highway bridges in moderate seismic zones in the United States, and reported that the ductilities of columns were

about 16 of the bridges considered in his study. Much larger column ductilities (about 30) were observed on the bridges reported by Ghee (1981). According to Dutta and Mander (2000), the piers will suffer slight damage if the ductility is 2.01, moderate damage if the ductility is 6.03, extensive damage if the ductility if 11.07, and the piers are considered complete collapse if the ductility is 23.65. According to this recommendation, Pier 1 might undergo slight damage if the seismic excitations are twice than those considered in the design. Regarding the column of Pier 2, in which expansion bearings were installed, the column behaves elastically at the intensity levels of $0.5Sa_{Area}$, $1.0Sa_{Area}$, and $2.0Sa_{Area}$, the curvature ductilities corresponding to these three intensity levels are well below 1.0. For example, the curvature ductility was about 0.25 at the intensity level of $0.5Sa_{Area}$, and was about 0.60 at $2.0Sa_{Area}$. The comparison between the bearing displacement and column curvature ductility shows that the bearing is a more critical component than the column during seismic excitations. This is mainly because the bearing considered in this study almost reached the limit of the deformation before it fails.

The response parameters (deck displacements, expansion bearing displacements, curvature ductilities at the end sections of the columns) discussed above represent deformation demands of the bridge under the seismic excitations. In addition, base shear was used as a force-response parameter on the selection of the most suitable set of accelerograms for the time-history analysis in this study. As mentioned previously, base shear is considered as a global force demand of the bridge due to seismic loading. It is also an indicator of moments in a bridge due to seismic loads (i.e., larger shear force leads to larger bending moment on a column). The results for base shear are presented in Fig. 4.5. Note that the base shear shown in the figure is the total shear forces on the Piers 1 and 2 of 6 columns. It is seen in Fig. 4.5 that the average base shear from the 4 sets of accelerograms at the intensity level of $0.5Sa_{Area}$

was about 1900 kN, at $1.0Sa_{Area}$ was about 3500 kN, at $2.0Sa_{Area}$ was about 4900 kN. The increase of the base shear was not linearly proportional to the increase of the intensity level. This is because Pier 1 behaves inelastically during the seismic response as discussed above.

4.3 Analysis Results of the Bridge #2

4.3.1 Statistics results

The results for the response of the Bridge #2, are presented in Figs. 4.11 to 4.15. The response results (Figs. 4.11 to 4.15) from the four excitation sets show that the largest responses correspond to the excitations of Set 3 (Simulated accelerograms). The ranges of the differences between the largest and the smallest mean responses obtained from the four sets are 2% to 12% for deck displacements, 3% to 14% for expansion bearing displacement, 2% to 19% for curvature ductilities of columns of the Pier 1, 16% to 23% for curvature ductilities of columns of the Pier 2, and 1% to 12% for base shears (see Table 4.2).

Table 4.2 Ranges of the differences (in percentage) between the largest and smallest mean responses values from the selected sets of excitations for Bridge #2.

Intensity level	Deck displ.	Exp. displ.	Column curvature ductility@ Pier1	Column curvature ductility@ Pier2	Base shear
$0.5Sa_{Area}$	6 to 12	3 to 14	6 to 12	16 to 21	4 to 12
$1.0Sa_{Area}$	2 to 12	4 to 14	2 to 11	16 to 23	2 to 12
$2.0Sa_{Area}$	3 to 10	7 to 14	8 to 19	16 to 23	1 to 9

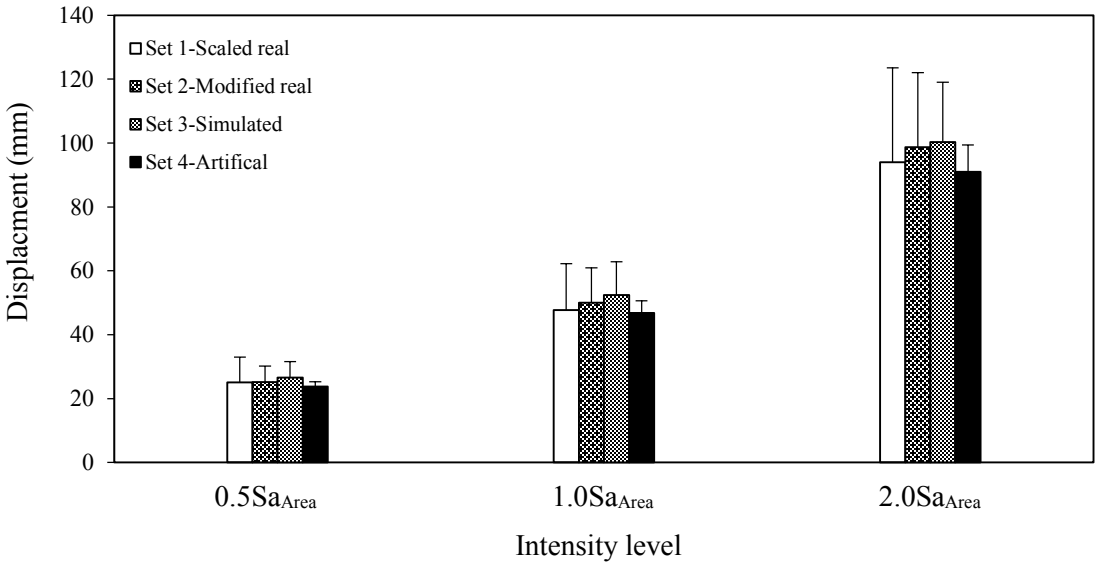

Figure 4.11 Deck displacements of Bridge #2.

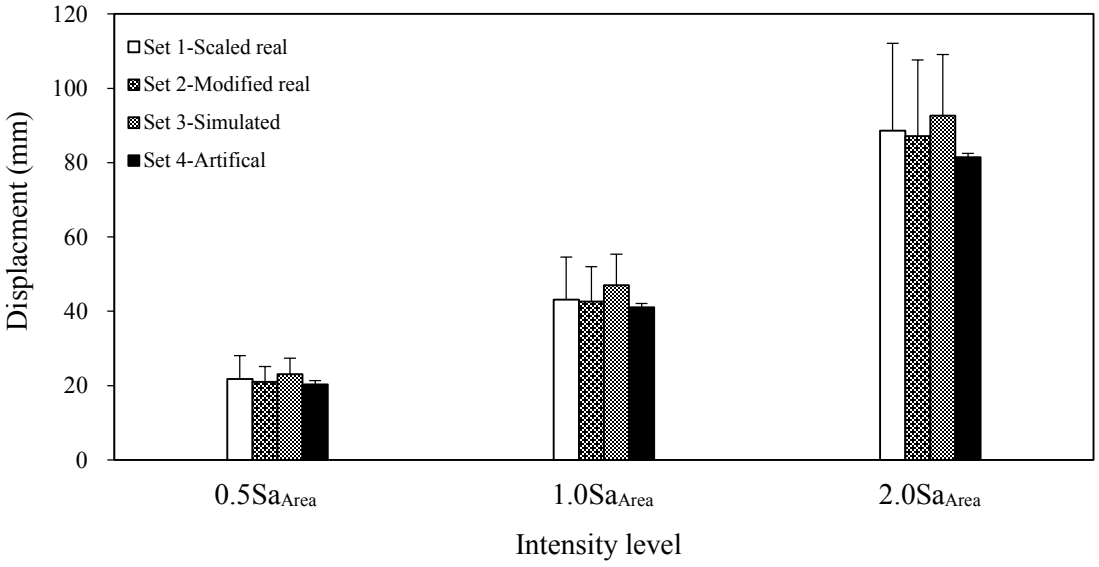

Figure 4.12 Expansion bearing displacements of Bridge #2.

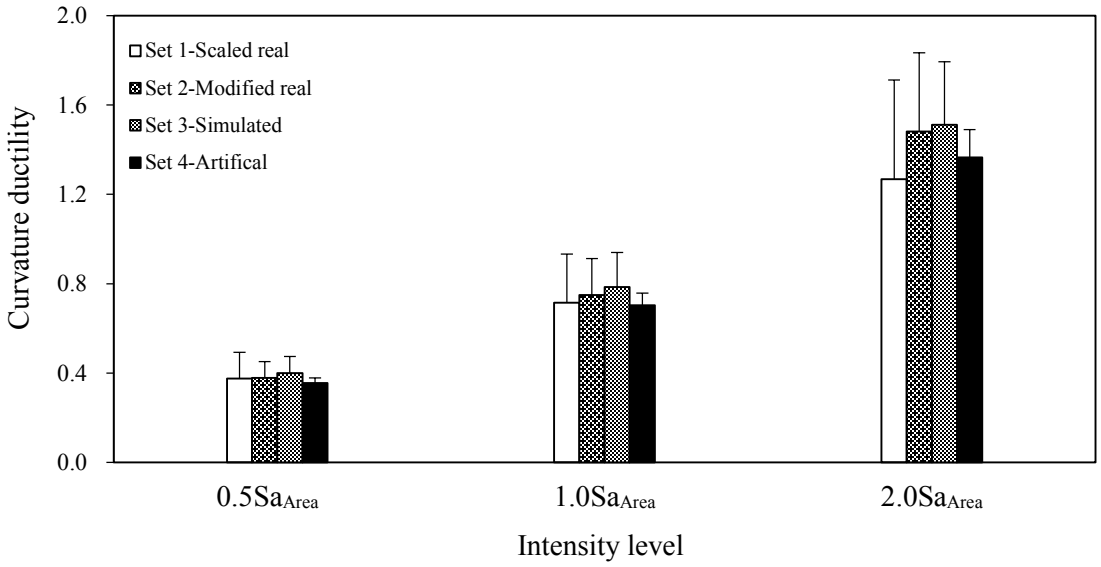

Figure 4.13 Column curvature ductilities of Bridge #2 (Pier 1).

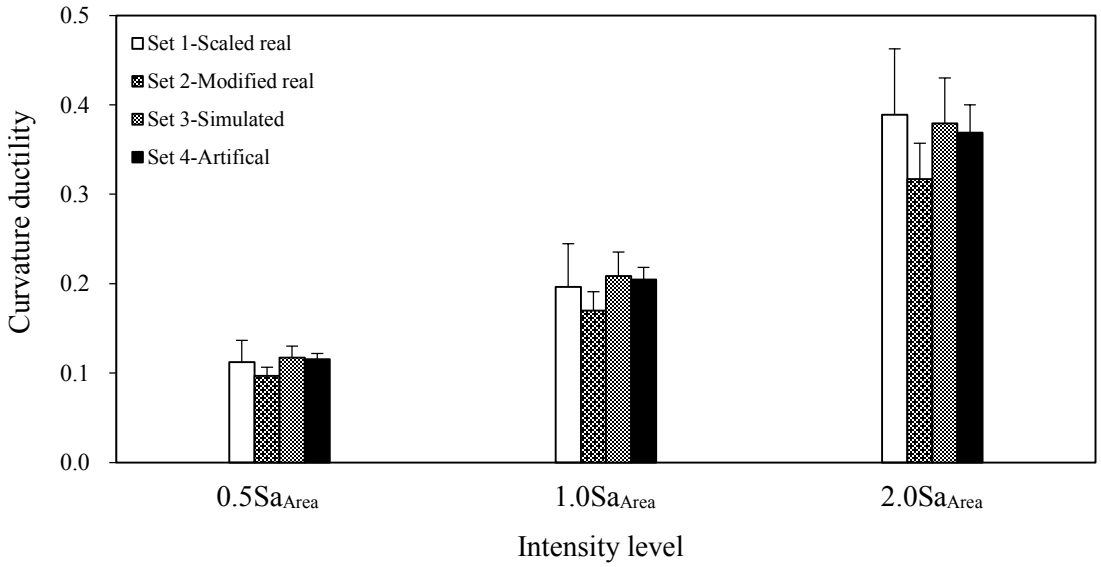

Figure 4.14 Column curvature ductilities of Bridge #2 (Pier 2).

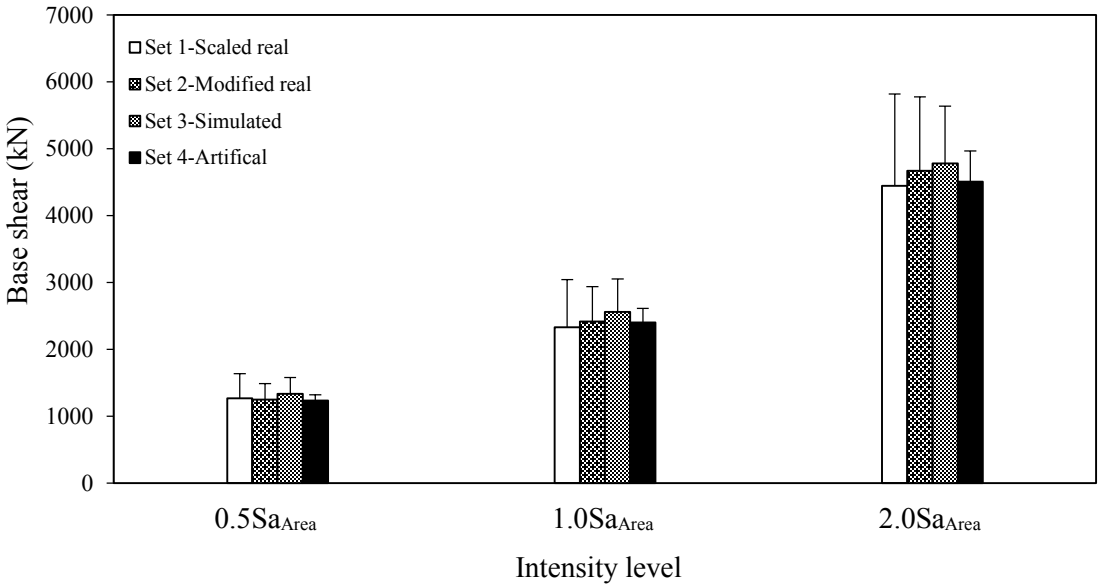

Figure 4.15 Base shears of Bridge #2.

It is interesting to notice that the ranges of the differences of each response parameter are almost the same for the three intensity levels considered. Among the five response parameters used in the analysis, the largest difference for the response parameter from the analyses was observed on the column curvature ductilities of Pier 2. Note that the displacements of bearings of the Bridge #2 are the same as those of the Bridge #1, i.e., fixed bearings are used on the Pier 1, and expansion bearings are used on the Pier 2. However, the dimensions of bearings used in the two bridges are different, the bearing size is 600 mm x 600 mm x 130 mm for Bridge #1, and 450 mm x 350 mm x 100 mm for Bridge #2.

As shown in the Table 4.2 and Figs. 4.11 to 4.15, the differences of the response parameter from the four sets of accelerograms are compatible with each other. As mentioned above, the maximum mean values for the response parameters are associated with the accelerograms of Set 3 (Simulated accelerogram), while the maximum M+SD values correspond to either accelerograms of Set 1 (Scaled real accelerograms) or Set 3 (Simulated

accelerograms) depending on the response parameter and the intensity level considered (see Table 4.3). For example, for the deck displacement, at the intensity level of $0.5Sa_{Area,}$ the maximum value for M+SD corresponds to Set 1; and at the intensity level of $2.0Sa_{Area,}$ it corresponds to Set 3.

The findings of the results for COV of Bridge # 2 (Figs. 4.16 to 4.20) are similar to those for Bridge #1, i.e., the responses for the accelerograms of Set 4 (Artificial accelerograms) have the smallest COV, and those of Set 1 (Scaled real accelerograms) have the largest COV. The accelerograms of Sets 2 (Modified real accelerograms) and 3 (Simulated accelerograms) provide very similar COV. More specifically, COVs of the responses corresponding to accelerograms of Sets 1, 2, 3, and 4 are about 0.31, 0.21, 0.18, and 0.07, respectively. It is necessary to mention that the COVs of the five response parameters of the Bridge #2 considered in this study are almost uniformly distributed except for the column curvature ductilities of the Piers 1 and 2.

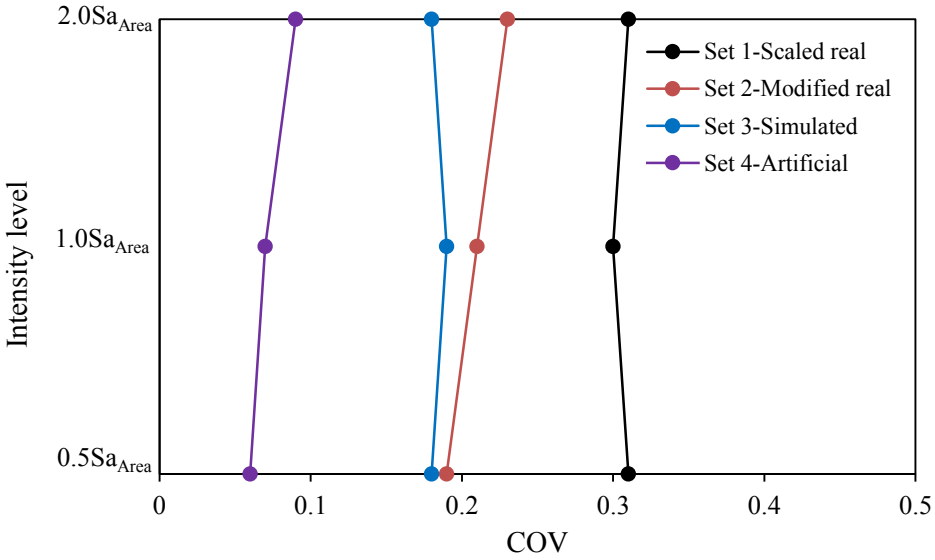

Figure 4.16 Coefficients of variation (COV) of deck displacements of Bridge #2.

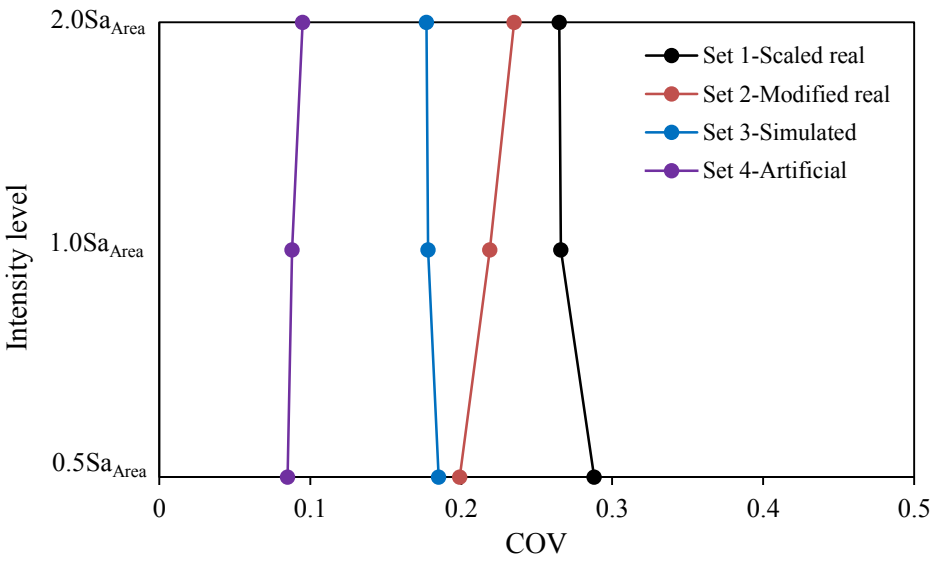

Figure 4.17 Coefficients of variation (COV) of expansion bearing displacements of Bridge #2.

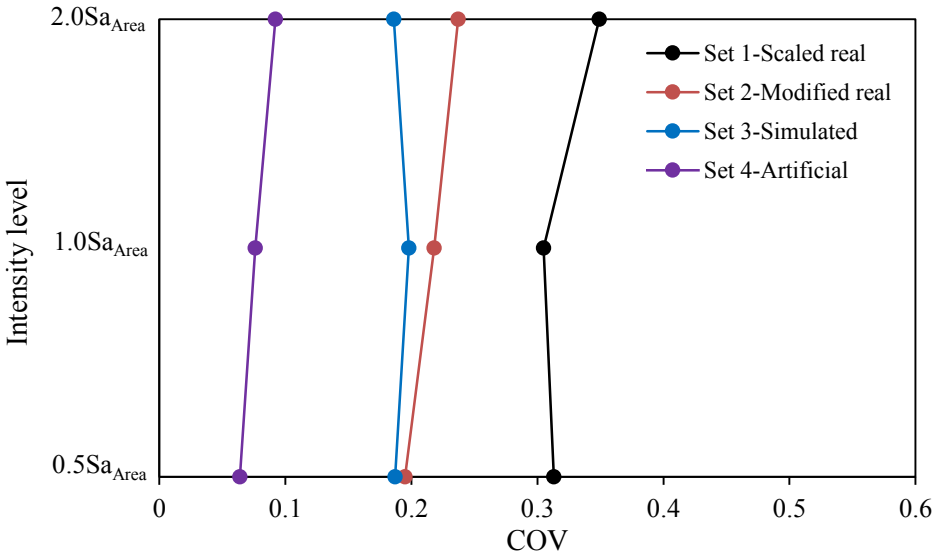

Figure 4.18 Coefficients of variation (COV) of column curvature ductilities of Bridge #2 (Pier 1).

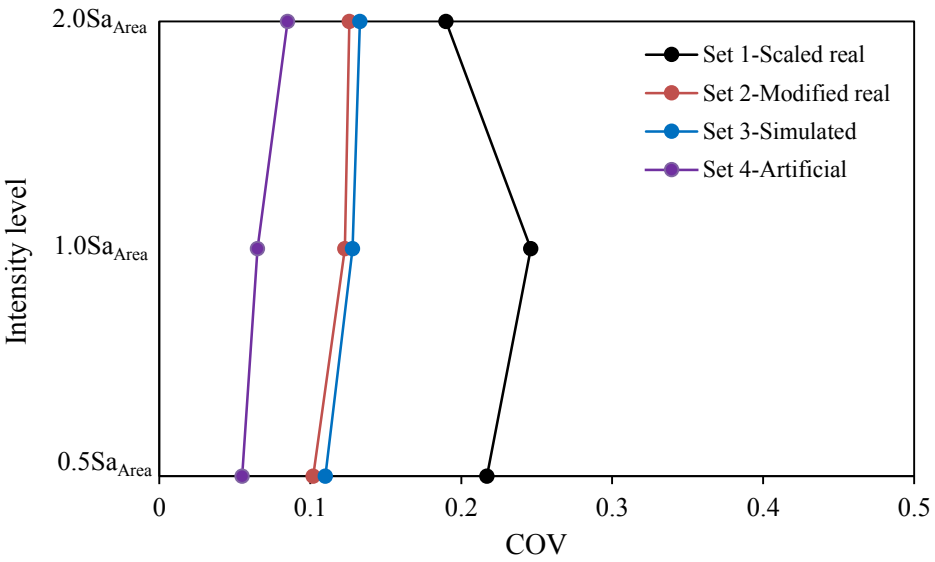

Figure 4.19 Coefficients of variation (COV) of column curvature ductilities of Bridge #2 (Pier 2).

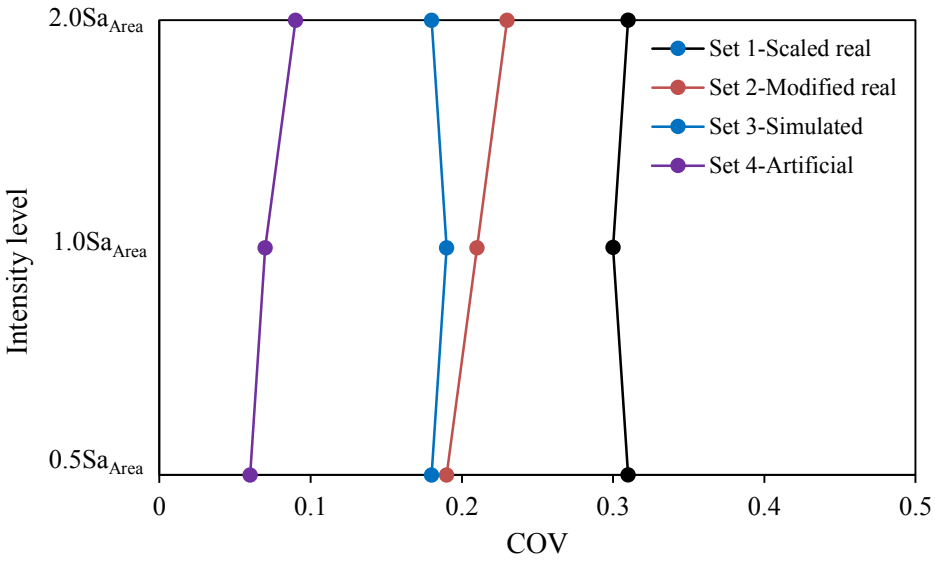

Figure 4.20 Coefficients of variation (COV) of base shears of Bridge #2.

4.3.2 Behavior of the Bridge #2

The performance of Bridge #2 was also investigated in this study. It should be noted that the intensities of seismic excitations used to scale the four sets of accelerograms for the time-history analysis of the Bridge #1 and the Bridge # 2 are the same. The structural systems of the two bridges considered in the study are slightly different. The superstructure of Bridge # 1 consists of a solid slab while the superstructure of Bridge #2 consists of a slab supported by girders. The substructure of the two bridges is very similar; both have three columns at each pier. The only difference is, circular columns are used in Bridge #1 and rectangular columns are used in Bridge #2. Detailed descriptions of the two bridges are given in Chapter 2.

The results for the deck displacements (Fig. 4.11 and Table 4.3) show that the displacement is almost linearly proportional to the intensity level. For example, the deck displacement was about 27 mm for the records scaled to $0.5Sa_{Area}$, and was about 52 mm for the records scaled to $1.0Sa_{Area}$, i.e., the deck displacement at $1.0Sa_{Area}$ is approximately twice the displacement at $0.5Sa_{Area}$. The displacement at $2.0Sa_{Area}$ is slightly less than two times the displacement at $1.0Sa_{Area}$. It indicates very small nonlinear deformations occurred in bearings and/or columns of the substructure system during the response. The observation of results for the deck displacement for the Bridge #2 is different that for the Bridge #1. As discussed above, it has been noticed that significant nonlinear deformations occurred in the substructure.

The expansion bearing displacement of the Bridge #2 is very close to the deck displacement. This finding is the same as that of the Bridge #1 due to the mechanism of the bridge structures. It can be seen in Table 4.3 that the expansion bearing displacement of the Bridge #2 is almost the same as that of the Bridge #1 for the accelerograms scaled to $0.5Sa_{Area}$. However, the bearing displacements of the Bridge #2 are about 27% and 70% larger than those

of the Bridge #1 for the intensity levels of $1.0Sa_{Area}$ and $2.0Sa_{Area}$, respectively. Such results indicate that the bearings used in the Bridge #2 are much flexible than those in the Bridge #1. This can also been seen in Table 2.1 in Chapter 2 in which the ultimate lateral deformation of the expansion bearing used in the Bridge #2 (75 mm) is much larger than that used in the Bridge #1 (50 mm).

As expected the column curvature ductilities of the Bridge #2 are much smaller than those of the Bridge #1. More specifically, the ductilities of the Bridge #2 are about half of the ductilities of the Bridge #1. The results for the column curvature ductilites in Table 4.3 show that the columns of the Piers 1 and 2 of the Bridge #2 behave elastically (ductility is less than 1.0) for all the three seismic excitation levels considered in the analysis except that the columns of the Pier 1 behave inelastically at the intensity level of $2.0Sa_{Area}$. The maximum curvature ductility of the columns of the Pier 1 of the Bridge #2 was only about 1.5 which shows very small nonlinear deformation occurred in the column during the response.

The total shear forces at the bases of the Piers 1 and 2 of the Bridge #2 are significantly smaller than that of the Bridge #1. For example, the base shear of the Bridge #2 is about 65% of the Bridge #1 for the intensity level of $0.5Sa_{Area}$, 70% for the intensity level of $1.0Sa_{Area}$, and 90% for the intensity level of $2.0Sa_{Area}$. A larger difference of the base shear between the Bridge #1 and the Bridge #2 was observed at the intensity level of $0.5Sa_{Area}$. It is due to the difference between the effective weight of the bridge, i.e., the weight of the Bridge #2 is much smaller (about 50%) than that of the Bridge #1. It is necessary to mention that both bridges behave almost elastically at the intensity level of $0.5Sa_{Area}$ except the expansion bearings.

Table 4.3 Maximum mean and mean + standard deviation (M+SD) response values from the selected sets of excitations.

Bridge	Intensity level	Deck displ. (mm)		Exp. displ. (mm)		Column curvature ductility @Pier1		Column curvature ductility @Pier2		Base shear (kN)	
		Mean	M+SD	Mean	M+SD	Mean	M+SD	Mean	M+SD	Mean	M+SD
#1	$0.5Sa_{Area}$	27 (Set 3)	32 (Set 3)	23 (Set 3)	28 (Set 1)	0.93 (Set 3)	1.10 (Set 3)	0.28 (Set 3)	0.32 (Set 3)	2072 (Set 3)	2425 (Set 3)
	$1.0Sa_{Area}$	45 (Set 3)	54 (Set 1)	37 (Set 3)	42 (Set 1)	1.68 (Set 3)	1.92 (Set 1)	0.47 (Set 3)	0.52 (Set 3)	3653 (Set 3)	4182 (Set 3)
	$2.0Sa_{Area}$	70 (Set 3)	77 (Set 3)	54 (Set 3)	60 (Set 3)	2.47 (Set 3)	2.71 (Set 3)	0.69 (Set 3)	0.75 (Set 3)	5343 (Set 3)	5841 (Set 3)
#2	$0.5Sa_{Area}$	26 (Set 3)	33 (Set 1)	23 (Set 3)	28 (Set 1)	0.40 (Set 3)	0.49 (Set 1)	0.12 (Set 3)	0.14 (Set 1)	1334 (Set 3)	1637 (Set 1)
	$1.0Sa_{Area}$	52 (Set 3)	63 (Set 3)	47 (Set 3)	55 (Set 3)	0.79 (Set 3)	0.94 (Set 3)	0.21 (Set 3)	0.25 (Set 1)	2558 (Set 3)	3052 (Set 3)
	$2.0Sa_{Area}$	100 (Set 3)	77 (Set 3)	92 (Set 3)	112 (Set 1)	1.51 (Set 3)	1.79 (Set 3)	0.38 (Set 3)	0.46 (Set 1)	4781 (Set 3)	5819 (Set 1)

4.4 Summary

The main findings from the results of the time-history analyses using the four sets of accelerograms considered in this Chapter are summarized as follows:

- The maximum mean values of the response parameters are from the accelerograms of Set 3 (Simulated accelerograms) whereas the minimum values are provided by the accelerograms of Set 4 (Artificial accelerograms).
- The maximum M + SD values of the response parameters are from the accelerograms of either Set 3 or Set 1 (Scaled real accelerograms).
- The responses from the accelerograms of Set 1 have the largest COV (i.e., coefficient of variation), while those of Set 4 have the smallest COV. The COVs of the responses using accelerograms of Set 2 (Modified real accelerograms) and Set 3 are very close.
- Among the four sets of the accelerograms, simulated accelerograms (Set 3) are preferred for the time-history analysis given the smaller standard deviation of the response parameters.

Chapter 5

Minimum Number of Accelerograms Required for Time-history Analysis

5.1 Introduction

The nonlinear time-history analysis is the most reliable method for the assessment of the behavior of bridges subjected to seismic loads. It has been widely used in research on the performance of bridges with the purpose of the validation and the improvement of the code provisions for seismic design. In recent years, the nonlinear time-history analysis has been extensively used for research related to performance-based earthquake engineering (Moehle and Deierlein 2004). In design practice, the application of nonlinear analysis is very limited, and has been used only for the seismic evaluation of important bridges.

Given the progress in earthquake engineering in the last few decades and the availability of new-developed advanced methods and software for nonlinear modelling and analysis of bridges, recent editions of modern bridge codes allow the use of nonlinear dynamic analysis in the design of bridges located in seismic regions (e.g., AASHTO 2007; ASCE 2010; CHBDC 2010).

To conduct time-history analysis, the number of accerlerograms used in the analysis should be decided first. According to ASCE/SEI-7 (2010), three accelerograms (as a minimum) or more than seven accelerograms should be used for the nonlinear time-history analysis. If less than seven accelerograms are used, the maximum values of the response parameters from

the analyses should be considered for the design. If seven or more accelerograms are used, then the average values of the response parameters should be used. However, the minimum number of accelerograms required for the time-history analysis specified in NIST (2011) is 30, which is much larger than that in ASCE/SEI-7 (2010). Both AASHTO (2007) and CHBDC (2010) stated that five spectrum-compatible time histories should be used when site-specific time histories are not available. Tremendous research on the evaluation of the seismic performance of building and bridges has been conducted in the past decades. The number of records used in the time-history analysis in these studies is quite different. For example, Cordova et al. (2000) used eight records to investigate the behavior of two composite frame and one steel frame buildings. Lin et al. used 80 records on the development of new intensity measures for the probabilistic seismic demand analysis of reinforced concrete buildings. Based on the discussion above, it can be seen that the number of records required for the time-history analysis in the code is different, i.e., from 3 accelerograms to 30 accelerograms. Meanwhile, the number of time histories used in the research is also different from researcher to researcher.

Given these, the second objective of this study is to investigate the minimum number of accelerograms that should be used in the time-history analysis. It is believed that the finding in the study will be beneficial for the code authorities to improve the seismic provisions of the code. It will be also useful for the design engineers and researchers such that they can use a small number of records in the analysis, but achieve accurate results on the estimation of the seismic response of structures.

Chapter 4 discussed four different methods for obtaining spectrum-compatible acceleration time histories of seismic motions, and it concluded that simulated accelerograms (i.e., Set 3) were appropriate for use for the time-history analysis of the two bridges considered

in this study. For the purpose of investigation of the minimum number of accelerograms that can be used in the time-history analysis, three ensembles of accelerograms were selected from Set 3 - Simulated accelerograms. The ensembles consisted of 5, 10, and 20 accelerograms, respectively, and they were randomly selected from the Set 3 accelerograms. The accelerograms in these ensembles may not be the same due to the randomness of the selection. The response parameters considered in this chapter are the same as those used in Chapter 4, which are the deck displacements, expansion bearing displacements, column curvature ductilities of the Piers 1 and 2, and the base shears. It is necessary to mention that in total *four* ensembles of accelerograms were used in the analyses in this Chapter. They were comprised of 5, 10, 20, and 30 accelerograms in which the response from the 30 accelerograms was used as a *reference* in order to examine the suitability of using 5, 10, and 20 accelerograms in the time-history analysis. Note the number of 30 accelerograms is the total number of accelerograms included in the Set 3 of accelerograms that are used throughout the study.

Two methods were used to scale the accelerograms, one was the partial spectral area (Sa_{Area}) scaling method which was already used in the analyses in Chapter 4, the other was scaling the accelerograms according to $Sa(T_1)$. The latter is considered because $Sa(T_1)$ is currently the most used intensity measure by the practitioners for the design and analysis of bridges subjected to seismic loads. In addition, $Sa(T_1)$ is the intensity measure used in the development of the fragility curves to evaluate the vulnerability of bridges to earthquakes, and a larger number of records are always used for this purpose. Given this, the conclusion of the investigation on the minimum number of accelerograms required for the time-history analysis will be very beneficial for the study on the fragility analysis of bridges. In this Chapter, the results from the accelerograms using partial spectral area scaling method for two bridges are

presented first followed by those using $Sa(T_1)$.

5.2 Determination the Minimum Number of Accelerograms Based on Scaling to Partial Spectral Area Method

As described above, 5, 10, and 20 accelerograms were randomly selected from the Set 3 accelerograms in order to examine the minimum number of accelerograms for the time-history analysis. For ease of discussion, ensembles consisting of 5, 10, 20, and 30 accelerograms are referred to as Ens5, Ens10, Ens20, and Ens30, respectively, hereafter. Figure 5.1 shows the mean response spectra for the accelerograms of Ens5, Ens10, Ens20 using the partial spectral area scaling method, in which the range of the period considered in the calculation of the spectral area is between 0.14 s and 1.2 s. For the purpose of comparison, the design spectrum for Montreal for the probability of exceedance of 10% in 50 years and the mean spectrum for the 30 accelerograms of Set 3-Simulated Accelerograms are superimposed in the figure. Note that the mean spectrum of Ens30 is the same one used in the analyses in Chapter 4. It can be seen in Fig. 5.1 that the mean spectra of the Ens5, Ens10, and Ens20 are above the design spectrum as required by ASCE (2010). It should be noted that in the scaling process the mean spectra of Ens5, Ens10, and Ens20 should be as close as possible to the mean spectrum of Ens30 in which the response is used as a *reference*. The purpose of doing this is to have the accelerograms of the four ensembles scaled to approximately the same intensity

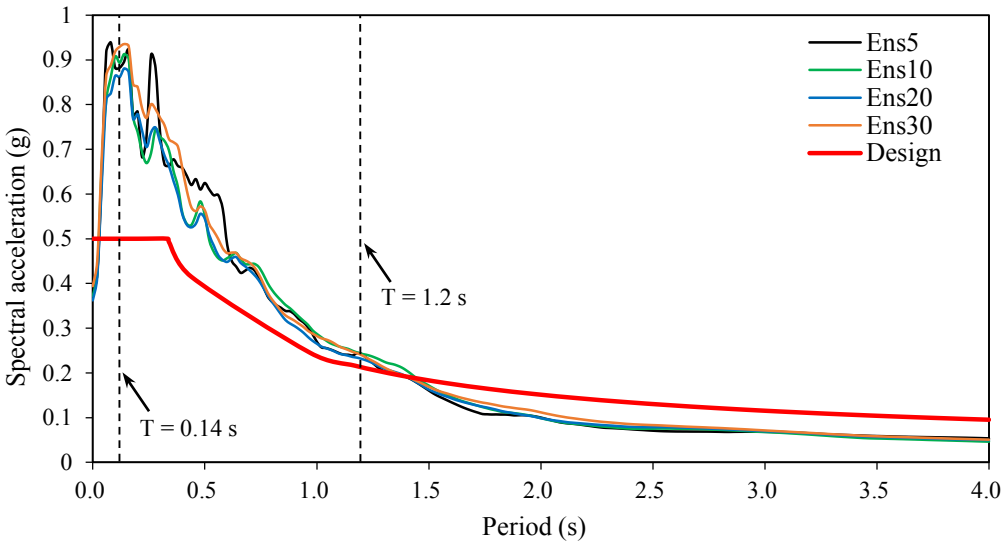

Figure 5.1 Mean response spectra from simulated accelerograms of Ens5, Ens10, Ens 20, and Ens30 using the partial spectral area scaling method.

level such that the responses can be compared to each other. The intensity level used to achieve the mean spectra shown in Fig. 5.1, i.e., the area under the mean spectrum for accelerograms of each ensemble is close to the area under the design spectrum for the period range of 0.14 s to 1.2 s, is referred to as $1.0Sa_{Area}$. Similarly, the intensity levels that the areas under the mean spectrum of the ensemble are half and twice those under the design spectrum for the range of the period mention above are referred to as $0.5Sa_{Area}$ and $2.0Sa_{Area}$, respectively.

5.2.1 Results for Bridge #1

The results for the Bridge #1 using the accelerograms of Ens5, Ens10, Ens20, and Ens30 scaled to the three intensities levels described above are presented in Figs. 5.2 to 5.6. Figure 5.2 shows the results for the mean deck displacements from the four ensembles, Fig. 5.3 presents the results for the mean expansion bearing displacements, while Figs. 5.4 and 5.5 illustrate the results for the mean column curvature ductilities of the pier 1 (fixed bearings were installed), mean column curvature ductilities of the pier 2 (expansion bearings were used),

respectively, and Fig. 5.6 shows the results for the mean base shears. The bar extensions shown in the figures represent the standard deviation. The main findings of the results are summarized as follows,

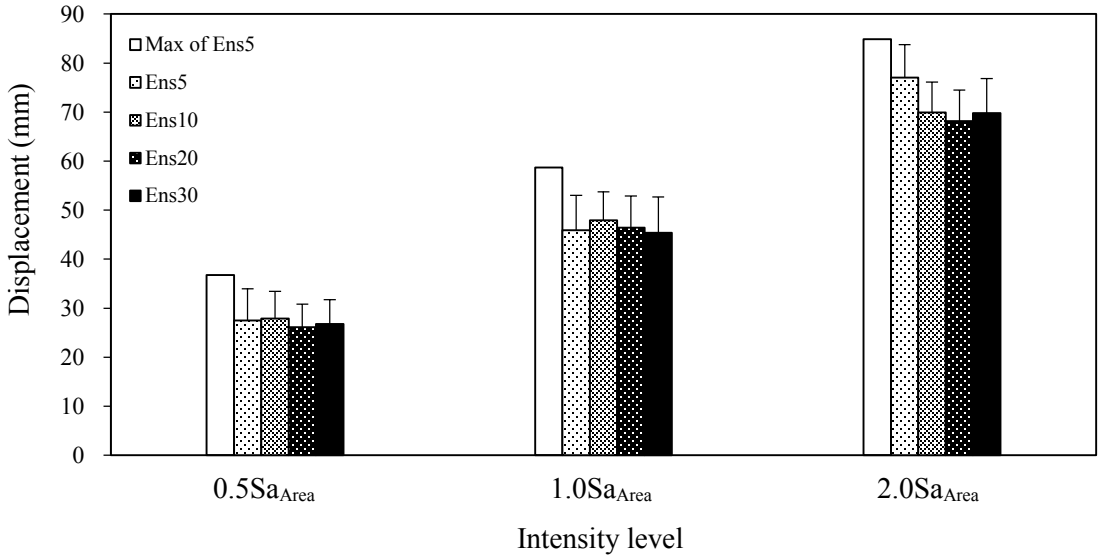

Figure 5.2 Deck displacements of Bridge #1 based on the intensity measure of Sa_{Area}.

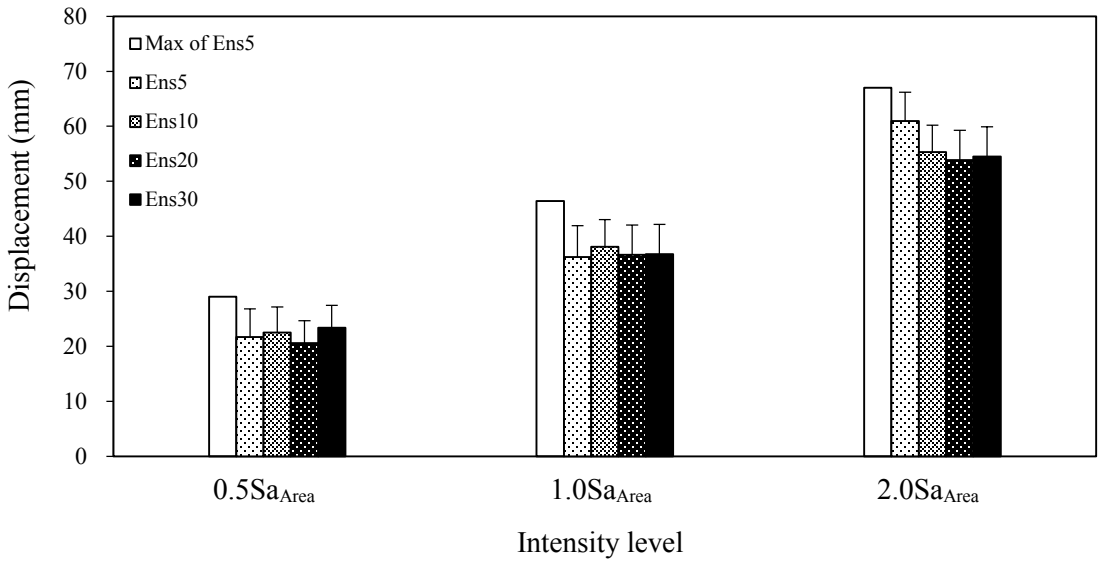

Figure 5.3 Expansion bearing displacements of Bridge #1 based on the intensity measure of Sa_{Area}.

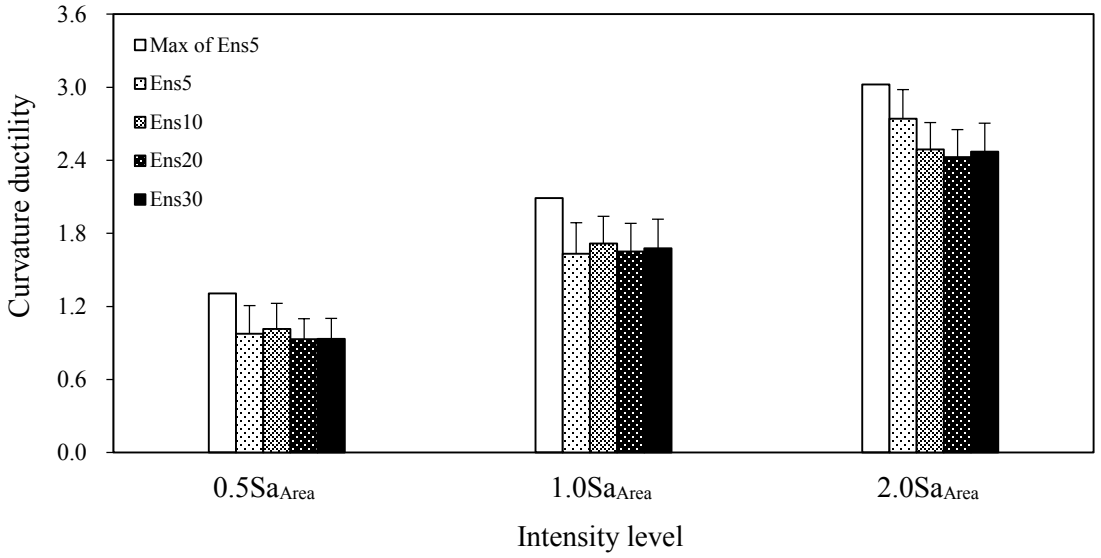

Figure 5.4 Column curvature ductilities of Bridge #1 based on the intensity measure of Sa_{Area} (Pier 1).

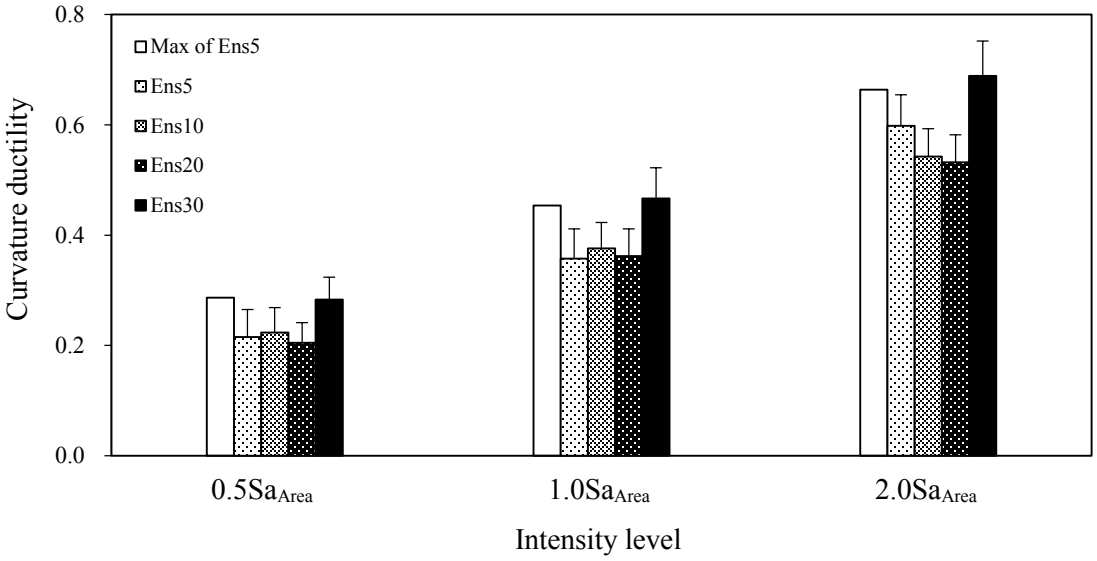

Figure 5.5 Column curvature ductilities of Bridge #1 based on the intensity measure of Sa_{Area} (Pier 2).

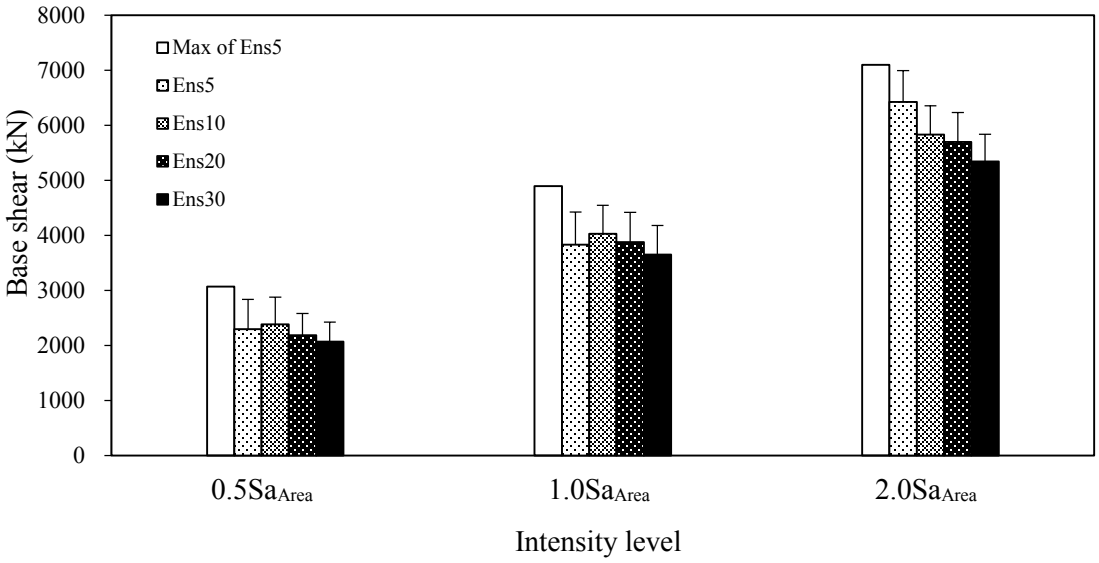

Figure 5.6 Base shears of Bridge #1 based on the intensity measure of Sa_{Area}.

Using 10 accelerograms in the time-history analysis (Ens10)

For the response parameters of the deck displacement, expansion bearing displacement, maximum column curvature ductility of the bridge (represented by the column of Pier 1), the results in the figures show that the responses using Ens10 were very close to those using Ens30 at the three intensity levels. It indicates that 10 accelerograms are sufficient to estimate these responses.

For the column curvature ductilities of the Pier 2 (which presents the minimum column curvature ductility of the bridge), the response using Ens10 was smaller than that using Ens30. More specifically, the difference between the responses using Ens10 and Ens30 was about 20% (Table 5.1) for all the three intensity levels considered in this study.

In terms of the base shear, the accelerograms of Ens10 provided relatively larger response than those of Ens30, the difference was about 15% at the intensity level of $0.5Sa_{Area}$, 10% at the intensity levels of $1.0Sa_{Area}$ *and* $2.0Sa_{Area}$.

Using 20 accelerograms in the time-history analysis (Ens20)

As shown in Table 5.1, using 20 accelerograms in the analysis slightly improved the response results for the base shear. The difference between the results using Ens20 and Ens30 was only about 5% which is negligible in practice. For the other four response parameters, using 20 accelerograms did not improve the results significantly.

Table 5.1 Differences (in percentage) between the response values from ensembles of simulated accelegrams and those from Ens30 for Bridge #1 based on Sa_{Area}.

Response parameter	Intensity level	Max of Ens5	Mean of Ens5	Mean of Ens10	Mean of Ens20
Deck displacement	$0.5Sa_{Area}$	37	3	4	3
	$1.0Sa_{Area}$	29	1	6	2
	$2.0Sa_{Area}$	22	10	0	2
Expansion bearing displacement	$0.5Sa_{Area}$	24	7	4	12
	$1.0Sa_{Area}$	26	1	4	0
	$2.0Sa_{Area}$	23	12	2	1
Column curvature ductility@ Pier 1	$0.5Sa_{Area}$	40	4	8	0
	$1.0Sa_{Area}$	25	3	2	1
	$2.0Sa_{Area}$	22	11	1	2
Column curvature ductility@ Pier 2	$0.5Sa_{Area}$	1	24	21	28
	$1.0Sa_{Area}$	3	23	19	22
	$2.0Sa_{Area}$	3	13	21	23
Base shear	$0.5Sa_{Area}$	48	11	15	5
	$1.0Sa_{Area}$	34	5	10	6
	$2.0Sa_{Area}$	33	20	9	7

Note: Percentage is expressed relative to the mean response value from Ens30.

Using 5 accelerograms in the time-history analysis (Ens5)

The current bridge design codes, i.e., AASHTO (2010) and CHBDC (2010) require using five accelerograms in the time-history analysis. Given this, the responses of the Bridge #1 using five accelerograms, i.e., Ens5, are also evaluated. According to ASCE/SEI 7-10 (ASCE 2010), if less than seven accelerograms are used, the maximum values of the responses should be considered in the design. However, it is not mentioned in either AASHTO (2010) or CHDBC (2010) whether the maximum or the mean response should be used. Therefore, both the maximum and the mean responses from the accelerograms of the Ens5 were considered in the study.

It can be seen in Figs. 5.2 to 5.6 that the mean responses from the accelerograms of Ens5 are very close to those of Ens30 for lower excitation levels (e.g., $0.5Sa_{Area}$ *and* $1.0Sa_{Area}$) except for the column curvature ductility of the Pier 2. It is because the bridge responds almost elastically at these two intensity levels as discussed in Chapter 4. However, at the intensity

level of $2.0Sa_{Area,}$ the mean response from the accelerograms of Ens5 is relatively larger (in average, about 15%) than that of the Ens30. In general, 5 accelergrams are sufficient for the elastic time-history analysis for the design purpose, and they might overestimate the structural response when significant nonlinear deformations occur in the substructure (i.e., piers).

The results in Figs. 5.2 to 5.6 clearly show that the maximum (instead of mean) response from the accelerograms of Ens5 is noticeably higher than that of Ens30. Table 5.1 shows that differences of each response parameter between the using of Ens5 and Ens30 for all the three seismic levels considered in this study. They are between 22% and 48% except for the column curvature ductility of the Pier 2, in which the maximum responses from Ens5 and Ens30 are quite close. It means that the mean response not the maximum response should be considered if five accelerograms are used in the analysis.

It is necessary to point out that the standard deviations of the responses based on Ens5, Ens10, Ens20, and Ens30 are almost the same as for the same intensity level as illustrated in Figs. 5.2 to 5.6.

5.2.2 Results for Bridge #2

The results for the deck displacements, expansion bearing displacements, column curvature ductilities of Piers 1 and 2, and base shears for Bridge #2 are presented in Figs. 5.7 to 5.11. In general, the observations of the results of the Bridge #2 are very similar to those of the Bridge #1. The detailed discussions on the results are given below.

- The results in the figures show that the responses from the accelerograms of Ens10 are very close to those of Ens30 for all the response parameters mentioned above and for

all the intensity levels considered in the analysis. It can be seen in Table 5.2 that the maximum difference of the response between using accelerograms of Ens10 and Ens30 was only about 5%, which was for the deck displacement for the seismic excitation level of $0.5Sa_{Area}$. For all other response parameters and intensity levels, the difference was about 2-4%. It can be concluded that 10 accelerograms are enough for the time-history analysis.

- It is surprising to notice that the mean responses from the accelerograms of Ens5 are almost the same as those of Ens30. As shown in Table 5.2, a relatively larger difference between the responses from Ens5 and Ens30 was observed on the column curvature ductility, which was 7%. For other responses parameters, the difference was about 1-4% which was compatible with that corresponding to Ens10.

- The maximum response provided by Ens5 was about 30% larger than by Ens.30. It indicates that maximum response from the Ens5 was not appropriate to estimate the seismic response of the bridge considered in this study. This conclusion is the same as that for the Bridge #1.

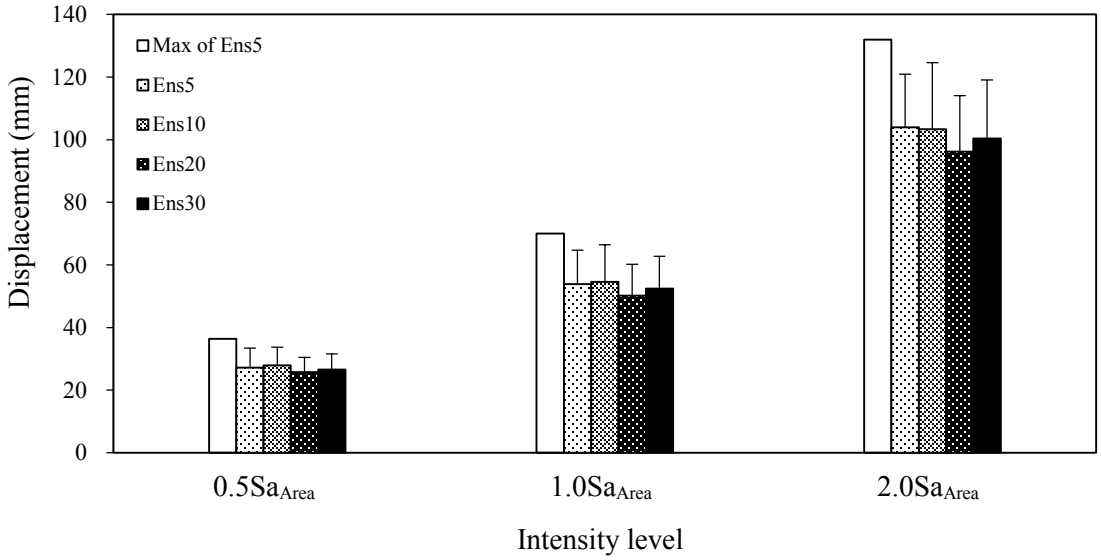

Figure 5.7 Deck displacements of Bridge #2 based on the intensity measure of Sa_{Area}.

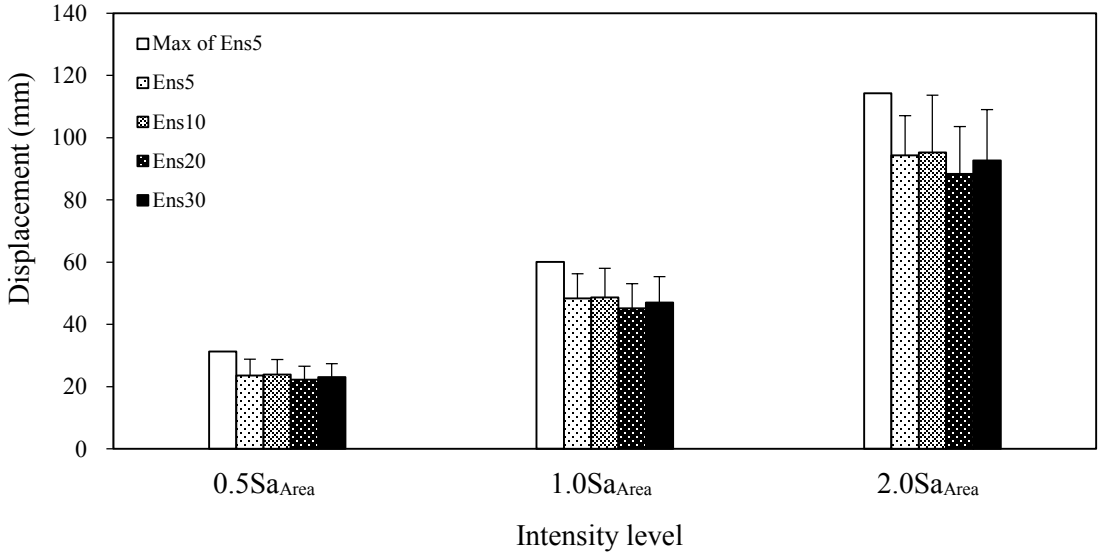

Figure 5.8 Expansion bearing displacements of Bridge #2 based on the intensity measure of Sa_{Area}.

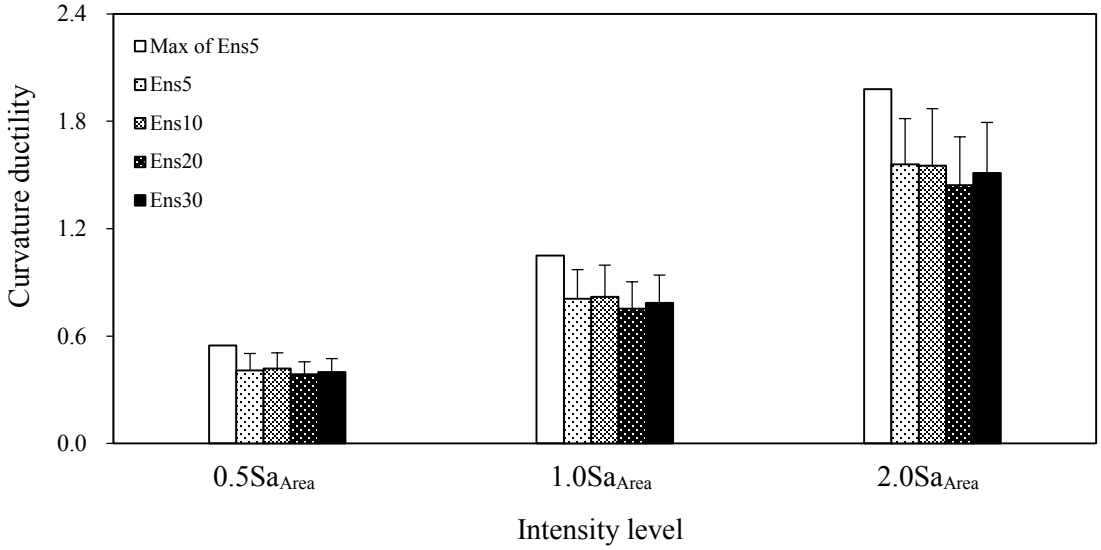

Figure 5.9 Column curvature ductilities of Bridge #2 based on the intensity measure of Sa_{Area} (Pier 1).

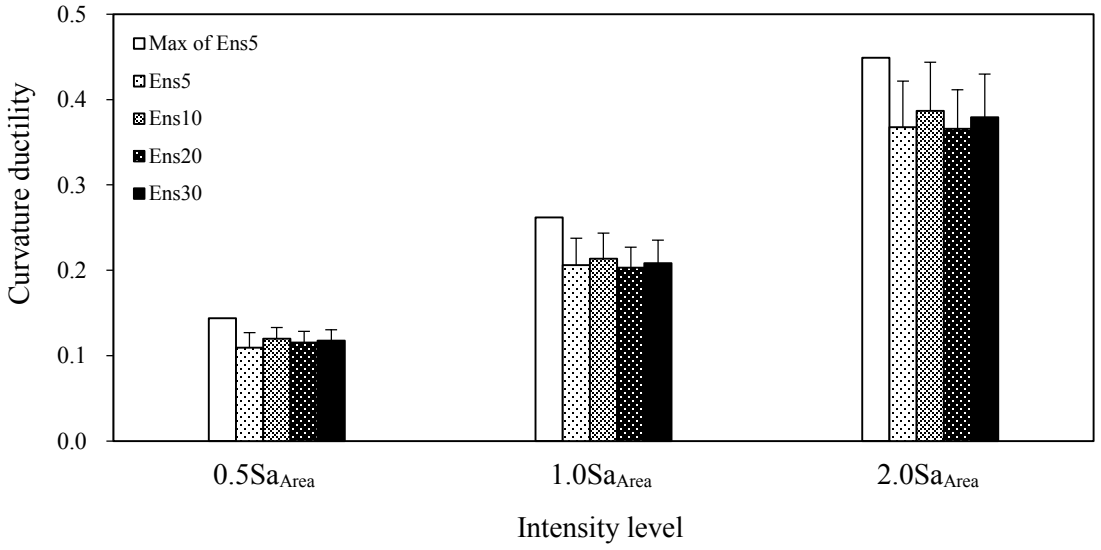

Figure 5.10 Column curvature ductilities of Bridge #2 based on the intensity measure of Sa_{Area} (Pier 2).

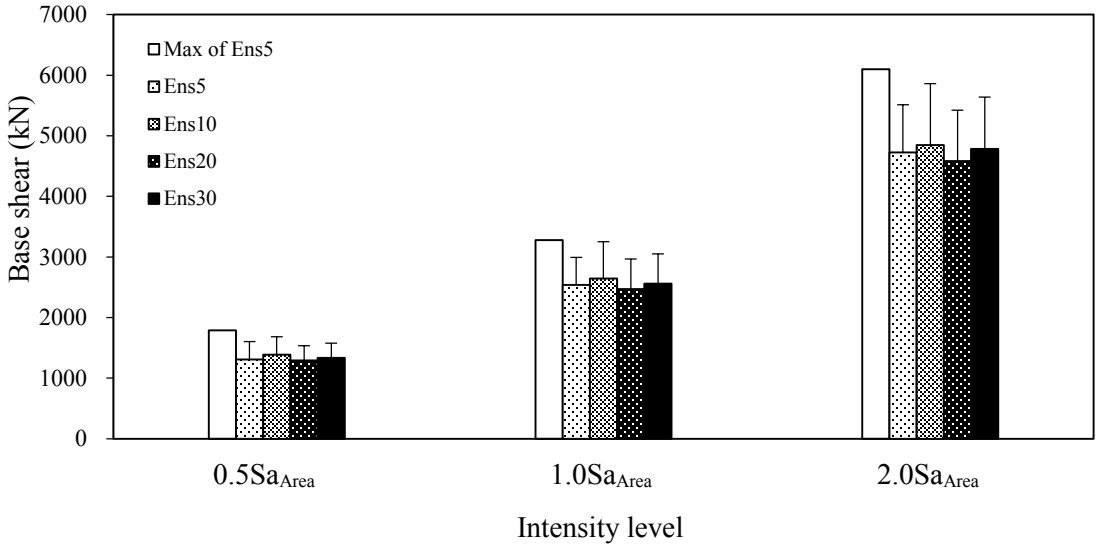

Figure 5.11 Base shears for the Bridge #2 based on the intensity measure of Sa_{Area}.

- The results in the figures and tables show that 10 accelerograms of the Ens10 set are sufficient for the time-history analysis of the bridge #2. This is because the maximum difference between the responses using Ens10 set and Ens30 set accelerograms was only about 5% (Table 5.2).

- The results indicate that the minimum number of accelerograms that can be used for the time-history analysis of the bridge #2 is five (Ens5 set). The maximum difference between the responses using 5 accelerograms (Ens5 set) and 30 (Ens30 set) accelerograms was only about 6% (Table 5.2). It was noted in Table 5.2 that the differences corresponding to Ens5 set were slightly larger than Ens10. However, they were still acceptable.

- The maximum response from the Ens5 set should not be used to represent the response of the bridge because it led to the response about 35% higher than that from the Ens30 set consisting of 30 accelerograms.

- It is interesting to notice that the standard deviations of the responses from the seismic excitations Ens5, Ens10, Ens20, and Ens30 are almost identical

Table 5.2 Differences (in percentage) between the response values from ensembles of simulated accelegrams and those from Ens30 for Bridge #2 based on Sa_{Area}.

Response parameter	Intensity level	Max of Ens5	Mean of Ens5	Mean of Ens10	Mean of Ens20
Deck displacement	$0.5Sa_{Area}$	37	2	5	3
	$1.0Sa_{Area}$	34	3	4	4
	$2.0Sa_{Area}$	31	4	3	4
Expansion bearing displacement	$0.5Sa_{Area}$	35	2	3	4
	$1.0Sa_{Area}$	28	3	4	4
	$2.0Sa_{Area}$	23	2	3	5
Column curvature ductility@ Pier 1	$0.5Sa_{Area}$	37	2	5	3
	$1.0Sa_{Area}$	34	3	4	4
	$2.0Sa_{Area}$	31	3	3	5
Column curvature ductility@ Pier 2	$0.5Sa_{Area}$	23	7	2	2
	$1.0Sa_{Area}$	26	1	2	3
	$2.0Sa_{Area}$	18	3	2	4
Base shear	$0.5Sa_{Area}$	34	2	4	3
	$1.0Sa_{Area}$	28	1	3	3
	$2.0Sa_{Area}$	28	1	1	4

Note: Percentage is expressed relative to the mean response value from Ens30.

5.3 Determination the Minimum Number of Accelerograms Based on the Intensity Measure of Sa(T_1)

As mentioned in the Section 5.1 "Introduction", the intensity measure Sa(T_1) was also used to scale the seismic excitations in order to investigate the minimum number of accelerograms for the time-history analysis. It should be noted herein that the partial spectral area under the spectrum of the accelerogram and Sa(T_1) are different intensity measures. Therefore, the responses obtained using these two intensity measures cannot be compared. This can be seen clearly on the results for the base shear for the two bridges (e.g., the results shown in Fig. 5.6 vs in Fig. 5.17), the detailed discussion is given below. It is logical that the intensity measure in terms of the partial spectral area is better than Sa(T_1) because the higher mode

effects are taken into account. The main reason that Sa(T_1) was considered is because it is widely used by the practitioners on the design and evaluation of bridges subjected to seismic loads.

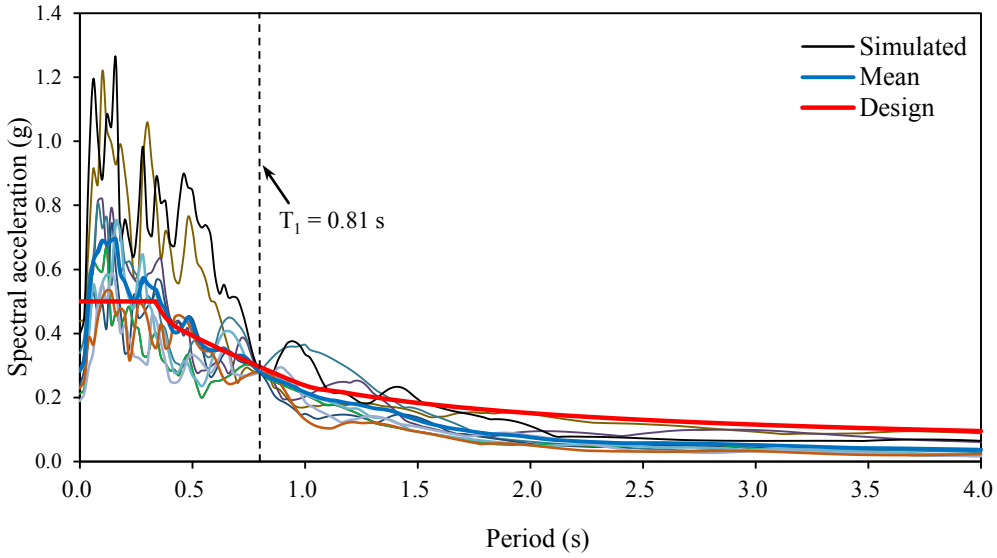

Figure 5.12 Acceleration response spectra for the records of the Ens10 scaled to spectral acceleration of 0.28g at the first mode period of the Bridge #1, T_1 = 0.81s; 5% damping.

Figure 5.12 shows the 5% damped spectra of the scaled accelerograms of Ens10 to spectra acceleration of 0.28g at the first mode period of the Bridge #1, T_1 = 0.81 s. It can be seen that this scaling provides a relatively small dispersion of the spectra in the vicinity of 0.81 s and for the periods longer than 0.81 s, but the dispersion is significant in the short period range. For comparison, Figure 5.13 presents the mean response spectra of the accelerograms of Ens5, Ens10, Ens20, and Ens30 sets scaled to Sa(0.81 s) = 0.28g, 5% damping along with the design spectrum for Montreal, for Soil Type I according to CHBDC, for the probability of exceedance of 10% in 50 years. It can be seen in the figure that the spectra of the accelerograms of the four sets are compatible. Three seismic excitation levels were used in the investigation,

and they were *0.5Sa(T1)*, *1.0Sa(T1)*, and 2.0*Sa(T1)*, in which T_1 = 0.81 s for the Bridge #1, and T_1 = 0.71 s for the Bridge #2.

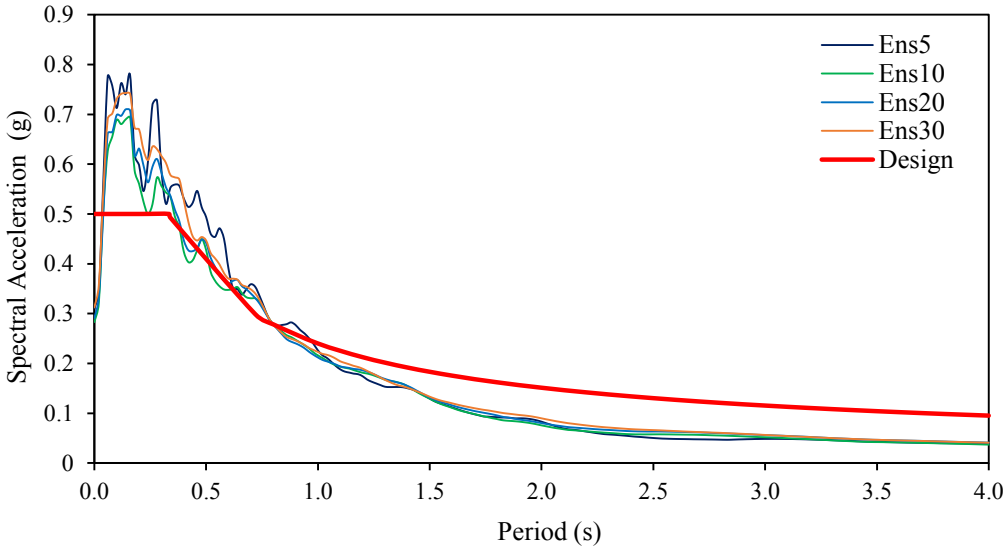

Figure 5.13 Mean response spectra for the records of the Ens5, Ens10, Ens20, and Ens30 scaled to spectral acceleration of 0.30g at the first mode period of the Bridge #1, T_1 = 0.81s; 5% damping.

5.3.1 Results for Bridge #1

The results for the five response parameters considered for the Bridge #1 using the accelerograms of Ens5, Ens10, Ens20, and Ens30 scaled to three excitation levels are presented in Figs. 5.14 to 5.18. Table 5.3 shows the differences of the responses from different sets (Ens5, Ens10, and Ens20) and those from the Ens30. In general, the observations of the results were very similar to those based on the partial spectral area scaling method discussed above. However, additional findings were obtained. The major conclusions are summarized as follows,

- The responses using the Ens10 set were the same as those using Ens30. The difference was only about 1% (Table 5.3). It indicates that 10 accelerograms are sufficient for the analysis.

- The accelerograms of Ens5 also provided the responses very close to those of Ens30. Relatively larger difference was observed of using Ens5 set, i.e., about 3% to 8%. However, the difference is still acceptable from the practical point of view.

- The maximum response from the Ens5 set was much larger than those from the Ens30 set. The difference was about 20% for the responses at the intensity levels of *0.5Sa(0.81s)* and *1.0 Sa(0.81s)*, while the difference was increase to about 40% for the seismic excitations of *2.0Sa(0.81s)* (Table 5.3).

- Comparing the differences shown in Table 5.1 to those in Table 5.3, larger difference was noticed in the results using the partial spectral area scaling method. This is mainly due to the fact that more modes other than only the first mode were considered in the scaling method using the partial spectral area.

- The intensity represented by the partial area under the spectrum is higher than by the $Sa(T_1)$ for a lower excitation level. For example, the mean base shear obtained using $0.5Sa_{Area}$ was about 2100 kN, and using $0.5Sa(T_1)$ was about 1700 kN, and the corresponding difference was about 20%. However, for a higher scaling level, the two intensities $2.0Sa_{Area}$ and $2.0Sa(T_1)$ generate approximately the same excitation level because the corresponding base shears were very close (5300 kN vs. 5200 kN).

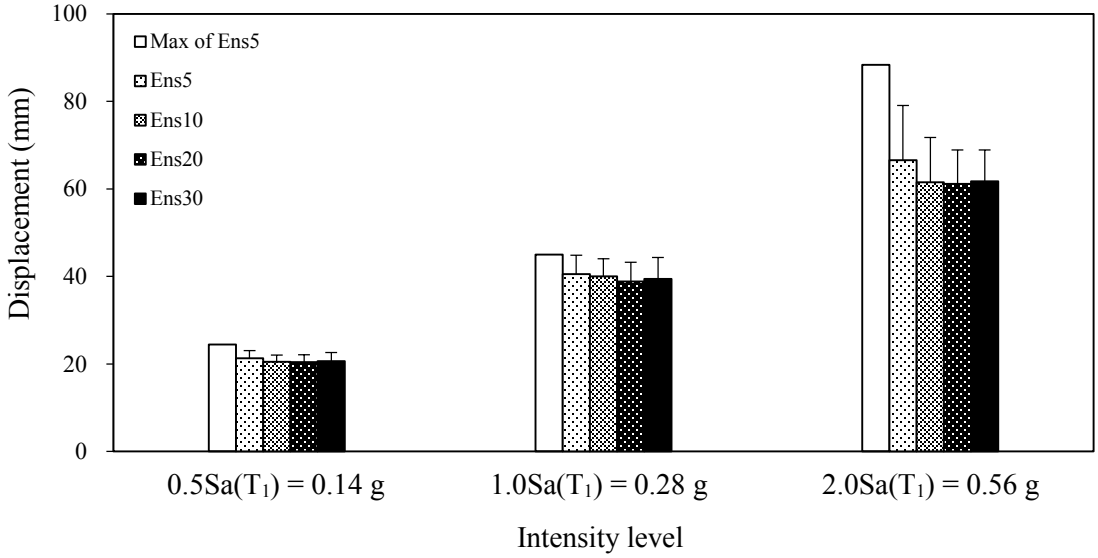

Figure 5.14 Deck displacements of Bridge #1 based on the intensity measure of $S_a(T_1)$.

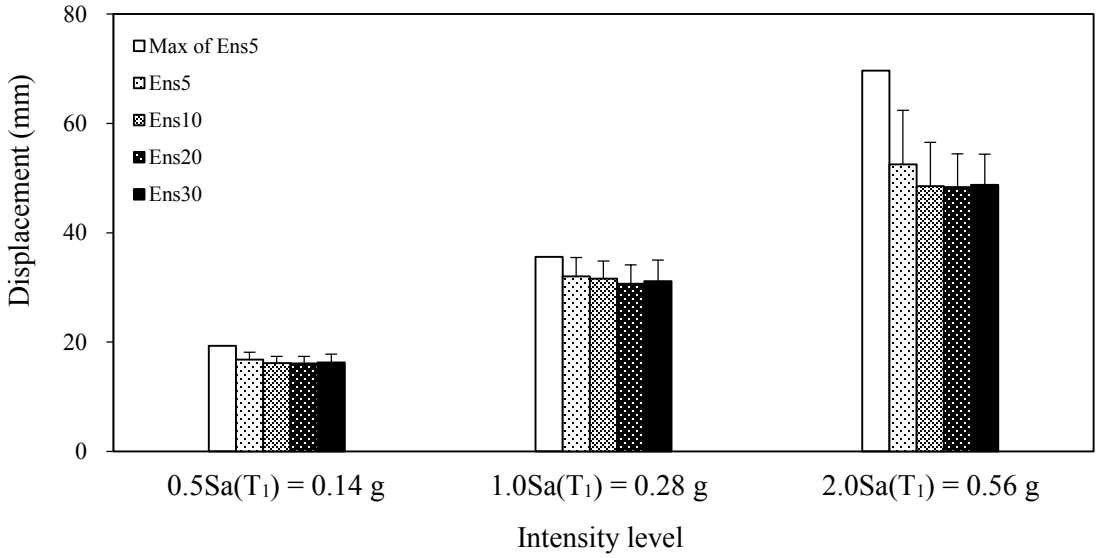

Figure 5.15 Expansion bearing displacements of Bridge #1 based on the intensity measure of $S_a(T_1)$.

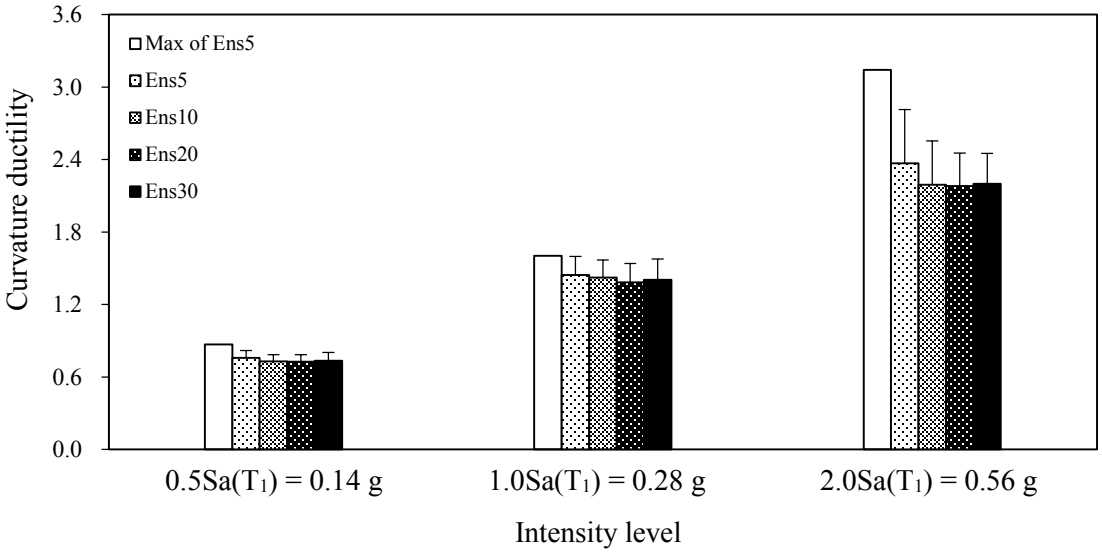

Figure 5.16 Column curvature ductilities of Bridge #1 based on the intensity measure of $S_a(T_1)$ (Pier 1).

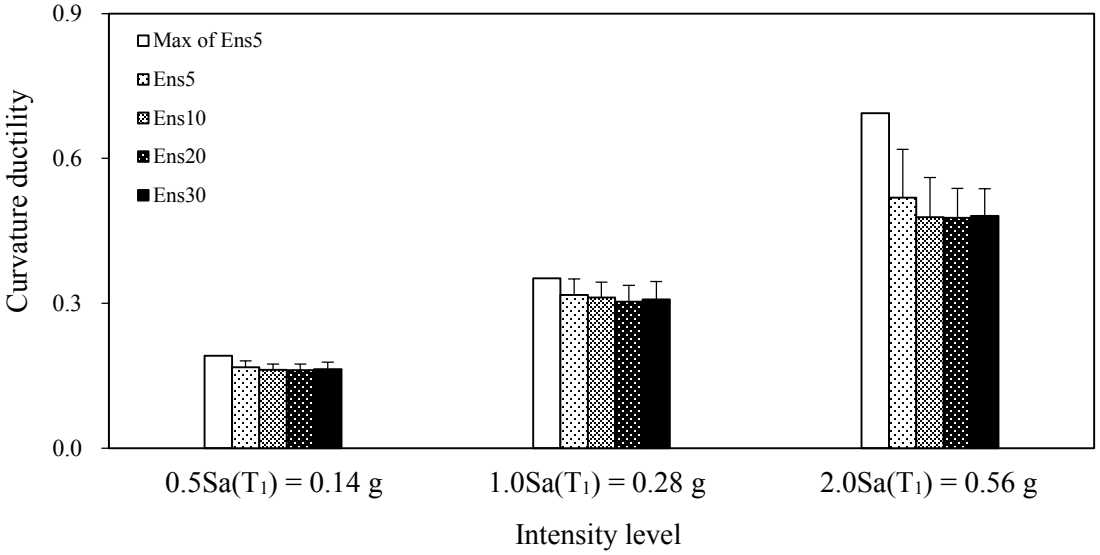

Figure 5.17 Column curvature ductilities of Bridge #1 based on the intensity measure of $S_a(T_1)$ (Pier 2).

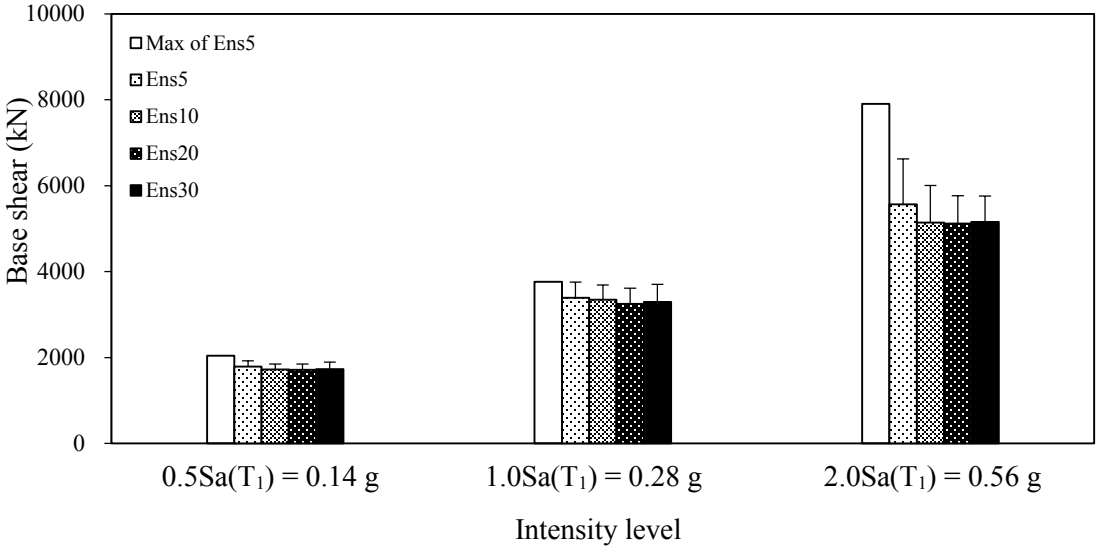

Figure 5.18 Base shears of Bridge #1 based on the intensity measure of $S_a(T_1)$.

Table 5.3 Differences (in percentage) between the response values from ensembles of simulated accelerograms and those from Ens30 for Bridge #1 based on $Sa(T_1)$.

Response parameter	Intensity level	Max of Ens5	Mean of Ens5	Mean of Ens10	Mean of Ens20
Deck displacement	0.5Sa(T_1)	19	3	1	1
	1.0Sa(T_1)	14	3	1	1
	2.0Sa(T_1)	43	8	0	1
Expansion bearing displacement	0.5Sa(T_1)	19	3	1	1
	1.0Sa(T_1)	14	3	1	2
	2.0Sa(T_1)	43	8	1	1
Column curvature ductility@ Pier 1	0.5Sa(T_1)	18	3	1	1
	1.0Sa(T_1)	14	3	1	1
	2.0Sa(T_1)	43	8	0	1
Column curvature ductility@ Pier 2	0.5Sa(T_1)	17	3	1	1
	1.0Sa(T_1)	14	3	1	1
	2.0Sa(T_1)	44	8	0	1
Base shear	0.5Sa(T_1)	18	3	1	1
	1.0Sa(T_1)	14	3	1	1
	2.0Sa(T_1)	44	8	0	1

Note: Percentage is expressed relative to the mean response value from Ens30.

5.3.2 Results for Bridge #2

The results for Bridge #2 using the four sets of accelerograms Ens5, Ens10, Ens20, and Ens30 are given in Figs. 5.19 to 5.23. The differences between the responses from each of the

three sets of accelerograms (Ens5, Ens10, and Ens20) and those from the Ens30 are provided in Table 5.4.

- The results in the figures and tables show that 10 accelerograms of the Ens10 set are sufficient for the time-history analysis of the Bridge #2. This is because the maximum difference between the responses using Ens10 set and Ens30 set accelerograms was only about 5% (Table 5.4).

- The results indicate that the minimum number of accelerograms that can be used for the time-history analysis of the Bridge #2 is five (Ens5 set). The maximum difference between the responses using 5 accelerograms (Ens5 set) and 30 (Ens30 set) accelerograms was only about 6% (Table 5.4). It was noted in Table 5.4 that the differences corresponding to Ens5 set were slightly larger than Ens10, they were still acceptable.

- The maximum response from the Ens5 set should not be used to represent the response of the bridge because it led to the response about 35% higher than that from the Ens30 set consisting of 30 accelerograms.

- It is interesting to notice that the standard deviations of the responses from the seismic excitations using Ens5, Ens10, Ens20, and Ens30 are almost identical.

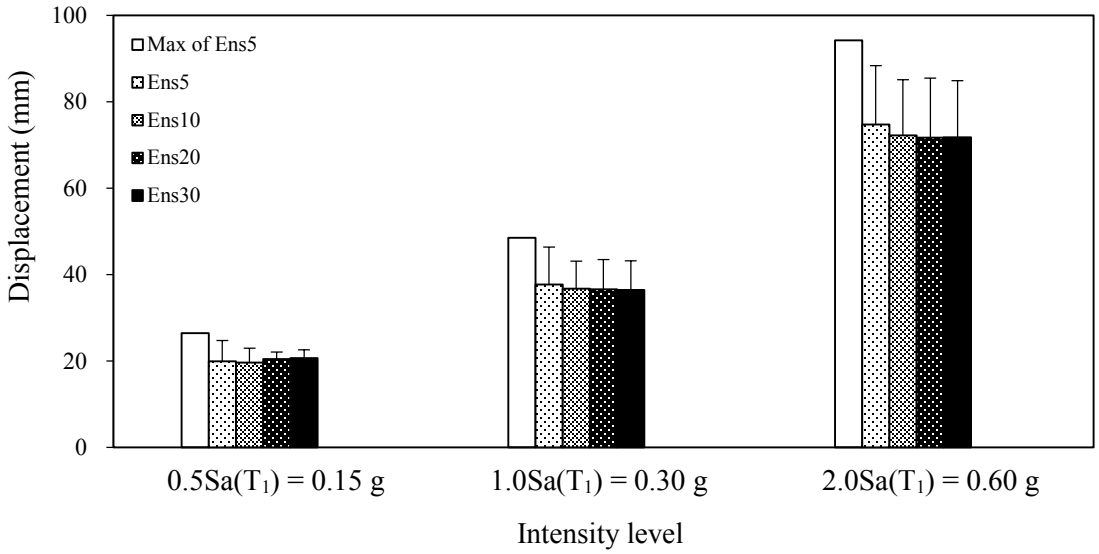

Figure 5.19 Deck displacements of Bridge #2 based on the intensity measure of $S_a(T_1)$.

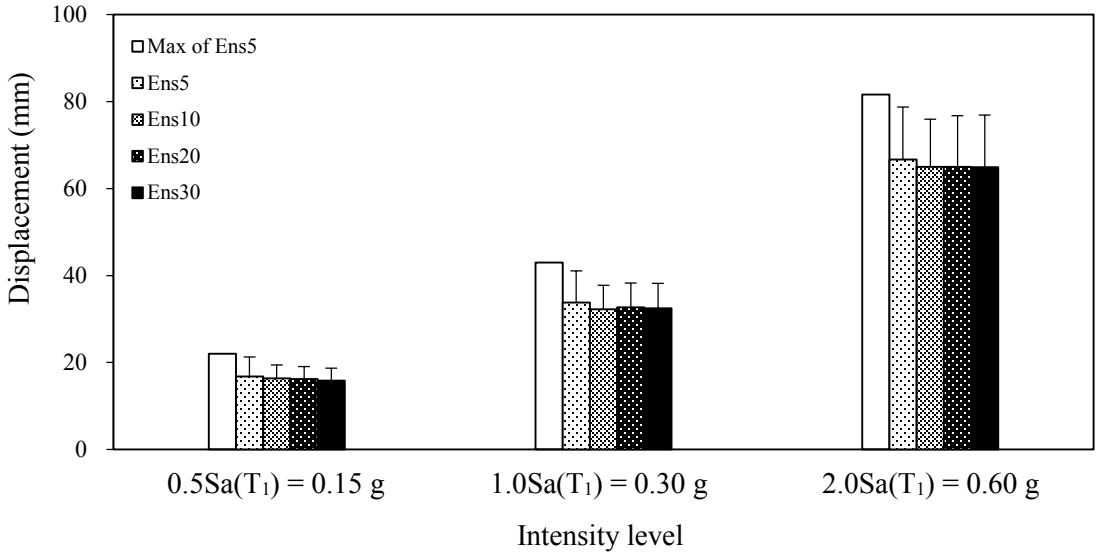

Figure 5.20 Expansion bearing displacements of Bridge #2 based on the intensity measure of $S_a(T_1)$.

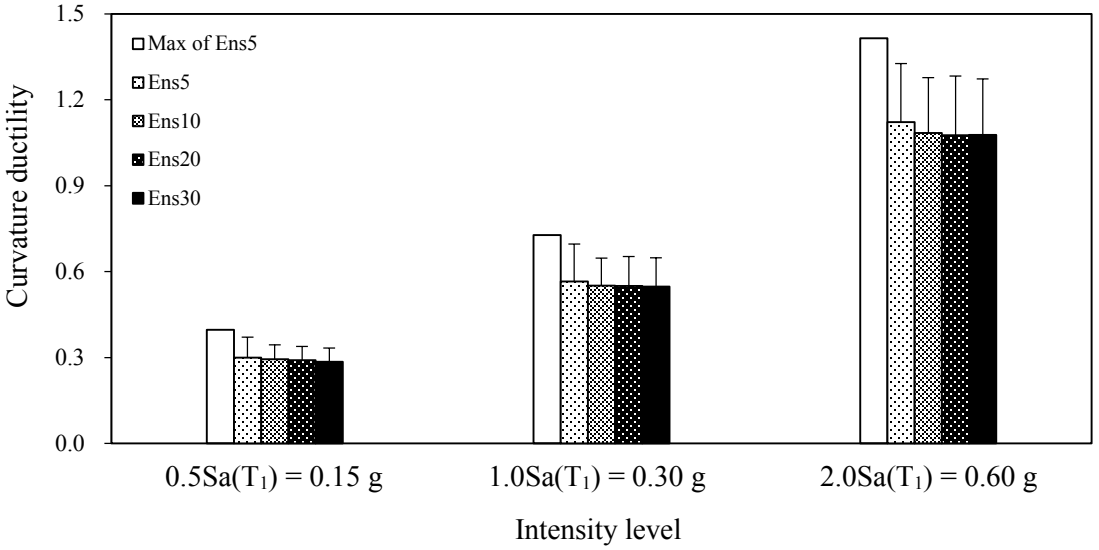

Figure 5.21 Column curvature ductilities of Bridge #2 based on the intensity measure of $S_a(T_1)$ (Pier 1).

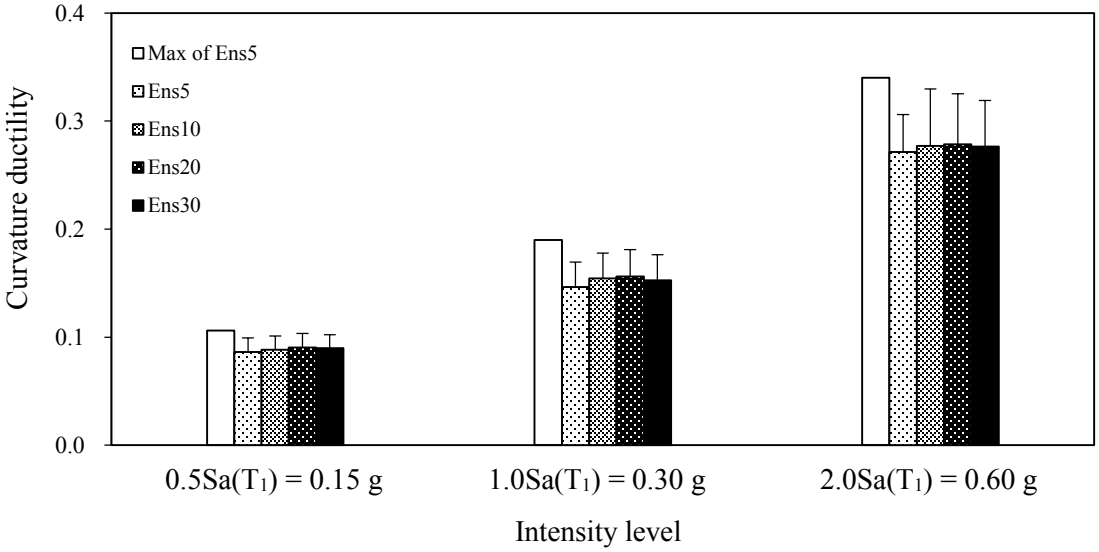

Figure 5.22 Column curvature ductilities of Pier 2 of Bridge #2 based on the intensity measure of $S_a(T_1)$ (Pier 2).

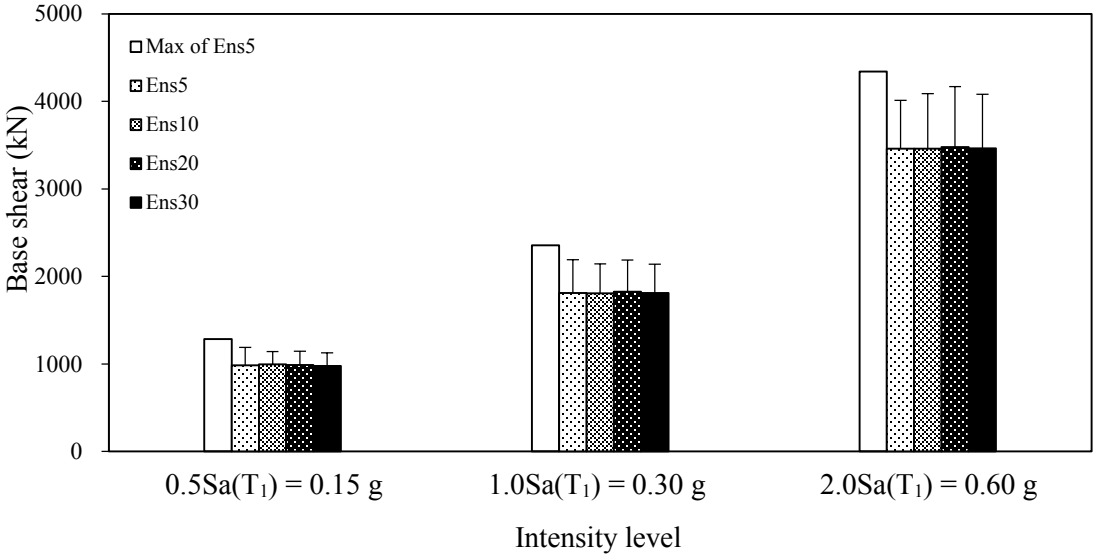

Figure 5.23 Base shears for the Bridge #1 based on the intensity measure of $S_a(T_1)$.

Table 5.4 Differences (in percentage) between the response values from ensembles of simulated accelegrams and those from Ens30 for Bridge #2 based on $Sa(T_1)$.

Response parameter	Intensity level	Max of Ens5	Mean of Ens5	Mean of Ens10	Mean of Ens20
Deck displacement	0.5Sa(T1)	28	3	5	1
	1.0Sa(T1)	33	3	1	0
	2.0Sa(T1)	31	4	1	0
Expansion bearing displacement	0.5Sa(T1)	39	6	3	2
	1.0Sa(T1)	32	4	1	1
	2.0Sa(T1)	26	3	0	0
Column curvature ductility@ Pier 1	0.5Sa(T1)	39	5	3	2
	1.0Sa(T1)	33	3	1	0
	2.0Sa(T1)	31	4	1	0
Column curvature ductility@ Pier 2	0.5Sa(T1)	18	4	2	0
	1.0Sa(T1)	24	4	1	2
	2.0Sa(T1)	23	2	0	1
Base shear	0.5Sa(T1)	31	1	2	1
	1.0Sa(T1)	30	0	0	1
	2.0Sa(T1)	25	0	0	0

Note: Percentage is expressed relative to the mean response value from Ens30.

5.4 Summary

The main findings of the study presented in this Chapter are summarized below:

- The standard deviation of the response of each set of accelerograms (Ens5, Ens10, Ens20, and Ens30) at a given intensity level is almost the same, and it increases with the increase of the seismic excitation level.

- If the partial spectral area scaling method is used, 5 accelerograms are sufficient for the *linear* time-history analysis for the *design* purpose. However, for the evaluation of the seismic performance of bridges (i.e., higher excitation levels are considered), 10 accelerograms are enough for the analysis.

- If $Sa(T_1)$ is used as an intensity measure, 5 accelerograms are adequate for both linear and nonlinear time-history analysis.

- If 5 accelerograms are considered, mean response instead of the maximum response from the 5 accelerograms should be used to present the seismic response of the bridge.

5.5 Additional Remarks

It is necessary to mention that investigation on the minimum number of accelerograms for the time-history analysis was also conducted using Set 1 - Scaled real accelerograms that was considered in Chapter 4. Same analyses as those described above were performed, i.e., additional three sets of accelerograms consisting of 5, 10, and 20 accelerograms were selected; two intensity measures (Sa_{Area}; $Sa(T_1)$); and three excitation levels ($0.5Sa_{Area}$, $1.0Sa_{Area}$, and $2.0\ Sa_{Area}$; 0.5 $Sa(T_1)$, 1.0 $Sa(T_1)$, and 2.0 $Sa(T_1)$) were used in the analysis. The observations of the results were almost the same as those using the simulated accelerograms. The detailed analysis results using real accelerograms are given in Appendix.

Chapter 6

Summary and Conclusions

6.1 General remarks

The Canadian Highway Bridge Design Code (CHBDC), as well as other modern bridge codes around the world (American code, New Zealand code, European code, etc.) specifies the requirements for the seismic analysis of multi-span bridges. According to the current edition of CHBDC, four methods can be used to conduct seismic analysis on bridges; they are uniform-load method, single-mode spectral method, multi-mode spectral method, and time-history method. Among the four methods, it is believed that the time-history analysis method is the most appropriate method to evaluate the seismic response of bridges. Note that time-history analysis is mandatory for irregular bridges, e.g., the number of spans is more than seven.

For the time-history analysis, the codes require the seismic excitations (i.e., the accelerograms) used in the analysis to be compatible with the design spectrum for the bridge location. The selection of spectrum-compatible accelerograms is one of the major issues for the time-history analysis of bridges. Another issue is the number of accelerograms that should be used in the analysis. Currently, the number of accelerograms required for the time-history analysis is different in the different codes and standards, e.g., *5* are required by CHBDC, *30* are required by NEHRP (National Earthquake Hazards Reduction Program).

Given these, the objectives of this study are: (i) to evaluate different methods for the selection of accelerograms in the estimation of the structural responses of bridges, (ii) to

investigate the minimum number of accelerograms that can be used in the time-history analysis including elastic analysis and inelastic analysis. For the purpose of analysis, two 3-span typical highway bridges located in Montreal were considered. Both bridges are reinforced concrete bridges. The total length of the bridges is about 50 m. These two bridges can be considered as regular bridges according to CHBDC. The location of the bridge, Montreal, was selected because (i) Montreal is in a moderate seismic hazard zone, (ii) not too many records from strong earthquakes in eastern Canada are available.

Four sets of accelerograms compatible with the design spectrum for Montreal were selected to examine the set of accelerograms which is the most suitable for the time-history analysis. These include: (i) Set 1 - scaled real accelerograms, (ii) Set 2 - modified real accelerograms, (iii) Set 3 - simulated accelerograms, and (iv) Set 4 - artificial accelerograms. Each set consists of 30 accelerograms. Nonlinear time-history analyses were conducted on the two bridges. Deck displacements, expansion bearing displacements, column curvature ductilities, and base shears were used in the evaluation of the effects of the selected excitations on the seismic response of bridges.

To achieve the second objective of this study, 5, 10, and 20 accelerograms were randomly selected from the 30 accelerograms of the Set which was preferable based on the conclusion of the analysis mentioned above. The accelerograms were scaled according to the partial spectral area and the spectral acceleration at the first mode period of the bridge $Sa(T_1)$, respectively. Three intensity levels were considered in the analysis in order to cover the response of the bridge from elastic to inelastic. The differences of the responses between the use of the small number of accelerograms (i.e., 5, 10, and 20 accelerograms) and the use of the 30 accelerograms were used to examine the minimum number of accelerograms that can be

used in the time-history analysis.

6.2 Summary of findings

The main findings from this study are given below:

- The major nonlinearity of bridge during seismic response occurs on the expansion bearing. Therefore, attention should be paid to the maximum translation of the expansion in the design and evaluation of bridges located in seismicity zones.

- For the two bridges considered in this study, it is found that the column curvature ductility is not significant. For example, it is about 2.5 when the seismic excitations are about two times higher than the design earthquake.

- Among the four sets of accelerograms used in the analysis, the spectra of the set with scaled real accelerograms and that with simulated accelerograms (i.e., sets designated (i) and (iii) above) show the largest dispersion around the mean spectra of the sets. Very small dispersion of the spectra is observed for the set with modified real accelerograms and that with artificial accelerograms (i.e., sets designated (ii) and (iv) above).

- The variability of the deformation responses (i.e., deck displacements, expansion bearing displacements, column curvature ductilities, and base shears) from the four sets of accelerograms is comparable for the two bridges. The maximum differences between the largest and the smallest mean values of the deformation responses (expressed as the percentage with respect to the smallest mean value) are about 15%, except for the Bridge #2, for the column curvature ductility of the pier 2 in which the expansion bearings are installed; the difference is about 25%.

- The largest mean response values are from the simuated accelerograms while the smallest are from the artificial accelerograms.

- The response from the scaled real accelerograms has the largest coefficient of variation (COV), and that from the artificial accelerograms has the smallest COV. The modified real accelerograms and simulated accelerograms have shown similar COV.

- The intensity represented by the partial area under the spectrum is about 20% lower than that represented by the spectral acceleration at the fundamental period of the bridge $Sa(T_1)$.

- The standard deviation of the response using the reduced number of accelerograms (i.e., 5, 10, and 20 accelerograms) is very close to that using the whole set of the 30 accelerograms.

- The maximum response from the 5 accelerograms is about 20-40% larger than that from the 30 accelerograms.

- The mean responses of the deck displacement, expansion bearing displacement, maximum column curvature ductility, and base shear from the 10 accelerograms are very close to those from the 30 accelerograms using the partial area scaling method. Note the base shear of Bridge #1 using 10 accelerograms is about 10-15% than those using 30 accelerograms. If 5 accelerograms are used, smaller difference of the responses with respect to those from 30 accelerograms is observed at the lower seismic excitation level while larger difference is observed at the higher excitation level.

- The mean values of all the response parameters considered in this study from 5

accelerograms are the same as those from the 30 accelerograms when the accelerograms are scaled according to $Sa(T_1)$.

- The maximum response from the 5 accelerograms is extremely larger than that from the 30 accelerograms.

- Either 5 accelerograms or 10 accelerograms can be used in the time-history analysis depending on the purpose of the analysis, i.e., to determine the design response or to estimate the nonlinear response due to larger earthquakes.

6.3 Conclusions

Based on the foregoing discussion, the main conclusions can be summarized as follows:

- Given the considerations of both the spectral characteristics of the selected sets and the response results from the analysis, *Simulated Accelerograms* are preferred for use in time-history analyses of bridges. The methods for the generation of such accelerograms take into account certain seismological characteristics of the region considered.

- For *linear time-history analysis* and for the *design purpose*, *5 accelerograms* are sufficient for the analysis. In addition, mean (not the maximum) response from the *5 accelerograms* should be used to estimate the seismic response of the bridges.

- For *nonlinear time-history analysis* for higher excitation levels, the minimum number of accelerograms depends on the scaling method. If the accelerograms are scaled according to $Sa(T_1)$, 5 accelerograms are enough. However, if the accelerograms are scaled based on the partial area under the spectrum, 10 accelerograms should be used. Given this, it is recommended to use *10 accelerograms* in the *nonlinear time-history analysis*.

- *Standard deviation* of the response parameters should not be a concern on the use of a smaller number of accelerograms in the analysis, such as, development of fragility curves. This is because it does not change with the number of accelerograms based on the results of this study.

6.4 Recommendations for future work

The research work presented in this thesis is based on considerations of the two selected bridge models located in Montreal, accelerograms respresentative of the characteristics of ground motions in eastern Canada. These may limit the conclusions of the study. Given this, further research needed is summarized hereafter:

- The research in this thesis is conducted using structural models of two reinforced concrete bridges, i.e., a slab bridge and a slab-girder type bridge. Other types of bridges, for example, box girder bridges, shear-connected beam bridges, etc. need to be analyzed to verify the conclusions of this study.

- The longitudinal direction of the bridge is considered in this thesis, similar study can also be conducted by applying the seismic excitations in the transverse direction to investigate the effects of accelerograms on the seismic response of bridges.

- The two bridges considered in this study are in eastern Canada. It will be useful if similar study is performed on bridges located in western Canada. This is because the characteristics of seismic ground motions in western Canada is very different than those in eastern Canada. Earthquake records from California are generally used for the seismic analysis of structures in western Canada including both buildings and bridges. However,

it is worth investigating the suitability of using simulated accelerograms on the estimation of the seismic response of bridges in western Canada.

Appendix

Analysis Results Using Set 1-Real Accelerograms

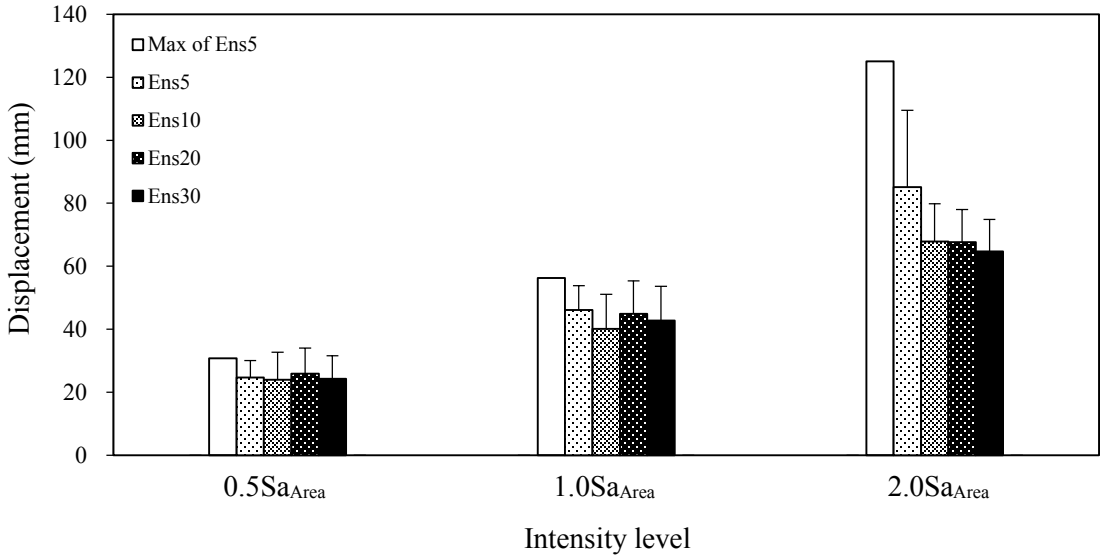

Figure A.1 Deck displacements of Bridge #1 based on Sa_{Area}.

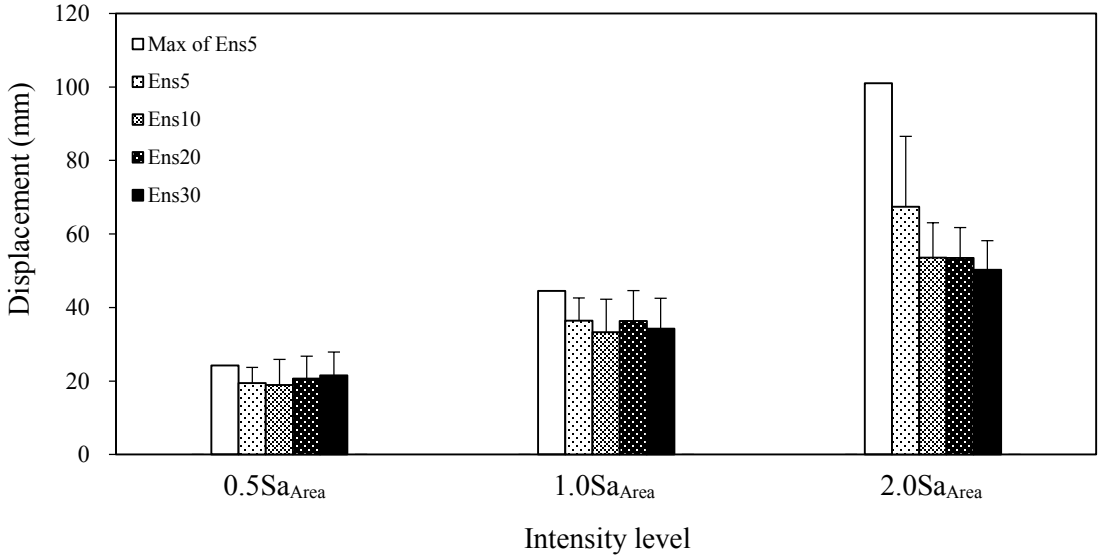

Figure A.2 Expansion bearing displacements of Bridge #1 based on Sa_{Area}.

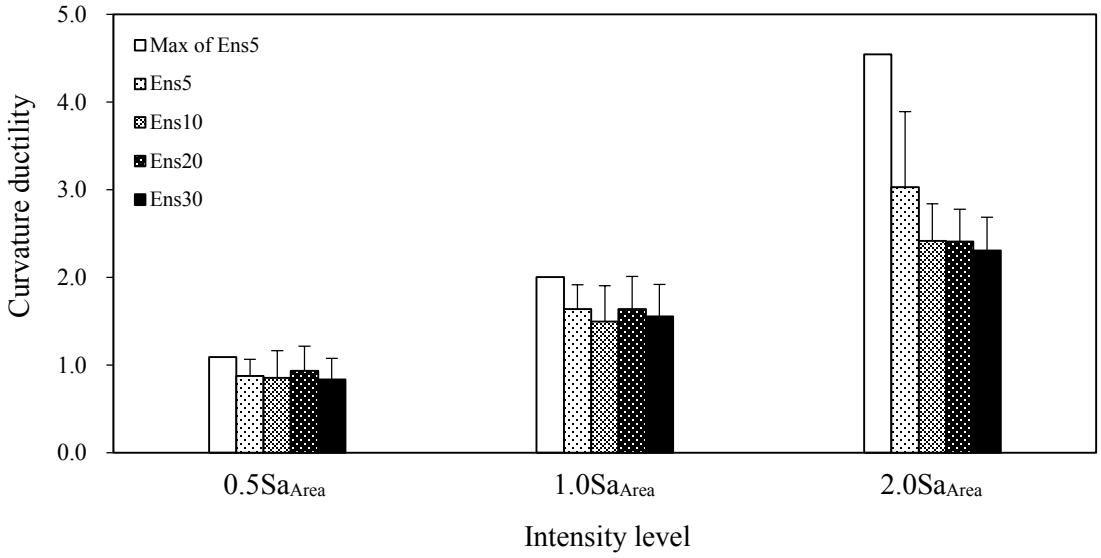

Figure A.3 Column curvature ductilities of Bridge #1 based on Sa_{Area} (Pier 1).

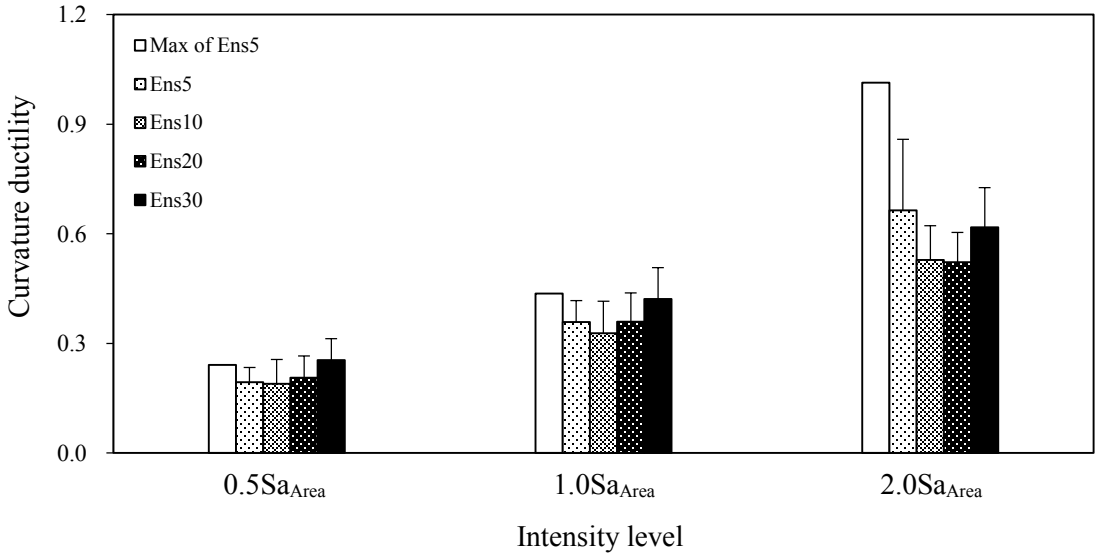

Figure A.4 Column curvature ductilities of Bridge #1 based on Sa_{Area} (Pier 2).

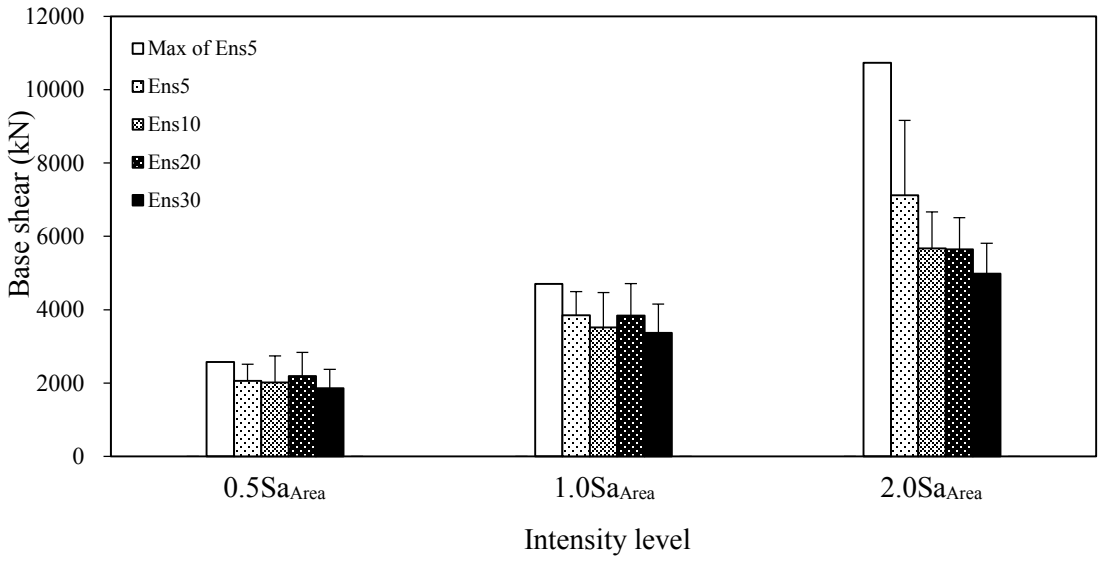

Figure A.5 Base shears of Bridge #1 based on Sa_{Area}.

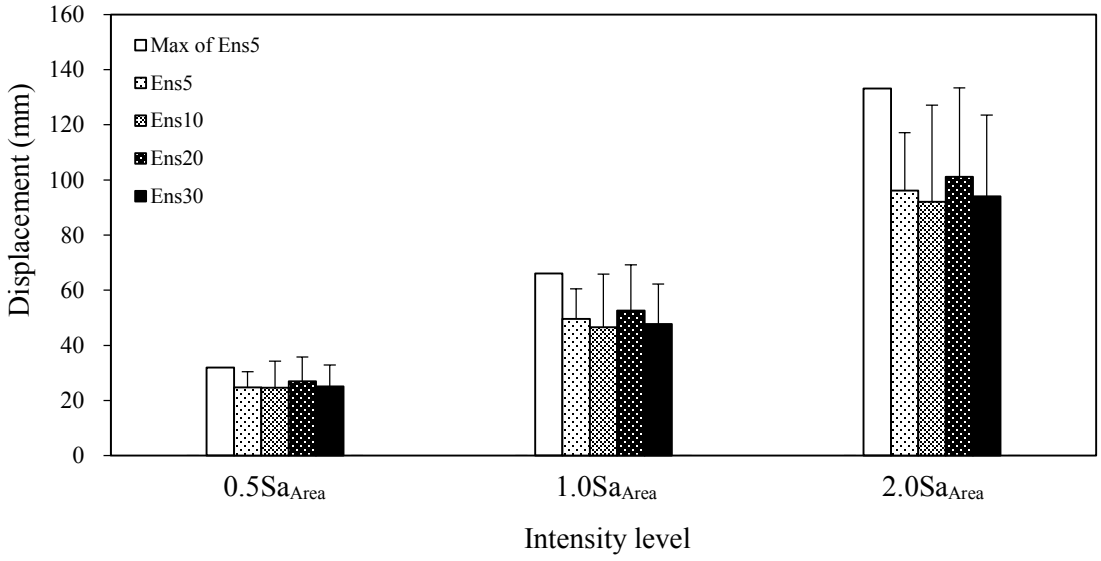

Figure A.6 Deck displacements of Bridge #2 based on Sa_{Area}.

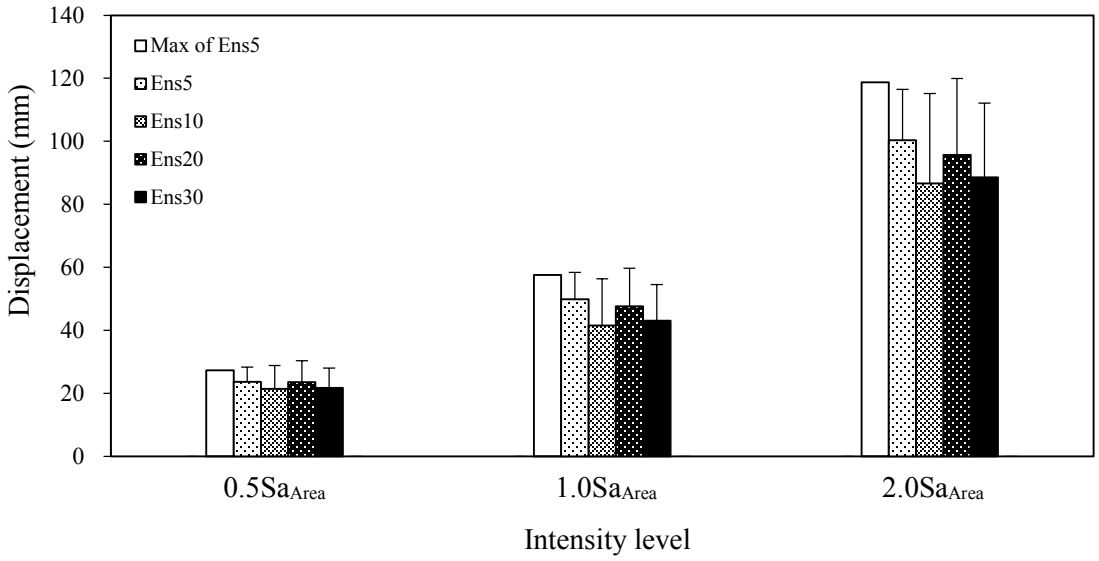

Figure A.7 Expansion bearing displacements of Bridge #2 based on Sa_{Area}.

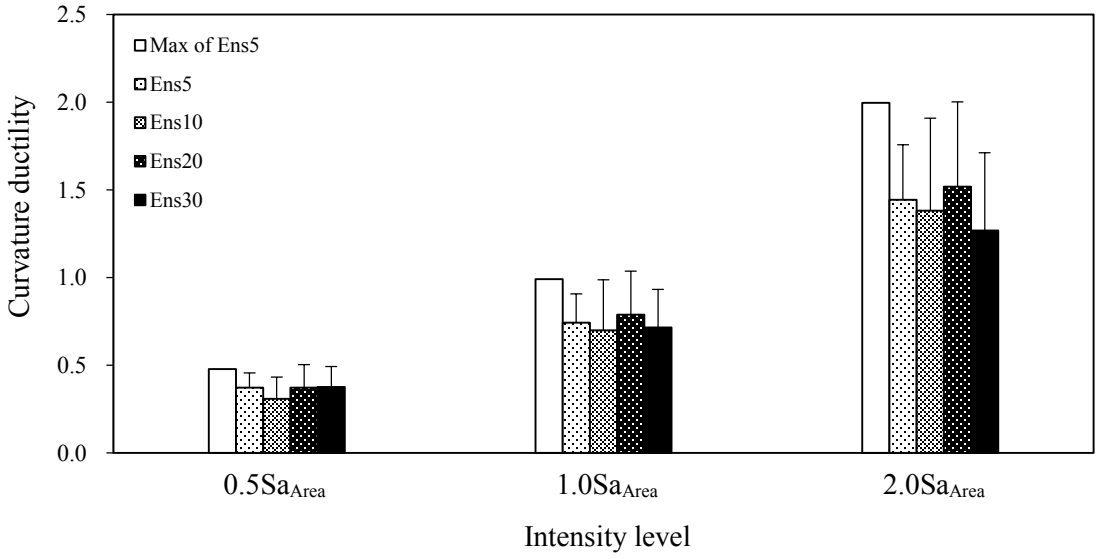

Figure A.8 Column curvature ductilities of Bridge #2 based on Sa_{Area} (Pier 1).

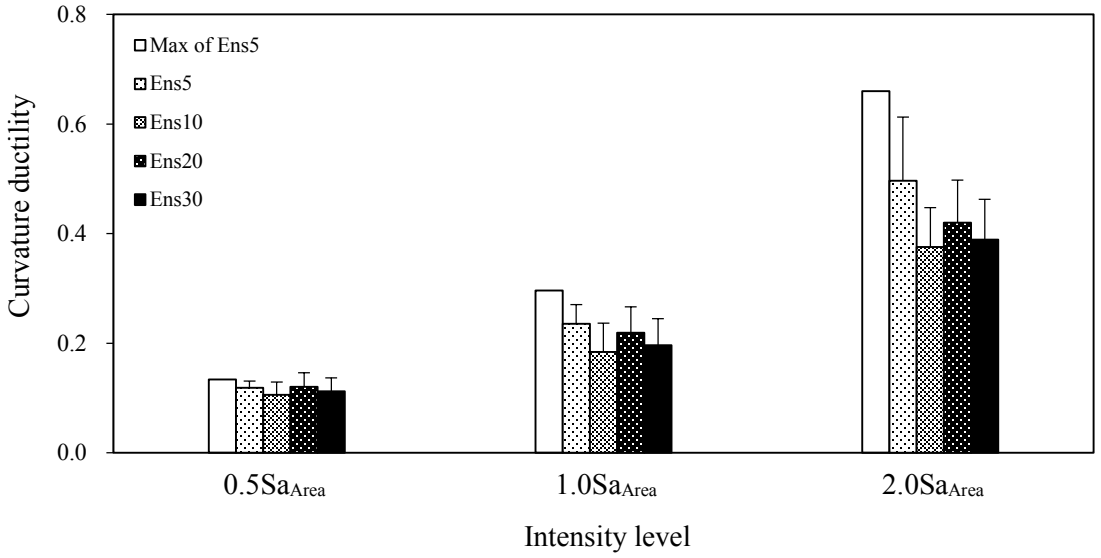

Figure A.9 Column curvature ductilities of Bridge #2 based on Sa_{Area} (Pier 2).

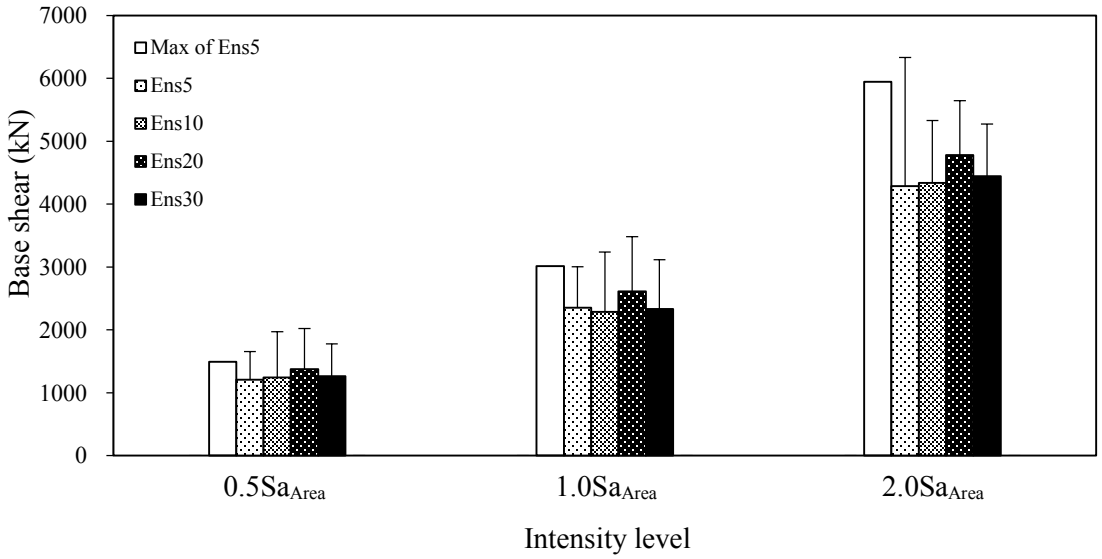

Figure A.10 Base shears of Bridge #2 based on Sa_{Area}.

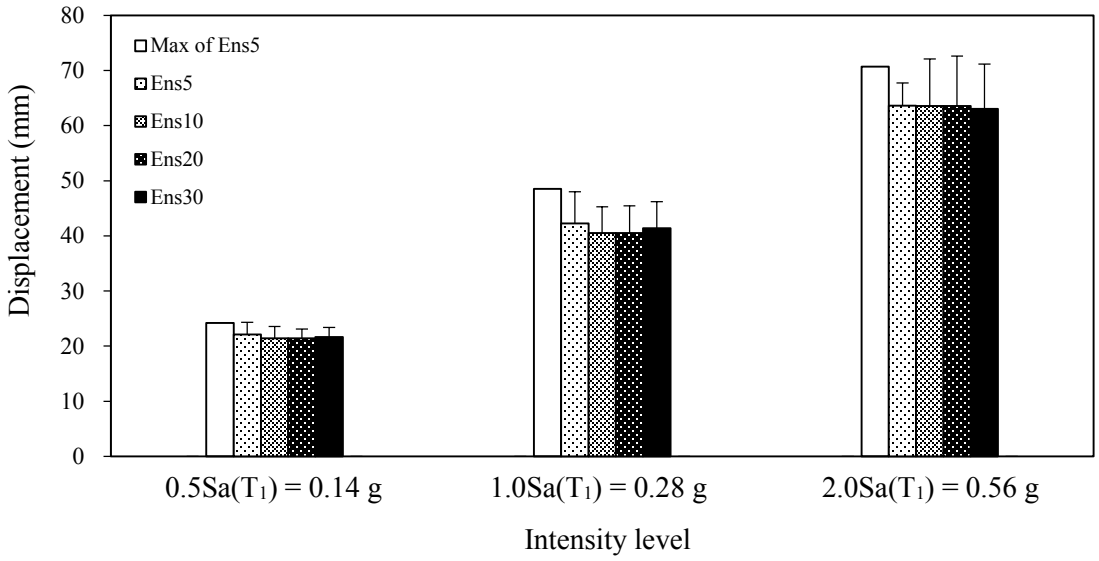

Figure A.11 Deck displacements of Bridge #1 based on $S_a(T_1)$.

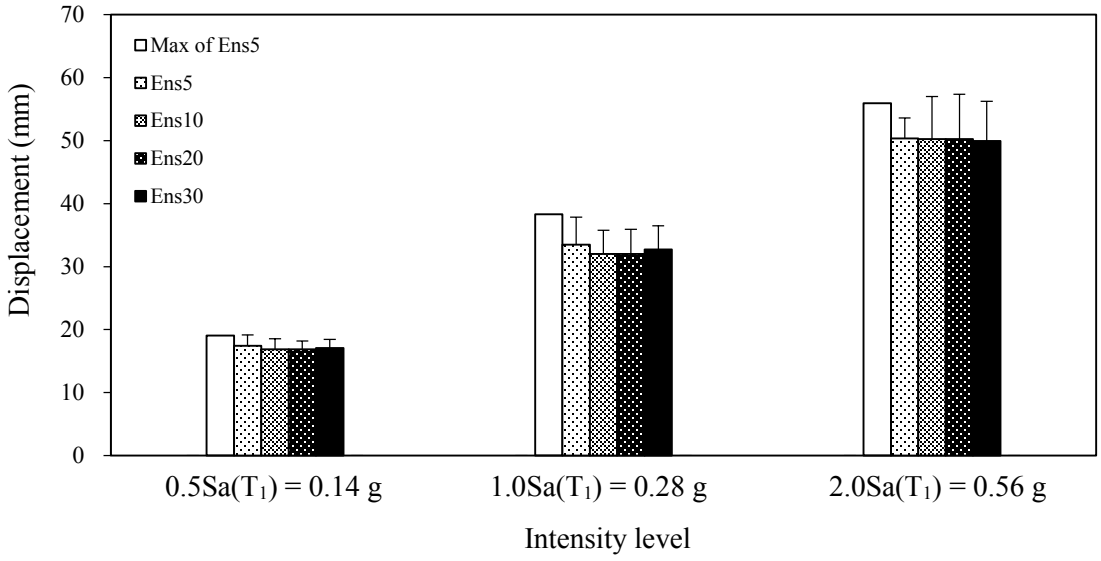

Figure A.12 Expansion bearing displacements of Bridge #1 based on $S_a(T_1)$.

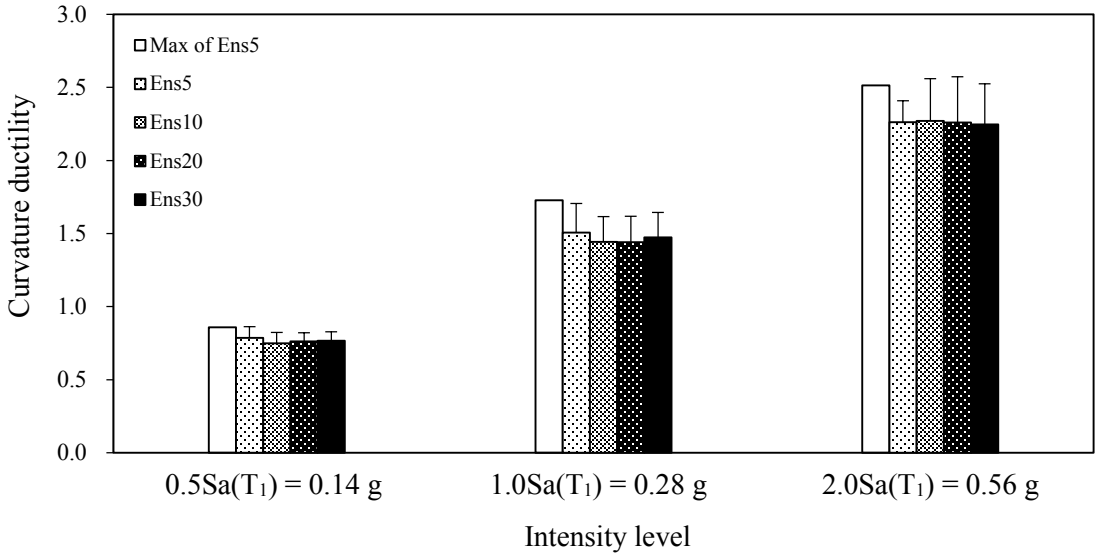

Figure A.13 Column curvature ductilities of Bridge #1 based on $S_a(T_1)$ (Pier 1).

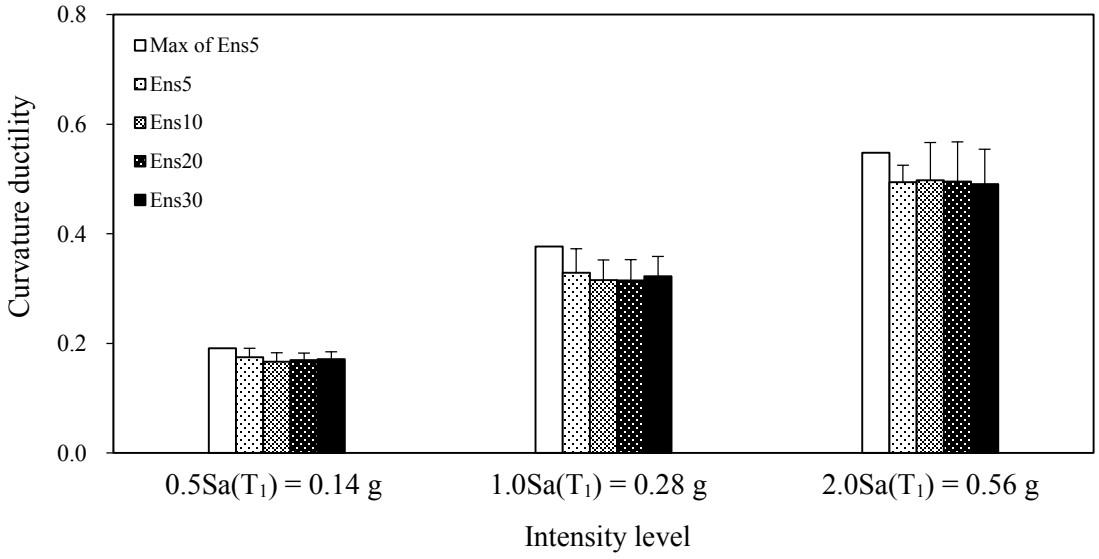

Figure A.14 Column curvature ductilities of Bridge #1 based on $S_a(T_1)$ (Pier 1).

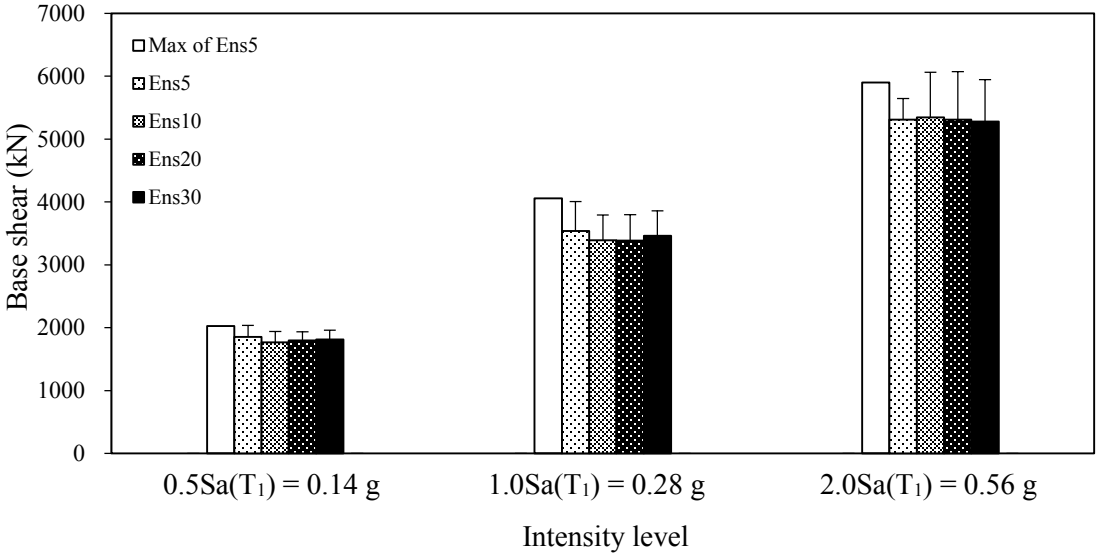

Figure A.15 Base shears of Bridge #1 based on $S_a(T_1)$.

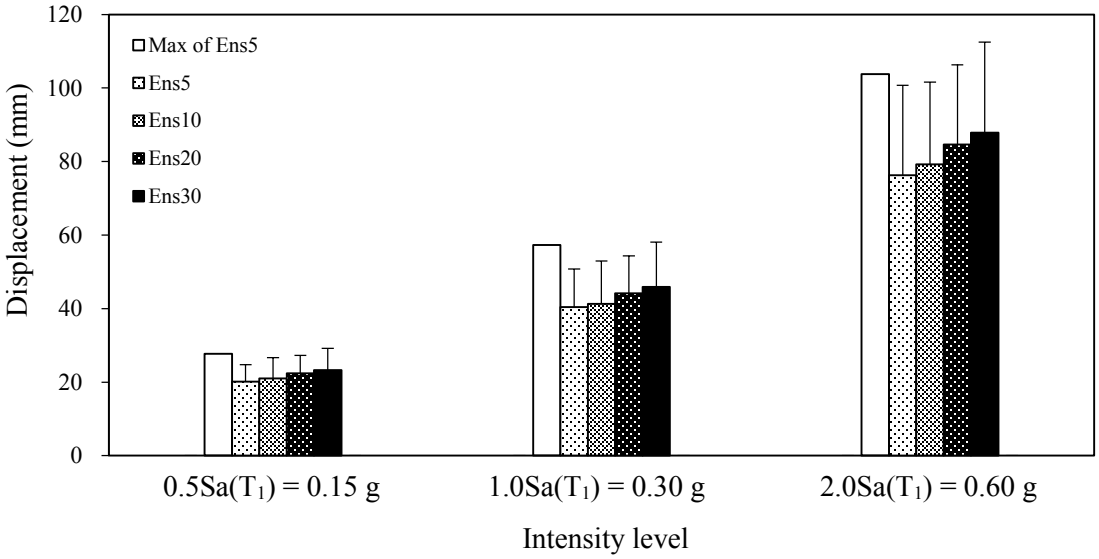

Figure A.16 Deck displacements of Bridge #2 based on $S_a(T_1)$.

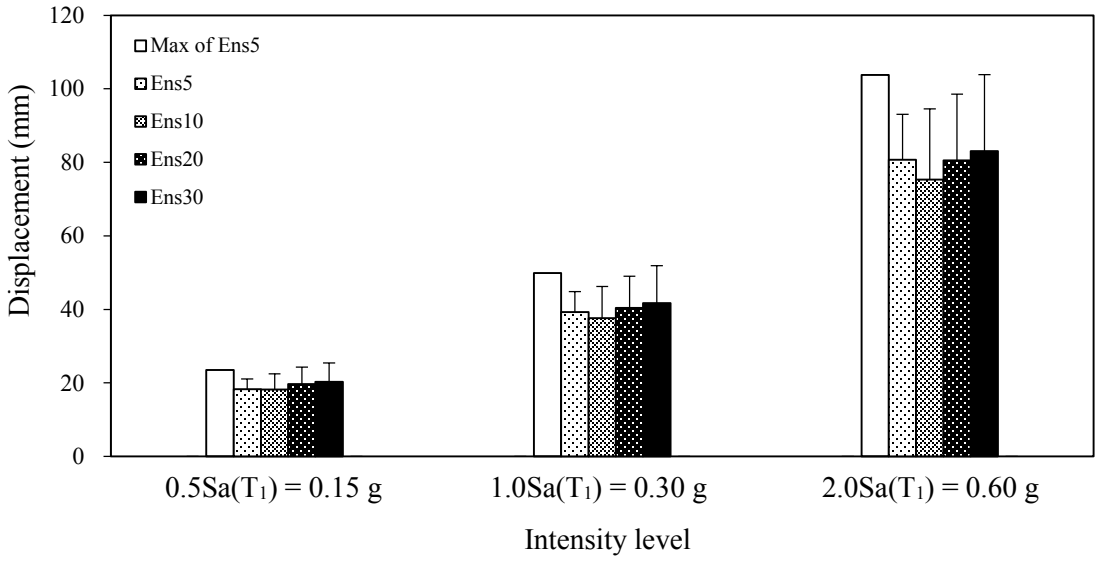

Figure A.17 Expansion bearing displacements of Bridge #2 based on $S_a(T_1)$.

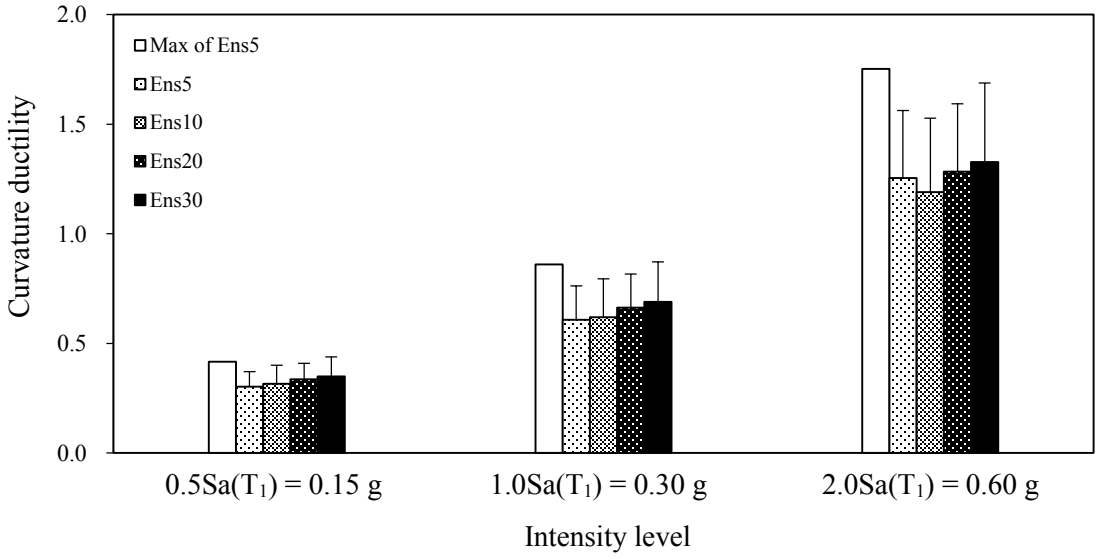

Figure A.18 Column curvature ductilities of Bridge #2 based on $S_a(T_1)$ (Pier 1).

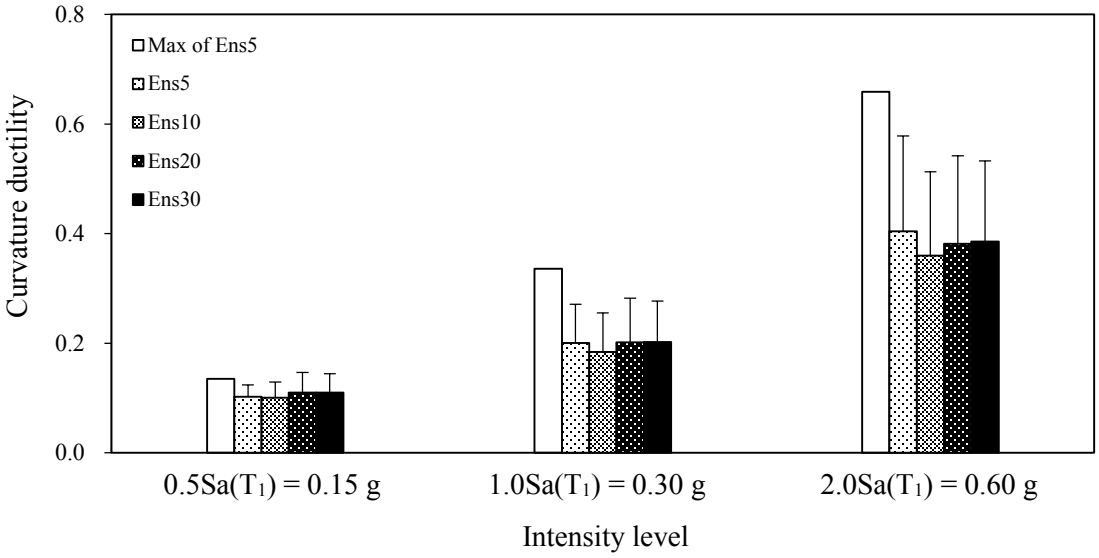

Figure A.19 Column curvature ductilities of Bridge #2 based on $S_a(T_1)$ (Pier 2).

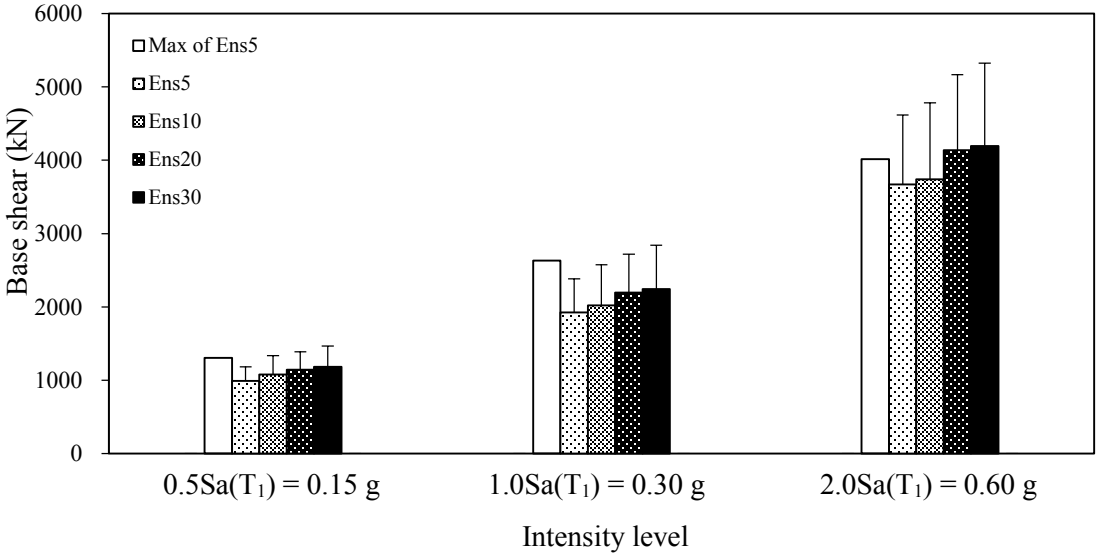

Figure A.20 Base shears of Bridge #2 based on $S_a(T_1)$.

References

AASHTO (2007). LRFD Bridge design specifications. American Association of State Highway and Transportation Officials. SI Units, 4th edition, Washington, DC.

Adams, J. (2011). Seismic hazard maps for the National Building Code of Canada. Proceedings of the CSCE 2011 General Conference, Ottawa, Ontario, 10 p.

Adams, J., and Atkinson, G. (2003). Development of seismic hazard maps for the proposed 2005 edition of the National Building Code of Canada. Canadian Journal of Civil Engineering, 30(2): 255-271.

Adams, J., and Halchuk, S. (2003). Fourth generation seismic hazard maps of Canada: Values for over 650 Canadian localities intended for the 2005 National Building Code of Canada. Open File Report 4459, Geological Survey of Canada, Ottawa, Ontario, 159 p.

Amiri-Hormozaki, K. (2004). Effects of scaling of earthquake excitations on dynamic response of reinforced concrete frame buildings. M.A.Sc thesis, Department of Civil and Environmental Engineering, University of Ottawa, Ontario.

Ang, B.G. (1981). Ductility of reinforced concrete bridge piers under seismic loading. M.A.Sc thesis, Department of Civil and Natural Resources Engineering, School of Engineering, University of Canterbury, Christchurch, New Zealand.

ASCE. (2010). Minimum design loads for buildings and other structures, ASCE standard ASCE/SEI7-10. American Society of Civil Engineers.

ATC-32 (1996). Improved seismic design criteria for California bridges: Provisional recommendations. Applied Technology Council, Redwood City, CA.

Atkinson, G.M. (2009). Earthquake time histories compatible with the 2005 National building code of Canada uniform hazard spectrum. Canadian Journal of Civil Engineering, 36(6): 991-1000.

Atkinson, G.M., and Beresnev, I.A. (1998). Compatible ground-motion time histories for new national seismic hazard maps. Canadian Journal of Civil Engineering, 25(2): 305-318.

Aviram, A., Mackie, K.R., and Stojadinovic, B. (2008a). Effect of abutment modeling on the seismic response of bridge structures. Earthquake Engineering and Engineering Vibration, 7(4): 395-402.

Aviram, A., Mackie, K.R., and Stojadinovic, B. (2008b). Guidelines for nonlinear analysis of bridge structures in California. PEER Report, Pacific Earthquake Engineering Research Center, Berkeley, California.

Caltrans (2013). Seismic design criteria version 1.7. California Department of Transportation, Sacramento, CA.

CHBDC (2010). Canadian highway bridge design code. Standards CAN/CSA-S6-88.Canadian Standards Association, Mississauga, Ontario.

Choi, E., DesRoches, R., and Nielson, B. (2004). Seismic fragility of typical bridges in moderate seismic zones. Engineering Structures, 26(2): 187-199.

Computers and Structures, Inc. (2011). SAP2000 – Computer program for three dimensional static and dynamic finite element analysis and design of structures. Berkley, CA.

Cordova, P. P., Deierlein, G.G., Mehanny, S.S.F., and Cornell, C.A. (2000). Development of two-parameter seismic intensity measure and probabilistic assessment procedure. Proceedings of the 2nd US-Japan Workshop on Performance-Based Earthquake Engineering Methodology for Reinforced Concrete Building Structures, Sapporo, Japan, pp. 187-206.

DesRoches, R., Leon, R.T., and Dyke, S. (2003). Response modification of bridges. MAE Center Project ST-12, Illinois.

Dhakal, R.P., Singh, S., and Mander, J.B. (2007). Effectiveness of earthquake selection and scaling method in New Zealand. Bulletin of the New Zealand Society for Earthquake Engineering, 40(3): 160-171.

Dincer, E. (2003). Seismic drift demands of reinforced concrete buildings. Ph.D dissertation, Department of Civil and Environmental Engineering, University of Ottawa, Ontario.

Dowell, R.K. (2012). Nonlinear time-history seismic analysis of bridge frame structures. Proceedings of the 15th World Conference on Earthquake Engineering, Lisbon, Portugal, 10 p.

European Committee for Standardization. (2004). Eurocode 8: Design of strcutures for earthquake resistance, Part 1–General rules, seismic actions and rules for buildings, Brussels, Belgium.

Fu, G. (2013). Bridge design and evaluation: LRFD and LRFR. John Wiley & Sons, Inc. New York.

Galin, S. (2012). Selection and scaling of seismic excitations for time-history analysis of reinforced concrete frame buildings, M.A.Sc thesis, Department of Civil and Environmental Engineering, University of Ottawa, Ontario.

Gao, Y.L. (2013) (In progress). Effects of modeling parameters on the seismic response of typical highway bridges. M.A.Sc thesis, Department of Building, Civil and Environmental Engineering, Concordia University, Montreal, Quebec.

Gao, Y.L., and Lin, L. (2012). Elongation of the fundamental periods of highway bridges during nonlinear seismic response. Proceedings of the 7th National Seismic Conference on Bridges and Highways, Oakland, CA.

Gasparini, D.A., and Vanmarcke, E.H. (1976). SIMQKE: A program for artificial motion generation. User's manual and documentation, Department of Civil Engineering, Massachusetts Institute of Technology, Cambridge, Massachusetts.

Haselton, C.B., Whittaker, A.S., and Hortacsu, A. (2012). Selection and scaling earthquake ground motions for performing response-history analyses. Proceedings of the 15th World Conference on Earthquake Engineering, Lisbon, Portugal.

Hartzell, S.H. (1978). Earthquake aftershocks as Green's functions. Geophysical Research Letters, 5(1): 1-4.

Heidebrecht, A.G., and Naumoski, N. (2002). The influence of design ductility on the seismic performance of medium height reinforced concrete buildings. ACI Special Publications SP-197, American Concrete Institute, Farmington Hills, MI, 239-264.

Kelly, J.M. (1997). Earthquake-Resitance Design with Rubber. Springer, London, 2nd Edition.

Lew, M., Naeim, F., Hudson, M.B., and Korin, B.O. (2008). Challenges in specifying ground motions for design of tall buildings in high seismic regions of the United States. Proceedings of the 14th World Conference on Earthquake Engineering, Beijing, China.

Lin, L. (2008). Development of improved intensity measures for probabilistic seismic demand analysis. Ph.D dissertation, Department of Civil and Environmental Engineering, University of Ottawa, Ontario.

Lin, L., Naumoski, N., Saatcioglu, M., Foo, S., Booth, E., and Gao, Y.L. (2012). Selection of seismic excitations for nonlinear analysis of reinforced concrete frame buildings. Canadian Journal of Civil Engineering, 40(5): 411-426.

Luco, N., and Cornell, C.A. (2007). Structure-specific scalar intensity measures for near-source and ordinary earthquake ground motions. Earthquake Spectra, 23(2): 357-392.

Mander, J.B., Priestley, M.J., and Park, R. (1988). Theoretical stress-strain model for confined concrete. Journal of Structural Engineering, 114(8): 1804-1826.

McKenna, F., Fenves, G.L., and Scott, M.H. (2000). Open system for earthquake engineering simulation, University of California, Berkeley, CA.

Moehle, J., and Deierlein, G.G. (2004). A framework methodology for performance-based earthquake engineering. Proceedings of the 13th World Conference on Earthquake Engineering, Vancouver, British Columbia.

Naeim, F., and Lew, M. (1995). On the use of design spectrum compatible time histories. Earthquake Spectra, 11(1): 111-127.

Naumoski, N. (2001). Program SYNTH – Generation of artificial accelerograms compatible

with a target spectrum. User's manual, Department of Civil and Environmental Engineering, University of Ottawa, Ottawa, Ontario.

Naumoski, N., Saatcioglu, M., and Amiri-Hormozaki, K. (2004). Effects of scaling of earthquake excitations on the dynamic response of reinforced concrete frame buildings. Proceedings of the 13th World Conference on Earthquake Engineering, Vancouver, British Columbia.

Naumoski, N., Heidebrecht, A.C., and Rutenberg, A.V. (1993). Representative ensembles of strong motion earthquake records. EERG report, 93-1, Department of Civil Engineering, McMaster University, Hamilton, Ontario.

Naumoski, N., Heidebrecht, A.C., and Tso, W.K. (1988). Selection of representative strong motion earthquake records having different A/V ratios. EERG report, 88-01, Department of Civil Engineering, McMaster University, Hamilton, Ontario.

Nielson, B.G. (2005). Analytical fragility curves for highway bridges in moderate seismic zones. Ph.D dissertation, School of Civil and Environmental Engineering, Georgia Institute of Technology, Georgia.

Nielson, B.G., and DesRoches, R. (2007). Analytical seismic fragility curves for typical bridges in the central and southeastern United States. Earthquake Spectra, 23(3): 615-633.

NIST. (2011). Selecting and scaling earthquake ground motions for performing response history analysis. NIST/GCR 11-917-15, prepared by NEHRP Consultants Joint Venture for the National Institute of Standards and Technology, Gaithersburg, Maryland.

NRCC. (2010). National Building Code of Canada 2010. Institute for Research in Construction, National Research Council of Canada, Ottawa, Ontario.

Pan, Y., Agrawal, A.K., Ghosn, M., and Alampalli, S. (2010). Seismic fragility of multispan simply supported steel highway bridges in New York State. I: Bridge modeling, parametric analysis, and retrofit design. Journal of Bridge Engineering, 15(5): 462-472.

Roeder, C.W., Stanton, J.F. and Taylor, A.W. (1987). Performance of elastomeric bearings. NCHRP Report 298, National Cooperative Highway Research Program, Transportation Research Board, Washington, DC.

Reyes, J.C., and Kalkan, E. (2011). Required number of records for ASCE/SEI 7 ground motion scaling procedure. US Geological Survey, Open File Report 108, 334 p.

Shafiei-Tehrany, R. (2008). Nonlinear dynamic and satic analysis of I-5 Ravenna Bridge. Ph.D dissertation, Washington State University, Washington. DC.

Somerville, P.G., Collins, N.F., Graves, R.W., and Pitarka, A. (2004). An engineering ground motion model for basin generated surface waves. Proceedings of the 13th World Conference on Earthquake Engineering, Vancouver, BC.

Tavares, D.H., Padgett, J.E., and Paultre, P. (2012). Fragility curves of typical as-built highway bridges in eastern Canada. Engineering Structures, Vol.40, 107-118.

TNZ. (2003). Bridge Manual, 2nd Edition. Transit New Zealand, Wellington, New Zealand.

Tremblay, R., and Atkinson, G.M. (2001). Comparative study of the inelastic seismic demand of eastern and western Canadian sites. Earthquake Spectra, 17(2): 333-358.

Wald, D.J., Burdick, L.J., and Somerville, P.G. (1988). Simulation of acceleration time histories close to large earthquakes. Earthquake Engineering and Soil Dynamics I-Recent Advances in Ground-Motion Evaluation, American Society of Civil Engineers, 430-444.

Waller, C.L. (2011). A Methodology for Probabilistic Performance-Based Seismic Risk Assessment of Bridge Inventories. M.A.Sc thesis, Department of Civil and Environmental Engineering, Carleton University, Ottawa, Ontario.

Wilson, J.C., and Tan, B.S. (1990). Bridge abutments: formulation of simple model for earthquake response analysis. Journal of Engineering Mechanics, 116(8): 1828-1837.